Novel Functional Membrane Precursors based on Triblock Terpolymer Thin Films

DISSERTATION

zur Erlangung des akademischen Grades eines
Doktors der Naturwissenschaften
- Dr. rer. nat. -
der Fakultät Biologie, Chemie und Geowissenschaften
der Universität Bayreuth

vorgelegt von
Alexandra Sperschneider
aus Coburg

Bayreuth 2009

Die vorliegende Arbeit wurde in der Zeit von November 2005 bis März 2009 an den Lehrstühlen für Physikalische Chemie II und Makromolekularen Chemie II der Universität Bayreuth unter der Betreuung von Herrn Prof. Dr. Axel Müller angefertigt.

Vollständiger Abdruck der von der Fakultät Biologie, Chemie und Geowissenschaften der Universität Bayreuth genehmigten Dissertation zur Erlangung des akademischen Grades Doktor der Naturwissenschaften (Dr.rer.nat.).

Amtierender Dekan: Prof. Dr. Stephan Clemens
Tag des Einreichens der Dissertation: 27. Juli 2009
Tag des wissenschaftlichen Kolloquiums: 22. Januar 2010

Prüfungsausschuss:
Prof. Dr. Axel Müller (Erstgutachter)
Prof. Dr. Georg Krausch (Zweitgutachter)
Prof. Dr. Mukundan Thelakkat
Prof. Dr. Helmut Alt (Vorsitzender)

Meiner Familie

Perché, secondo l'opinion mia,
A chi vuole una cosa ritrovare,
Bisogna adoperar la fantasia.

Galileo Galilei, *Contro il portar la toga*

Contents

Summary

In this study novel functional thin film membrane precursors based on polybutadiene-*block*-poly(2-vinylpyridine)-*block*-poly(*tert*-butyl methacrylate) (BVT) triblock terpolymer systems have been identified. By perfect combination of the rubber-like polybutadiene (PB), the pH-responsive and metal-charging poly(2-vinylpyridine) (P2VP) and the irradiation sensitive poly(*tert*-butyl methacrylate) (P*t*BMA), the most promising conditions for synthetic membrane precursors have been given regarding block copolymer synthesis.

Thin films (thickness less than 100 nm) were prepared by both spin-casting and combinatorial mapping onto different substrates. Subsequently, the morphologies have been thermodynamically equilibrated by a controlled solvent annealing procedure.

As an initial milestone, both bulk and thin film microphase separation behavior of four $B_xV_yT_z{}^{M_w}$ ternary systems with different volume fractions (x, y, z) and total weight-average molecular weights (M_w in kg/mol) were investigated with respect to the film thickness. Two interesting polymer compositions were shortlisted for further detailed studies. Scanning force microscopy (SFM), scanning electron microscopy (SEM) and grazing-incidence small-angle X-ray scattering (GISAXS) experiments revealed that $B_{16}V_{21}T_{63}{}^{145}$ self-assembles in thin films in well-defined, hexagonally ordered core-shell morphologies where the pH-responsive P2VP shell surrounds the soft PB core. For $B_{48}V_{27}T_{15}{}^{78}$ thin films, an inverse morphology was identified with a flexible PB top layer that covered subjacent cylindrical structures.

In comparison with previous studies of the well-characterized polystyrene-*block*-poly(2-vinyl pyridine)-*block*-poly(*tert*-butyl methacrylate) (SVT) triblock terpolymer thin films, the novel BVT core-shell morphologies were considered to be attractive precursors for nanoporous separation membranes. SFM, SEM and transmission electron microscopy (TEM) prove several useful features: similar equilibrum morphologies on substrates with different wettability, homogenous film thicknesses, the feasibility of transferring the thin films onto further substrate materials and the stabilization of the thin films by internal cross-linking.

Due to the low surface tension, PB tends to segregate to the free air interface. To tune the microphase separation behavior in thin films to obtain nanoporous structures, $B_{14}V_{18}T_{68}{}^{165}$ and $B_{53}V_{24}T_{23}{}^{85}$ triblock terpolymers have been chemically modified. The hydroxylation of the polybutadiene compartment resulted in an increase of both polarity and surface tension and, hence, in a stronger attraction by the polar silicon substrate. For hydroxylated $B_{14}V_{18}T_{68}{}^{165}$ thin films, a porous hybrid morphology was identified whereas the hydroxylated $B_{53}V_{24}T_{23}{}^{85}$ thin films showed a sponge-like architecture. Both structures were characterized by a film thickness independence.

To investigate the microphase separation and the homogenity of the pores within thin film volumes, we applied the high-depth resolution quasi *in-situ* (QIS) SFM nano-tomography guaranteeing a distinctive reliability, practicability and manageability. The obtained data sets, emanated from single plasma abrasion steps, were converted into three-

dimensional reconstructions, providing insights into the structural behavior in very thin volume elements. For $B_{14}V_{18}T_{68}{}^{165}$, the presumed core-shell microphase separation morphology was supplemented by QIS SFM nanotomography revealing a perforated lamella morphology which is distorted by surface fields. The strong effect of hydroxylation of $B_{14}V_{18}T_{68}{}^{165}$ caused a hybrid morphology with persistent 'open' pores after the selective destruction of the P*t*BMA compartment.

With thickness independence and a large homogenity of patterns over macroscale areas, these novel synthetic membrane precursors revealed highly promising morphologies for membrane technology, for example as 'skin' top layers of thin film composite membranes improving separation and flux properties. Moreover, the directed control of the pore diameter is facilitated by the pH-responsive poly(2-vinylpyridine) compartment.

Zusammenfassung

In dieser Studie wurden neuartige, funktionelle Vorstufen für Dünnfilm-Membranen auf Basis von Polybutadien-*block*-poly(2-vinylpyridin)-*block*-poly(*tert*-butylmethacrylat) (BVT) Dreiblockterpolymeren identifiziert. Durch geschickte Kombination des gummiartigen Polybutadiens (PB), des pH-responsiven und mit Metallen beladbaren Poly(2-vinylpyridin) (P2VP) und des strahlungsempfindlichen Poly(*tert*-butylmethacrylats) (P*t*BMA), sind seitens der Polymersynthese die besten Voraussetzungen für synthetische Membranvorstufen geschaffen.

Dünnfilme mit einer Dicke von kleiner 100 nm wurden sowohl mittels Lackschleudern als auch mittels Ziehvorrichtung zur Erstellung von Dickegradienten auf unterschiedlichen Substraten hergestellt. Im Anschluss wurden die selbstangeordneten Strukturen während des kontrollierten Lösungsmittelbedampfens in ein thermodynamisches Gleichgewicht überführt.

Im ersten Schritt der Arbeit wurde die Mikrophasenseparation im Volumen und in dünnen Filmen von vier $B_xV_yT_z{}^{M_w}$ Dreiblockterpolymeren mit unterschiedlichen Volumenanteilen (x, y, z) und totalen Molekulargewichten (M_w in kg / mol) in Abhängigkeit von der Filmdicke untersucht. Zwei interessante Polymerzusammensetzungen kamen in die engere Wahl für weitergehende detaillierte Studien. SFM, SEM und GISAXS Experimente zeigten, dass sich $B_{16}V_{21}T_{63}{}^{145}$ im Dünnfilm in definierten, hexagonal ausgerichteten Kern-Schale-Strukturen anordnet, wobei die pH-responsive P2VP Hülle den weichen PB Kern umschliesst. Für $B_{48}V_{27}T_{15}{}^{78}$ im Dünnfilm wurde eine inverse Morphologie identifiziert. Eine flexible Oberflächenschicht aus Polybutadien bedeckt eine darunter liegende zylindrische Struktur.

Im Vergleich zu früheren Dünnfilmstudien des sehr gut charakterisierten Dreiblockterpolymersystems Polystyrol-*block*-poly(2-vinylpyridin)-*block*-poly(*tert*-butylmethacrylat) (SVT), kommen die neuartigen BVT Kern-Schale-Morphologien als attraktive Vorstufen für nanoporöse Separationsmembranen in Betracht. SFM, SEM und TEM haben folgende effektive Eigenschaften bestätigt: identische Gleichgewichtsstrukturen auf Substraten mit unterschiedlicher Benetzbarkeit, homogene Filmdicken, die Realisierbarkeit des Dünnfilmtransfers auf andere Substrate sowie die Stabilisierung durch interne Vernetzung.

Aufgrund der niedrigen Oberflächenspannung neigt der Polybutadienblock dazu, an die freie Luftgrenzfläche zu segregieren. Um die Mikrophasenseparation in dünnen Filmen zur Herstellung poröser Strukturen gezielt einzustellen, wurden die Dreiblockterpolymere $B_{14}V_{18}T_{68}{}^{165}$ und $B_{53}V_{24}T_{23}{}^{85}$ chemisch modifiziert. Die selektive, oxidative Hydroborierung des Polybutadienblocks resultierte in einer Zunahme der Polarität und der Oberflächenspannung. Somit ergab sich auch eine stärkere Anziehungskraft durch das polare Substrat.
Hydroxyliertes $B_{14}V_{18}T_{68}{}^{165}$ ordnet sich im dünnen Film selbst in einer Art Hybridstruktur an, wohingegen hydroxyliertes $B_{53}V_{24}T_{23}{}^{85}$ eine schwamm-ähnliche Architektur aufweist. Beide Morphologien werden durch ihre Unabhängigkeit von der Filmdicke bestimmt.

Um die Mikrophasenseparation und die Homogenität der Poren innerhalb der dünnen Filme zu analysieren, nutzten wir die hochauflösende quasi *in-situ* (QIS) SFM Nanotomographie Methode, welche eine ausgeprägte Verlässlichkeit, Verwendbarkeit und Handlichkeit garantiert. Um Einblicke in das strukturelle Verhalten in extrem dünnen Volumenelementen zu ermöglichen, wurden die aus einzelnen Plasmaabtragungsschritten generierten Datensätze in eine dreidimensionale Rekonstruktion übertragen.
Für $B_{14}V_{18}T_{68}$[165] wurde die frühere Annahme einer Kern-Schale-Mikrophasenseparation durch QIS SFM Nanotomographie erweitert. Dieses Dreiblockterpolymersystem ordnet sich selbst als perforierte Lamelle an, welche durch Oberflächeneffekte deformiert wird. Der starke Effekt der Hydroxylierung von $B_{14}V_{18}T_{68}$[165] äussert sich in der Selbstanordnung einer Hybridmorphologie, welche nach der gezielten Zerstörung des P*t*BMA-Blocks über durchgehend 'offene' Poren verfügt.

Aufgrund ihrer Filmdickenunabhängigkeit und der Homogenität der Strukturen über makroskopische Bereiche, weisen diese neuartigen synthetischen Membranvorstufen ein enormes Potential für die Membrantechnologie auf. Ein möglicher Einsatzbereich ist beispielsweise die Verwendung als dünne Oberflächenschicht bei Dünnfilmkompositmembranen um dort Separierungs- und Flusseigenschaften zu verbessern.
Darüber hinaus wird die gezielte Kontrolle des Durchmessers der offenen Poren durch den pH-responsiven Poly(2-vinylpyridin)block gesteuert.

Chapter 1

Introduction

This thesis was motivated by the aim of developing novel, functional membrane precursors based on ABC triblock terpolymer thin films. By exploiting the self-assembling properties and the continuous improvement in block copolymer synthesis, well-defined thermodynamically and mechanically stable thin film morphologies could be developed. By incorporating responsive compartments which may be stimulated externally by light, pH or temperature, a high potential in the application as smart membranes is provided.

During the last decade, the technological demand for miniaturization down to nanoscale objects increased significantly. This nanotechnology hype is mostly driven by the continuous size reduction of semiconductor devices in combination with the incessant improvement of high-resolution characterization methods [Cao04].

Two different approaches can be classified. On the one hand, the 'top-down' strategy focuses on the fabrication of devices based on traditional lithography techniques [Par03, Cao04] and novel soft lithography processes, for example nanografting [WM99] or microcontact printing [Jac95]. Hence, difficulties concerning effort and final control of the designed nanostructures still remain [Laz03].

Adopted from self-assembling biological systems [Bal97], current scientific investigations focus on the 'bottom-up' approach of chemical self-assembly of auspicious block copolymer materials. This class has evolved from the standard application fields like adhesives or elastomers to ideal nanoscale tools because of their large variety of chemical and physical properties [Li02, Ish03, Ols08]. These features can be nowadays exactly tuned, with respect to the corresponding purpose, due to the permanent progress in polymer synthesis [Haw97, Had05]. Block copolymers consist of at least two chemically different macromolecules, which are covalently linked, resulting in spontaneously thermodynamically driven self-organized nanostructures. In dependence of the preparation procedures,

block copolymer thin films exhibit highly ordered domains representing a basis for nanolithography applications including nanoimprinting templates [Man91, Man96, Par97, Far99, Asa02, Men04, Bra06, Cho96, Sol08], electronics [Gre93, Pei95, Bla07], nanoparticle templates [Fog97, Fog97a] and polymeric matrices for metal nanoclusters [Cie98].

Moreover, inspired by nature, the focus of current research is put on highly-promising novel functional synthetic membranes with tailored properties. The selectivity of traditional state-of-the-art membranes is still often limited due to the random pore size distribution. Thus, novel composite membranes are of outstanding relevance in this field.

In general, three different kinds of composite membranes are distinguished as shown schematically in Figure 1.1. Initially, the large pores of support membranes may be filled by graft polymerization, in-situ polymerization or cross-linking of a polymeric precursor (scheme in Figure 1.1 A). By introducing responsive polymers (for example pH or solvent sensitive), the control of the permeability is obtained. Yamaguchi et *al.* studied these pore-filled composite membranes in detail [Yam91, Yam93, Yam96, Yam97, Cho03, Kai05]. A second approach, introduced by Saito and Furusaki [Lee99], deals with the functionalization of interior pore walls via grafting-from process (scheme in Figure 1.1 B). This procedure enables the control of pore-size, e.g. by chemical vapor deposition [Als03] and responsiveness resulting from grafted smart hydrogels [Shi93, Kop02] or polymer brushes [Ito97, Reb98]. Moreover, addtional functionalities like the immobilization of nanoparticles as emzyme

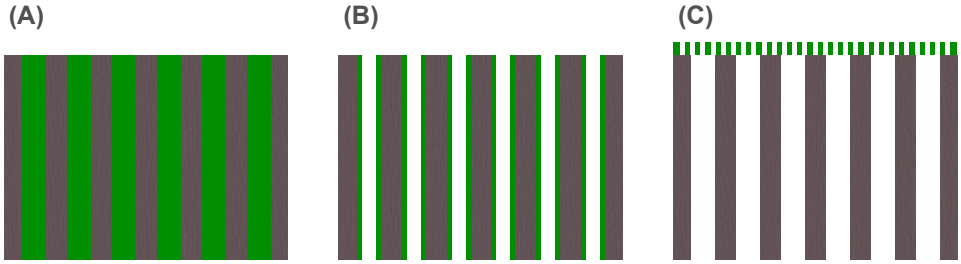

Figure 1.1: *Three different kinds of composite membranes are distinguishable:* ***(A)*** *pore filling composite membranes,* ***(B)*** *surface modified composite membranes and* ***(C)*** *thin film composite membranes.*

carriers on the inner pore walls were studied. Figure 1.2 displays a scanning electron microscopy (SEM) image of such a track-etched poly(ethylene terephthalate) (PET) support membrane including covalently bond nanoparticles [Hic06].

The most promising approach in membrane technology are thin film composite (TFC) membranes where support membranes are coated with thin films as 'skin' top layers (scheme in Figure 1.1 C). Pioneering studies on multi-polyelectrolyte layers applied via

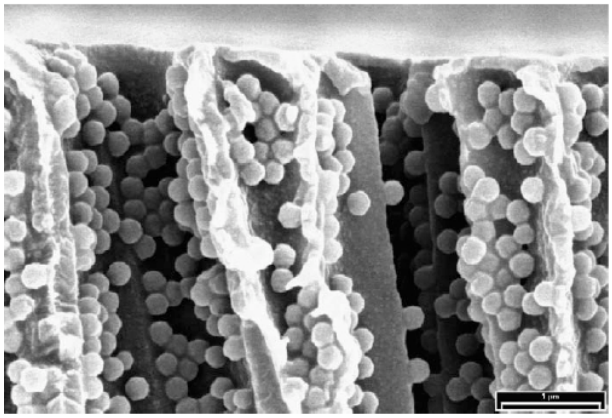

Figure 1.2: *Track-etched PET support membrane including covalently bond nanoparticles. (from Ref. [Hic06]. Copyright 2006, Elsevier)*

layer-by-layer technique onto support membranes were made by Tieke et *al.* [Tie03]. However, it is still not possible to coat the supporting material with defect-free, selective 'skin' layers thinner than 50 nm [Ulb06]. Early studies using Langmuir-Blodgett techniques failed in reproducing ultra thin film morphologies [Pen06].

The motivation of the presented study based on the generation of complex periodically nanoporous structures as candidates for the membrane application. By choosing suitable physical parameters, a guided self-assembly of ABC triblock terpolymers in thin films reveals the desired nanopatterns which can be susbsequently transferred onto support materials. The resulting novel TFC membranes possess optimized features like periodic pore sizes, surface functionalization, high flux, sufficent long-term stability and a vast selectivity representing a promising basis for various membrane applications in industry [Nun01, Ulb06].

Lee et *al.* established the basis for a meanwhile general implemented method of generating nanoporous films by the selective removal of the ordered minority phase [Lee88]. Smith and Meier degraded the polydiene compartments of polystyrene-*block*-polybutadiene (PS-PB) and polystyrene-*block*-polyisoprene (PS-PI), respectively, by ozonolysis. The corresponding PS domains had not been influenced during the treatment [Smi92]. More recent studies showed the universal use of this procedure. Beside complex nanoporous thin films, based on polyisoprene-*block*-polystyrene-*block*-polylactide (PS-PI-PLA), also bicontinuous gyroid nanoporous networks were prepared by ozonolysis of the polyisoprene block in a blend consisting of poly(2-vinylpyridine)-*block*-polyisoprene (P2VP-PI) mixed with homopolymer PI [Guo06, Oku06]. Both hexagonally packed short cylinders oriented perpendicular to the substrate and continuous gyroid morphologies revealed consistent channel geometries which are also of interest for TFC membranes.

Another approach represents the specific depolymerization of polymer blocks, sensi-

tive to UV-irradiation, like poly(methyl methacrylate) to obtain nanoporous film volumes [Ban06, Joo06]. Concerning the purpose of developing functional synthetic membrane templates, ABC triblock terpolymer thin films represent the most promising systems as shown by Ludwigs et *al.*. The ample investigations of microdomain structures of polystyrene-*block*-poly(2-vinylpyridine)-*block*-poly(*tert*-butyl methacrylate) (SVT) revealed a tickness dependent, thermodynamically stable, three compartment perforated lamella morphology (PL) which is a promising structure formation for composite membranes. Depolymerization of the poly(*tert*-butyl methacrylate) (P*t*BMA) matrix phase by UV-irradiation provides a core-shell mesh-like pattern where the PS minority phase forms the stabilizing core surrounded by a P2VP shell. Furthermore, by acid saponification of the poly(*tert*-butyl methacrylate) compartment, a pH-dependent nanostructure was created without changing the consistent microdomain morphologies [Lud05, Lud05a, Lud05b].

Until now, published studies lack of in-depth analysis of three-diensional microphase separation through a confined volume. However, these investigations are important for the analysis of the provided potential of ABC triblock terpolymer films used as functional membranes.

1.1 Microphase separation of block copolymers in bulk

The simplest class of block copolymers consists of two chemically different macromolecules (A, B) which are covalently attached to each other. Due to repulsion forces, both blocks tend to segregate forming equilibrium microphase separated morphologies considering the minimization of both A-B contact area and interfacial energy [Bat90, Seg05]. The mean-field theory (MFT), a theoretical approach established by Leibler [Lei80], considers the driving forces for phase behaviour to be the Flory-Huggins segment-segment interaction parameter χ, which is indirect proportional to the temperature [Bat90], the overall degree of polymerization N and the volume fractions ϕ_{A} and ϕ_{B} (with $\phi_{\mathrm{B}} = 1 - \phi_{\mathrm{A}}$).

In detail, the Flory-Huggins interaction parameter describes the mixing free energy (monomer repulsion between A and B),

$$\chi_{AB} = (\frac{Z}{k_B T})\ [\epsilon_{AB} - (\frac{1}{2})(\epsilon_{AA} + \epsilon_{BB})] \tag{1.1}$$

with Z representing the number of nearest-neighbor monomers to a copolymer configuration cell and ϵ corresponding to the monomeric interaction energy between A and B. In case of a negative χ_{AB} value, a mixed state was found. On the contrary, positive values represent total repulsion resulting consequently in microphase separated domains [Bat99].

Furthermore, the product χN determines the degree of segregation which can be divided into three regimes: weak segregation limit ($\chi N \backsim 10$), strong segregation limit ($\chi N \gg 10$) and intermediate segregation region ($12 \backsim \chi N \backsim 50$) [Mei69, Hel78, Lei80, Bat90, Mat96]. A symmetric AB diblock copolymer system is dominated by entropic terms favouring a disorded phase, if $\chi N < 10$. In case of the strong segregation limit, the enthalpic terms dominate causing a disorder-to-order phase transition where the blocks start to segregate to different periodic morphologies [Lei80, Fre96, Abe05].

For AB diblock copolymers, four equlibrium microphase structures as shown in Figure 1.3 are determined. Starting with a small volume fraction ϕ_{A}, spheres in a body-

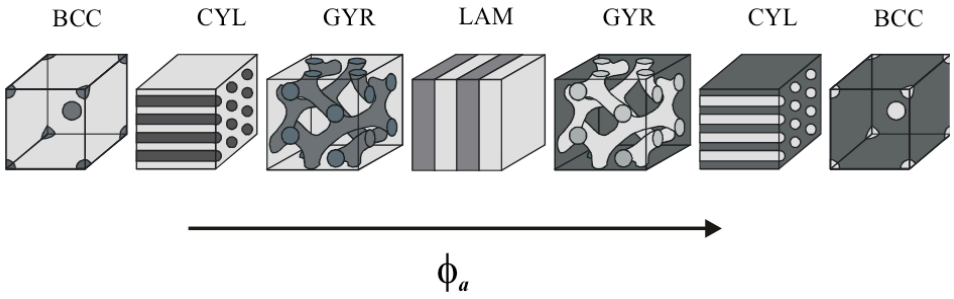

Figure 1.3: *Bulk morphologies of AB diblock copolymers in dependence of an increasing volume fraction ϕ_{A} of the A compartment with BCC: spheres orderd in a body centered lattice, CYL: cylinders ordered on a hexagonal lattice, GYR: gyroid, biscontinuous phase, LAM: lamellar morphology [Bök02].*

centered cubic (BCC) lattice are found. With a constant increase of ϕ_{A}, the domains form hexagonally ordered cylinders (CYL) passing into a bicontinous double gyroid structure (GYR) and resulting finally in lamellae (LAM) [Sch94, Haj94, Bat99]. The periodical domain spacing $\mathrm{L_0}$ what is typically determined in the range of 10 – 100 nm [Bat99, Kra02, Nie08], is also dependent on the molecular weight and the segmental interactions [Oht86, Bat90, Ham98, Laz03, Had02]. However, all presented investigations show a strong temperature dependence. For the majority of block copolymers, the segregation in nanoscale domains is driven by the volume fractions at low temperatures [Mol71]. By increasing the ambient temperature to the so-called order-to-disorder transition temperature ($\mathrm{T_{ODT}}$), the microphase order disappears entirely resulting in a disorded state [Lei80, Hel82, Bat90, Fre96].

By the additional incorporation of a third polymer compartment, the complexity of the phase diagram is enlarged considerably. In the 1990' s, important investigations of microphase separation in complex ABC triblock terpolymer systems were performed by Mogi et *al.* [Mog92a, Mog92, Mog93, Mog94] and Stadler et *al.* [Abe96, Bre97, Eru97] who

studied the microphase separation of polystyrene-*block*-polybutadiene-*block*-poly(methyl methacrylate) (SBM) in both weak and strong segregation limit. Since additional segmental interactions (BC, AC) factor into the periodic arrangement of nanoscale domains, phase diagrams of SBM (Figure 1.4), polystyrene-*block*-poly(2-vinylpyridine)-*block*-poly(*tert*-butyl methacrylate) (SVT) [Lud05b] and other triblock terpolymers clarify the intricacy of their microphase separated morphologies [Abe00].

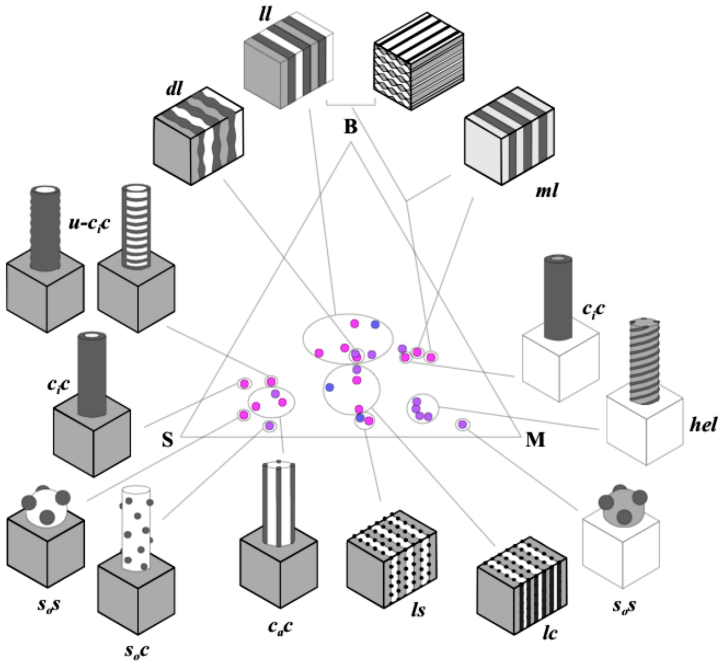

Figure 1.4: *Ternary phase diagram of polystyrene*-block-*polybutadiene*-block-*poly(methyl methacrylate) triblock terpolymers revealing a large structural variety. (from Ref. [Abe00]. Copyright 2000, Wiley VCH).*

The introduction of a third polymer compartment provides the oppurtunity of extra functionalities, e.g. responsiveness to external stimuli such as light, pH or temperature, resulting in distinctive features which can be tuned for particular applications.

1.2 Microphase separation of block copolymer in thin films

A special strategic focus is put on the high potential of block copolymer thin films as inherent part of nanoporous TFC membranes.

In contrast to bulk morphologies, additional driving forces near surfaces and in thin film volumes influence the structural arrangement in thin block copolymer films. Thus, in addition to molecular weight and temperature, thin film morphologies are also dependent on the film thickness [Rus91, Smi01] and surface energies [Man97, Epp07]. The polymer block containing the most minimal surface energy tend to segregate to the free surface whereas the compartment with the less interfacial tension wets the supporting substrate. Hence, thin film morphologies are the result of optimizing interfacial energies in the block copolymer systems [Kra95, Fas01, Kra02]. For lamellar AB diblock copolymers, two different microdomain orientations have been found. In case of symmetric wetting, one polymer compartment is located on both substrate and air interface. If the initial film thickness t equals $t = n * L_0$ (where n is an integer and L_0 corresponds to the periodical domain spacing), smooth films result. This commensurability was investigated theoretically [Pic97, Gei99, Gei99a] and experimentally [Lam94, Kon95]. On the contrary, asymmetric wetting is observed, if the two interfaces attract different blocks. Thus, a continuous layer is found if the initial film thickness equals $t = (2n + 1)\ \frac{L_0}{2}$ [Seg05, Dar07].

For technical approaches in nanoscience, in general, thin block copolymer films are faced with asymmetric boundary conditions, e.g. substrate supporting films. For that very reason, it is absolutely indispensable to obtain a profound understanding of the subsiding processes occuring near surfaces and in thin film volumes. The overall determination of control factors is likewise crucial for the utilization of the whole material potential and the resulting tuned nanstructures in thin films [Kra02]. More complex ABA triblock copolymer thin film morphologies were investigated profoundly [Sza03, Hor04, Hor07, Reh08]. Knoll et *al.* investigated a phase diagram of surface structures for polystyrene-*block*-polybutadiene-*block*-polystyrene (SBS) block copolymer thin films which was confirmed by corresponding computer simulations. Previous bulk studies provided hexagonally packed polystyrene cylinders embedded in a soft polybutadiene matrix. The thin film studies, however, revealed much more complex morphologies depending on the film thickness [Kno01, Kno02, Kno04].

In Figure 1.5, starting with a complete disorded state (dis), an increase in the film tickness results initially in cylinders oriented perpendicular to the silicon substrate ($C_\perp$) switching to cylinders oriented parallel to the substrate ($C_{\parallel,1}$). Furthermore, a stable mesh-like perforated lamella morphology (PL) was detected. By additional increase of the film thickness, parallel cylinders with necks ($C_{\parallel,1}$) followed by vertically oriented cylinders ($C_\perp$) and two layers of parallel oriented cylinders ($C_{\parallel,2}$) were found both on experimental and computer simulation way.

The equilibrium morphologies of AB and ABA block copolymers have been studied in-

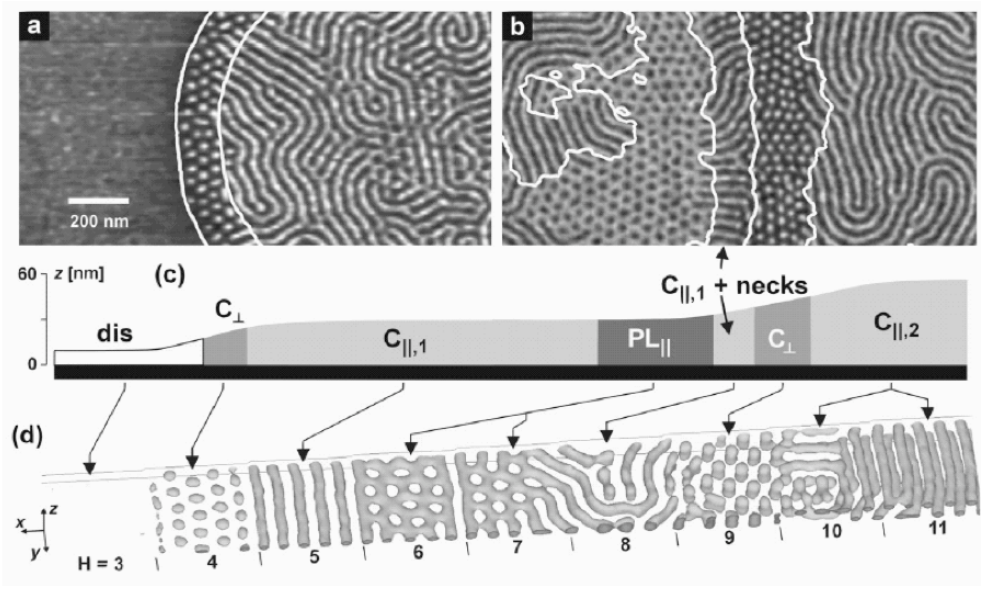

Figure 1.5: *Tapping Mode SFM phase images of thin polystyrene-block-polybutadiene-block-polystyrene (SBS) block copolymer film on silicon substrates after annealing in chloroform vapor. The surface is everywhere covered with an 10nm thick layer of poly(butadiene) [Kno01]. The bright color correspond to polystyrene whereas the dark represents to softer polybutadiene. Contour lines calculated from the corresponding height images are superimposed.* ***(c)*** *Schematic height profile of the phase images shown in* ***(a, b)****.* ***(d)*** *Simulation of an $A_3B_{12}A_3$ block copolymer film in one large simulation box with an increasing film thickness. (from Ref. [Kno02]. Copyright 2002, American Physical Society.)*

tensively. However, the identification of the potential of even more complex ABC triblock terpolymer thin films is still a challenge of outstanding relevance. Their phase behavior is determined by three Flory-Huggins interaction parameters (χ_{AB}, χ_{AC}, χ_{BC}), three volume fractions (ϕ_A, ϕ_B, ϕ_C), the total degree of polymerization N and the sequence of the three compartments, e.g. ABC or BCA [Kim08]. As a remark, already 30 different microphase separated bulk morphologies have been forecast by self-consistent mean field (SCMF) theory [Zhe95]. For thin films, complex structural designs were theoretically studied by Chen et *al.* [Che02] and Ludwigs et *al.* [Lud05]. Moreover, experimental studies revealed a large variety of different morphologies [Sto96]. Krausch and coworkers studied systematically the thin film microphase separation behavior of polystyrene-*block*-poly(2-vinylpyridine)-*block*-poly(*tert*-butyl methacrylate) (SVT) triblock terpolymer in dependence of the volume fraction ratios [Elb99, Fuk00, Elb01, Fuk02, Elb02, Fuk03, Lud03, Lud03a, Lud05b, Lud05]. Beside conventional microphase separation morphologies, a thermodynamically stable, mesh-like structure was found. This perforated lamella (PL) represents high potential as a template for nanoporous membranes (Figure 1.6). The polystyrene (white) represents the

core surrounded by the poly(2-vinylpyridine) compartment (red). The core-shell structure is embedded in the poly(*tert*-butyl methacrylate) matrix. Due to the incorporation of the pH-sensitive poly(2-vinylpyridine) middle block (red), the system may react on external stimuli.

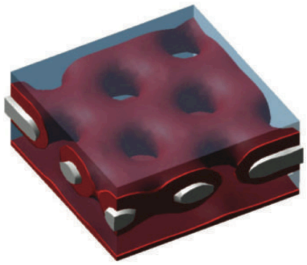

Figure 1.6: *MesoDyn calculation for a polystyrene*-block-*poly(2-vinylpyridine)*-block-*poly(*tert*-butyl methacrylate) triblock terpolymer thin film reveals a perforated lamella morphology. (from Reference [Lud03]. Copyright 2003, Nature Materials)*

1.3 Long-range, lateral order by external fields

With respect to the technological application of polybutadiene-*block*-poly(2-vinylpyridine)-*block*-poly(*tert*-butyl methacrylate) thin films as nanoporous templates for composite membranes, both long-range lateral order and directed microdomain orientation are essential. In order to minimize defects or grain boundaries, several technical approaches were presented such as both chemically and topographically patterned substrates [Roc99, Par01, Seg01, Sto05, Dao06], temperature gradients [Bod99], controlled interfacial interactions [Man97], optical alignment [Mor06], external shear [Che98, Ang04, Ang05] and electric fields [Amu91, Amu94, Mor96, Bök02a, Bök03, Ols06].

Moreover, microdomain ordering is triggered by solvent fields which can be distinguished into two different methods. Thin film studies of both AB diblock and ABA triblock copolymers dealed with the effect of the solvent evaporation rate on the morphology. Vertically well-aligned cylindrical microdomains were achieved over long ranges by exploiting the consisting polymer/solvent concentration gradient with the highest solvent concentration in the film volume and the lowest at the surface, respectively. With the fast solvent evaporation, the microphase separation initially starts at the film surface determining the structure of the whole film volume [Kim98, Kim98a, Lin02, Kim04, Ho05, Par09].

The second approach, controlled solvent annealing treatment, deals with solvents as plasticizers increasing the mobility on the molecular scale. For certain time periods, block copolymer thin films are exposed to a saturated solvent vapor environment by using a

special sample treatment set-up as displayed in Figure 1.7. With calibrated multi gas flow

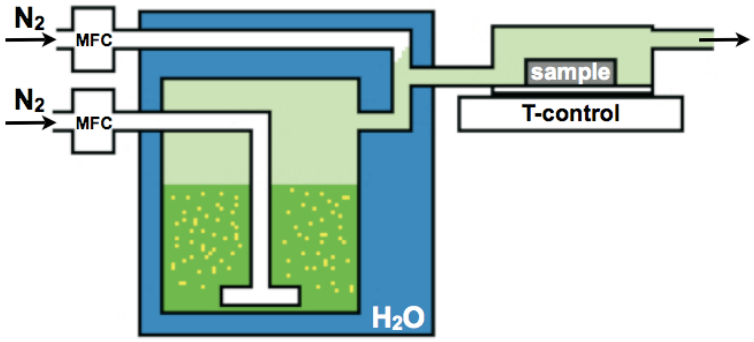

Figure 1.7: *Schematic of solvent annealing setup. Both solvent reservoir (green) and sample chamber may be temperature-controlled separately. Two N_2 flows can be adjusted by using calibrated mass flow controllers (MFC). By distinctive solvent vapor saturation of one N_2 flow, both flows mix and stream lamellar into the sample chamber. After annealing, the samples are quenched by a flow of pure dried air in order to freeze the developed morphologies. The fast quenching procedure ensures reproducibility.*

controllers, the desired vapor saturation in the sample chamber can be easily adjusted. Both solvent reservoir and sample temperature can be regulated separately. The final partial vapor pressure p_c in the sample chamber results from the temperature difference of solvent and sample and can be described by Clausius-Clapeyron

$$p_c = \frac{p}{p_{sat}} = exp\left[\frac{\Delta H_{solvent}}{R}\left(\frac{1}{T_{sample}} - \frac{1}{T_{solvent}}\right)\right] \tag{1.2}$$

p_{sat} : saturation vapor
$\Delta H_{solvent}$: evaporation enthalpy of the used solvent
R : ideal gas constant
T_{sample} : temperature of the sample
$T_{solvent}$: temperature of the solvent

Due to the solvent absorption, the film swells resulting in a highly concentrated polymer solution where long-range ordering occurs [Kra02, Kno04, Ols09]. This swelling behavior of the polymer is associated with the partial vapor pressure p_c according the Flory-Huggins theory [Flo89].

$$ln(p/p_{sat}) = \frac{\mu_v}{RT} = \frac{\mu_s}{RT} = \chi_{P,S}\ \Phi_P^2 + ln(1-\Phi_P) + (1-\frac{1}{N})\Phi_P \tag{1.3}$$

In general, the consequently induced microphase separation is accompanied by a surface roughening on the macroscale, e.g. formation of terraces and dewetting structures.

Both dynamic processes affect the thin film morphology and stability. However, block copolymers with relatively high molecular weights, such as discussed in this study, show a considerable high viscosity resulting in a retarded terrace formation [Tsa07]. Moreover, experimental investigations of these block copolymers display their comparatively stability towards dewetting [Geo03]. Krausch and coworkers demonstrated the successful long-range orientation of mesostructures [Elb99, Fuk00, Fuk02, Kno02, Lud03a, Lud05b, Ols06].

References

[Abe96] V. Abetz, R. Stadler, and L. Leibler. *Polymer Bulletin*, **37**(1), 135–142 (1996)

[Abe00] V. Abetz and T. Goldacker. *Macromolecular Rapid Communications*, **21**(1), 17–34 (2000)

[Abe05] V. Abetz and P. F. W. Simon. *Advances in Polymer Science*, **189**, 125–212 (2005)

[Als03] H. Alsyouri, G. Langheinrich, Y. S. Lin, Z. B. Ye, and S. P. Zhu. *Langmuir*, **19**(18), 7307–7314 (2003)

[Amu91] K. Amundson, E. Helfand, D. D. Davis, X. N. Quan, S. S. Patel, and S. D. Smith. *Macromolecules*, **24**(24), 6546–6548 (1991)

[Amu94] K. Amundson, E. Helfand, X. N. Quan, S. D. Hudson, and S. D. Smith. *Macromolecules*, **27**(22), 6559–6570 (1994)

[Ang04] D. E. Angelescu, J. H. Waller, D. H. Adamson, P. Deshpande, S. Y. Chou, R. A. Register, and P. M. Chaikin. *Advanced Materials*, **16**(19), 1736–1740 (2004)

[Ang05] D. E. Angelescu, J. H. Waller, R. A. Register, and P. M. Chaikin. *Advanced Materials*, **17**(15), 1878+ (2005)

[Asa02] K. Asakawa, T. Hiraoka, H. Hieda, M. Sakurai, and Y. Kamata. *Journal of Photopolymer Science and Technology*, **15**(3), 465–470 (2002)

[Bal97] P. Ball. *Made to Measure*. Princeton University Press, New York, chapter 4 edition (1997)

[Ban06] J. Bang, S. H. Kim, E. Drockenmuller, M. J. Misner, T. P. Russell, and C. J. Hawker. *Journal of American Chemical Society*, **128**(23), 7622–7629 (2006)

[Bat90] F. S. Bates and G. H. Fredrickson. *Annual Review of Physical Chemistry*, **41**, 525–557 (1990)

[Bat99] F. S. Bates and G. H. Fredrickson. *Physics Today*, **52**(2), 32–38 (1999)

[Bla07] C. T. Black, R. Ruiz, G. Breyta, J. Y. Cheng, M. E. Colburn, K. W. Guarini, H. C. Kim, and Y. Zhang. *Ibm Journal of Research and Development*, **51**(5), 605–633 (2007)

[Bod99] J. Bodycomb, Y. Funaki, K. Kimishima, and T. Hashimoto. *Macromolecules*, **32**(6), 2075–2077 (1999)

[Bök02] A. Böker. *Dissertation - Self-Assembly of Block Copolymers in External Fields*. Bayreuth (2002)

[Bök02a] A. Böker, H. Elbs, H. Hänsel, A. Knoll, S. Ludwigs, H. Zettl, V. Urban, V. Abetz, A. H. E. Müller, and G. Krausch. *Physical Review Letters*, **89**(13), 135502 (2002)

[Bök03] A. Böker, H. Elbs, H. Hänsel, A. Knoll, S. Ludwigs, H. Zettl, A. V. Zvelindovsky, G. J. A. Sevink, V. Urban, V. Abetz, A. H. E. Müller, and G. Krausch. *Macromolecules*, **36**(21), 8078–8087 (2003)

[Bra06] D. Bratton, D. Yang, J. Dai, and C. K. Ober. *Polymers for Advanced Technologies*, **17**, 94–103 (2006)

[Bre97] U. Breiner, U. Krappe, V. Abetz, and R. Stadler. *Macromolecular Chemistry and Physics*, **198**(4), 1051–1083 (1997)

[Bro79] H. C. Brown and R. A. Coleman. *Journal of Organic Chemistry*, **44**(13), 2328–2329 (1979)

[Cao04] G. Cao. *Nanostructures & Nanomaterials. Synthesis, Properties and Applications*. Imperial College Press, London, 1 edition (2004)

[Che98] Z.-R. Chen and J. A. Kornfield. *Polymer*, **39**(19), 4679–4699 (1998)

[Che02] H. Y. Chen and G. H. Fredrickson. *Journal of Chemical Physics*, **116**(3), 1137–1146 (2002)

[Cho96] S. Y. Chou, P. R. Krauss, and P. J. Renstrom. *Journal of Vacuum Science & Technology B*, **14**(6), 4129–4133 (1996)

[Cho03] Y. J. Choi, T. Moon, S. H. Yamaguchi, and S. I. Nakao. *Journal of Polymer Science Part A-Polymer Chemistry*, **41**(9), 1216–1224 (2003)

[Chu88] T. C. Chung, M. Raate, E. Berluche, and D. N. Schulz. *Macromolecules*, **21**(7), 1903–1907 (1988)

[Cie98] J. F. Ciebien, R. T. Clay, B. H. Sohn, and R. E. Cohen. *New Journal of Chemistry*, **22**(7), 685–691 (1998)

[Dao06] K. C. Daoulas, M. Muller, M. P. Stoykovich, S. M. Park, Y. J. Papakonstantopoulos, J. J. de Pablo, P. F. Nealey, and H. H. Solak. *Physical Review Letters*, **96**(3), 036104 (2006)

[Dar07] S. B. Darling. *Progress on Polymer Science*, **32**, 1152–1204 (2007)

[Elb99] H. Elbs, K. Fukunaga, R. Stadler, G. Sauer, and G. Magerle, R.and Krausch. *Macromolecules*, **32**(4), 1204–1211 (1999)

[Elb01] H. Elbs, V. Abetz, G. Hadziioannou, C. Drummer, and G. Krausch. *Macromolecules*, **34**(423), 7917–7919 (2001)

[Elb02] H. Elbs, C. Drummer, V. Abetz, and G. Krausch. *Macromolecules*, **35**(14), 5570–5577 (2002)

[Epp07] T. H. Epps, D. M. DeLongchamp, M. J. Fasolka, D. A. Fischer, and E. L. Jablonski. *Langmuir*, **23**(6), 3355–3362 (2007)

[Eru97] I. Erukhimovich, V. Abetz, and R. Stadler. *Macromolecules*, **30**(24), 7435–7443 (1997)

[Far99] M. Farhoud, J. Ferrera, A. J. Lochtefeld, T. E. Murphy, M. L. Schattenburg, J. Carter, C. A. Ross, and H. I. Smith. *Journal of Vacuum Science & Technology B*, **17**(6), 3182–3185 (1999)

[Fas01] M. J. Fasolka and A. M. Mayes. *Annual Review of Materials Research*, **31**, 323–355 (2001)

[Flo89] P. J. Flory. *Principles of Polymer Chemistry*. Cornell University Press, Ithaca, 3rd edition (1989)

[Fog97] D. E. Fogg, L. H. Radzilowski, R. Blanski, R. R. Schrock, and E. L. Thomas. *Macromolecules*, **30**(3), 417–427 (1997)

[Fog97a] D. E. Fogg, L. H. Radzilowski, B. O. Dabbousi, R. R. Schrock, E. L. Thomas, and M. G. Bawendi. *Macromolecules*, **30**(26), 8433–8439 (1997)

[Fre96] G. H. Fredrickson and F. S. Bates. *Annual Reviews*, **26**, 501–550 (1996)

[Fuk00] K. Fukunaga, H. Elbs, R. Magerle, and G. Krausch. *Macromolecules*, **33**(2), 947–953 (2000)

[Fuk02] K. Fukunaga, T. Hasimoto, H. Elbs, and G. Krausch. *Macromolecules*, **35**(11), 4406–4413 (2002)

[Fuk03] K. Fukunaga, T. Hashimoto, H. Elbs, and G. Krausch. *Macromolecules*, **36**(8), 2852–2861 (2003)

[Gei99] T. Geisinger, M. Muller, and K. Binder. *Journal of Chemical Physics*, **111**(11), 5241–5250 (1999)

[Gei99a] T. Geisinger, M. Muller, and K. Binder. *Journal of Chemical Physics*, **111**(11), 5251–5258 (1999)

[Geo03] M. Geoghegan and G. Krausch. *Progress in Polymer Science*, **28**(2), 261–302 (2003)

[Gre93] N. C. Greenham, S. C. Moratti, D. C. C. Bradley, R. H. Friend, and A. B. Holmes. *Nature*, **365**(6447), 628–630 (1993)

[Guo06] S. W. Guo, J. Rzayev, T. S. Bailey, A. S. Zalusky, R. Olayo-Valles, and M. A. Hillmyer. *Chemistry of Materials*, **18**(7), 1719–1721 (2006)

[Had02] N. Hadjichristidis, S. Pispas, and G. Fluodas. *Block Copolymers. Synthetic Strategies, Physical Properties, and Applications.* Wiley–VCH, New York, 1 edition (2002)

[Had05] N. Hadjichristidis, M. Pitsikalis, and H. Iatrou. *Advances in Polymer Science*, **189**, 1–124 (2005)

[Haj94] D. A. Hajduk, P. E. Harper, S. M. Gruner, C. C. Honeker, G. Kim, E. L. Thomas, and L. J. Fetters. *Macromolecules*, **27**(15), 4063–4075 (1994)

[Ham98] I. W. Hamley. *The Physics of Block Copolymers.* Oxford University Press, Oxford (1998)

[Haw97] C. J. Hawker. *Accounts of Chemical Research*, **30**(9), 373–382 (1997)

[Hel78] E. Helfand and Z. R. Wassermann. *Macromolecules*, **11**(5), 960–966 (1978)

[Hel82] E. Helfand and Z. R. Wassermann. *Developments in Block Copolymers.* Elsevier Science, New York (1982)

[Hic06] H. G. Hicke, M. Becker, B. R. Paulke, and M. Ulbricht. *Journal of Membrane Science*, **282**(1-2), 413–422 (2006)

[Ho05] R.-M. Ho, W.-H. Tseng, H.-W. Fan, Y.-W. Chiang, C.-C. Lin, B.-T. Ko, and B.-H. Huang. *Polymer*, **46**(22), 9362–9377 (2005)

[Hor04] A. Horvat, K. S. Lyakhova, G. J. A. Sevink, A. V. Zvelindovsky, and R. Magerle. *Journal of Chemical Physics*, **120**(2), 1117–1126 (2004)

[Hor07] A. Horvat, A. Knoll, G. Krausch, L. Tsarkova, K. S. Lyakhova, G. J. A. Sevink, A. V. Zvelindovsky, and R. Magerle. *Macromolecules*, **40**(19), 6930–6939 (2007)

[Ish03] K. Ishizu, K. Tsubaki, A. Mori, and S. Uchida. *Progress in Polymer Science*, **28**(1), 27–54 (2003)

[Ito97] Y. Ito, Y. Park, and Y. Imanishi. *Journal of the American Chemical Society*, **119**(11), 2739–2740 (1997)

[Jac95] R. J. Jackman, J. L. Wilbur, and G. M. Whitesides. *Science*, **269**(5224), 664–666 (1995)

[Joo06] W. Joo, M. S. Park, and J. K. Kim. *Langmuir*, **22**(19), 7960–7963 (2006)

[Kai05] T. Kai, H. Goto, Y. Shimizu, T. Yamaguchi, S. I. Nakao, and S. Kimura. *Journal of Membrane Science*, **265**(1-2), 101–107 (2005)

[Kim98] G. Kim and M. Libera. *Macromolecules*, **31**(8), 2670–2672 (1998)

[Kim98a] G. Kim and M. Libera. *Macromolecules*, **31**(8), 2569–2577 (1998)

[Kim04] S. H. Kim, M. J. Misner, T. Xu, M. Kimura, and T. P. Russell. *Advanced Materials*, **16**(3), 226–231 (2004)

[Kim08] J. K. Kim, J. I. Lee, and D. H. Lee. *Macromolecular Research*, **16**(4), 267–292 (2008)

[Kno01] A. Knoll, R. Magerle, and G. Krausch. *Macromolecules*, **34**(12), 4159–4165 (2001)

[Kno02] A. Knoll, A. Horvat, K. S. Lyakhova, G. Krausch, G. J. A. Sevink, A. V. Zvelindovsky, and R. Magerle. *Physical Review Letters*, **89**(3), 035501 (2002)

[Kno04] A. Knoll, R. Magerle, and G. Krausch. *Journal of Chemical Physics*, **120**(2), 1105–1116 (2004)

[Kon95] N. Koneripalli, N. Singh, R. Levicky, F. S. Bates, P. D. Gallagher, and S. K. Satija. *Macromolecules*, **28**(8), 2897–2904 (1995)

[Kop02] J. Kopecek. *Nature*, **417**(6887), 388–390 (2002)

[Kra95] G. Krausch. *Materials Science & Engineering R-Reports*, **14**(1–2), 1–94 (1995)

[Kra02] G. Krausch and R. Magerle. *Advanced Materials*, **14**(21), 1579–1583 (2002)

[Lam94] P. Lambooy, T. P. Russell, G. J. Kellogg, A. M. Mayes, P. D. Gallagher, and S. K. Satija. *Physical Review Letters*, **72**(18), 2899–2902 (1994)

[Laz03] M. Lazzari and M. A. Lopez-Quintela. *Advanced Materials*, **15**(19), 1583–1593 (2003)

[Lee88] J.-S. Lee, A. Hirao, and S. Nakahama. *Macromolecules*, **21**(1), 274–276 (1988)

[Lee99] W. Lee, S. Furusaki, J. Kanno, K. Saito, and T. Sugo. *Chemistry of Materials*, **11**(11), 3091–3095 (1999)

[Lei80] L. Leibler. *Macromolecules*, **13**(6), 1602–1617 (1980)

[Li02] H. Li and W. T. S. Huck. *Current Opinion in Solid State and Materials Science*, **6**(1), 3–8 (2002)

[Lin02] Z. Q. Lin, D. H. Kim, X. D. Wu, L. Boosahda, D. Stone, L. LaRose, and T. P. Russell. *Advanced Materials*, **14**(19), 1373–1376 (2002)

[Lud03] S. Ludwigs, A. Böker, V. Abetz, A. H. E. Müller, and G. Krausch. *Polymer*, **44**(22), 6815–6823 (2003)

[Lud03a] S. Ludwigs, A. Böker, A. Voronov, N. Rehse, R. Magerle, and G. Krausch. *Nature Materials*, **2**, 744 (2003)

[Lud05] S. Ludwigs, K. G., R. Magerle, A. V. Zvelindovsky, and G. J. A. Sevink. *Macromolecues*, **38**(5), 1859–1867 (2005)

[Lud05a] S. Ludwigs, K. Schmidt, and G. Krausch. *Macromolecules*, **38**(6), 2376–2382 (2005)

[Lud05b] S. Ludwigs, K. Schmidt, C. M. Stafford, E. J. Amis, M. J. Fasolka, A. Karim, R. Magerle, and G. Krausch. *Macromolecules*, **38**(5), 1850–1858 (2005)

[Man91] P. Mansky, P. M. Chaikin, M. Shayegan, and L. J. Fetters. *Bulletin of the American Physical Society*, **36**, 1051 (1991)

[Man96] P. Mansky, C. K. Harrison, P. M. Chaikin, R. A. Register, and N. Yao. *Applied Physical Letters*, **68**(16), 2586–2588 (1996)

[Man97] P. Mansky, Y. Liu, E. Huang, T. P. Russell, and C. J. Hawker. *Science*, **275**(5305), 1458–1460 (1997)

[Mat96] M. W. Matsen and F. S. Bates. *Macromolecules*, **29**(4), 1091–1098 (1996)

[Mei69] D. J. Meier. *Journal of Polymer Science Part C-Polymer Symposium*, **26PC**, 81–+ (1969)

[Men04] R. Menon, A. Patel, E. E. Moon, and H. I. Smith. *Journal of Vacuum Science & Technology B*, **22**(6), 3032–3037 (2004)

[Mog92] Y. Mogi, H. Kotsuji, Y. Kaneko, K. Mori, Y. Matsushita, and I. Noda. *Macromolecules*, **25**(20), 5408–5411 (1992)

[Mog92a] Y. Mogi, K. Mori, Y. Matsushita, and I. Noda. *Macromolecules*, **25**(20), 5412–5415 (1992)

[Mog93] Y. Mogi, K. Mori, H. Kotsuji, Y. Matsushita, I. Noda, and C. C. Han. *Macromolecules*, **26**(19), 5169–5173 (1993)

[Mog94] Y. Mogi, M. Nomura, H. Kotsuji, K. Ohnishi, Y. Matsushita, and I. Noda. *Macromolecules*, **27**(23), 6755–6760 (1994)

[Mol71] G. E. Molau. *Colloidal and Morphological Behaviour of Block and Grafted Copolymers*. Plenum Press, New York (1971)

[Mor96] T. L. Morkved, M. Lu, A. M. Urbas, E. E. Ehrichs, H. M. Jaeger, P. Mansky, and T. P. Russell. *Science*, **273**(5277), 931–933 (1996)

[Mor06] Y. Morikawa, S. Nagano, K. Watanabe, K. Kamata, T. Iyoda, and T. Seki. *Advanced Materials*, **18**(7), 883–886 (2006)

[Nie08] Z. Nie and E. Kumacheva. *Nature Materials*, **7**, 277–290 (2008)

[Nun01] S. Nunes, K. V. Peinemann, and editors. *Membrane technology in the chemical industry*. Wiley-VCH, Weinheim (2001)

[Oht86] T. Ohta and K. Kawasaki. *Macromolecules*, **19**(10), 2621–2632 (1986)

[Oku06] A. Okumura, Y. Nishikawa, and T. Hashimoto. *Polymer*, **47**(22), 7805–7812 (2006)

[Ols06] V. Olszowka, M. Hund, V. Kuntermann, S. Scherdel, L. Tsarkova, A. Böker, and G. Krausch. *Soft Matter*, **2**(12), 1089–1094 (2006)

[Ols08] D. A. Olson, L. Chen, and M. A. Hillmyer. *Chemistry of Materials*, **20**, 869–890 (2008)

[Ols09] V. Olszowka, T. L., and A. Böker. *Soft Matter*, **5**(4), 812–819 (2009)

[Par97] M. Park, C. Harrison, P. M. Chaikin, R. A. Register, and D. H. Adamson. *Science*, **276**(5317), 1401–1404 (1997)

[Par01] C. Park, J. Y. Cheng, M. J. Fasolka, A. M. Mayes, C. A. Ross, E. L. Thomas, and C. DeRosa. *Applied Physics Letters*, **79**(6), 848–850 (2001)

[Par03] C. Park, J. Yoon, and E. L. Thomas. *Polymer*, **44**, 6725–6760 (2003)

[Par09] S. Park, B. Kim, J. Xu, T. Hofmann, B. M. Ocko, and T. P. Russell. *Macromolecules*, **42**(4), 1278–1284 (2009)

[Pei95] Q. B. Pei, G. Yu, C. Zhang, Y. Yang, and A. J. Heeger. *Science*, **269**(5227), 1086–1088 (1995)

[Pen06] F. Penacorada, A. Angelova, H. Kamusewitz, J. Reiche, and L. Brehmer. *Langmuir*, **11**(2), 612–617 (2006)

[Pic97] G. T. Pickett and A. C. Balazs. *Macromolecules*, **30**(10), 3097–3103 (1997)

[Reb98] N. Reber, R. Spohr, A. Wolf, H. Omchi, M. Tamada, and M. Yoshida. *Journal of Membrane Science*, **140**(2), 275–281 (1998)

[Reh08] S. Rehse, K. Mecke, and R. Magerle. *Physical Review E*, **77**(5), 051805 (2008)

[Roc99] L. Rockford, Y. Liu, P. Mansky, T. P. Russell, M. Yoon, and S. G. L. Mochrie. *Physical Review Letters*, **82**(2), 2602–2605 (1999)

[Rus91] T. P. Russell, A. Menelle, S. H. Anastasiadis, S. K. Satija, and C. F. Majkrzak. *Macromolecules*, **24**(23), 6263–6269 (1991)

[Sch94] M. F. Schulz, F. S. Bates, K. Almdal, and K. Mortensen. *Physical Review Letters*, **73**(1), 86–89 (1994)

[Seg01] R. A. Segalman, H. Yokohama, and E. J. Kramer. *Advanced Materials*, **13**(15), 1152+ (2001)

[Seg05] R. A. Segalman. *Materials Science and Engineering R-Reports*, **48**(6), 191–226 (2005)

[Shi93] M. Shibayama and T. Tanaka. *Advances in Polymer Science*, **109**, 1–62 (1993)

[Smi92] D. R. Smith and D. J. Meier. *Polymer*, **33**(18), 3777–3782 (1992)

[Smi01] A. P. Smith, J. F. Douglas, J. C. Meredith, E. J. Amis, and A. Karim. *Physical Review Letters*, **8701**(1), 015503 (2001)

[Sol08] C. L. Soles and Y. F. Ding. *Science*, **322**(5902), 689–690 (2008)

[Sto96] W. Stocker, J. Beckmann, R. Stadler, and J. P. Rabe. *Macromolecues*, **29**(23), 7502–7507 (1996)

[Sto05] M. P. Stoykovich, M. Müller, S. O. Kim, H. H. Solak, E. W. Edwards, J. J. de Pablo, and P. F. Nealey. *Science*, **308**(5727), 1442–1446 (2005)

[Sza03] G. Szamel and M. Muller. *Journal of Chemical Physics*, **118**(2), 905–913 (2003)

[Tie03] B. Tieke, M. Pyrasch, and A. Toutianoush. *Functional layer-by-layer assemblies with photo- and electrochemical response and selective transport of small molecules and ions. In: Decher, G., Schlenoff, J.B., editors. Multilayer thin films.* Wiley-VCH, Weinheim (2003)

[Tsa07] L. Tsarkova. *Nanostructured Soft Matter: Experiment, Theory, Simulation and Perspectives.* Springer Verlag, Heidelberg, ed. a.v. zvelindovsky edition (2007)

[Ulb06] M. Ulbricht. *Polymer*, **47**, 2217–2262 (2006)

[WM99] K. Wadu-Mesthrige, S. Xu, A. N. A., and G. Liu. *Langmuir*, **15**(25), 8580–8583– (1999)

[Yam91] T. Yamaguchi, S. I. Nakao, and S. Kimura. *Macromolecules*, **24**(20), 5522–5527 (1991)

[Yam93] T. Yamaguchi, S. I. Nakao, and S. Kimura. *Industrial & Engineering Chemistry Research*, **32**(5), 848–853 (1993)

[Yam96] T. Yamaguchi, S. I. Nakao, and S. Kimura. *Journal of Polymer Science Part A-Polymer Chemistry*, **34**(7), 1203–1208 (1996)

[Yam97] T. Yamaguchi, S. I. Nakao, and S. Kimura. *Journal of Polymer Science Part B-Polymer Physics*, **35**(3), 469–477 (1997)

[Zhe95] W. Zheng and Z. G. Wang. *Macromolecules*, **28**(21), 7215–7223 (1995)

Chapter 2

Overview of the Thesis

This thesis contains six chapters including four publications which are presented in Chapters 3 to 6.

With the focus on innovative synthetic composite membranes with tailored properties, this study investigated novel membrane precursors derived from poly<u>b</u>utadiene-*block*-poly(2-<u>v</u>inylpyridine)-*block*-poly(<u>*t*</u>*ert*-butyl methacrylate) (BVT) triblock terpolymer thin films. With respect to their future application as 'skin' top layers of smart composite membranes, the thin films were supposed to fulfill special conditions, e.g. homogenous film thickness, monodisperse porosity and controllable permeability by external stimuli (pH, light, temperature). Here, both poly(2-vinylpyridine) (P2VP) and poly(*tert*-butyl methacrylate) (P*t*BMA) (saponification possible) were incorporated being responsive elements to external pH changes providing auspicious potential for switchable membranes.

Based on the insight of the well-investigated polystyrene-*block*-poly(2-vinylpyridine)-*block*-poly(*tert*-butyl methacrylate) SVT triblock terpolymer microphase sepration behavior, a novel triblock terpolymer composition was successfully developed by replacing the brittle polystyrene (PS) compartment with a soft and flexible polybutadiene (PB) block. Both elasticity and mechanical stability of the investigated $B_xV_yT_z{}^{M_w}$ triblock terpolymer thin films with different volume fractions (x, y, z) and total weight-average molecular weights (M_w in kg / mol) were significantly improved. Subsequently, the film transfer of large areas onto support materials, for example track-etched poly(ethylene terephthalate) macroporous filters, was facilitated.

To obtain a reliable overview of the microphase separation behavior and self-assembling properties of $B_xV_yT_z{}^{M_w}$ triblock terpolymer thin films, the investigated samples were initially spin-cast and gradient-cast, respectively. Subsequently, the thin films were thermodynamically equilibrated by a controlled solvent annealing process facilitating the mi-

crophase separation within the thin film volumes. The established morphologies were characterised by scanning force microscopy (SFM), scanning electron microscopy (SEM), grazing-incidence small-angle X-ray scattering technique (GISAXS), transmission electron microscopy (TEM) and quasi *in-situ* SFM (QIS-SFM) nanotomography.

The following chapters are categorized in three evolution steps for developing porous self-assembled monolayers based on polybutadiene-*block*-poly(2-vinylpyridine)-*block*-poly (*tert*-butyl methacrylate). In Chapter 3, the systematic investigations about the influence of block ratio and molecular weight on the microphase separation behaviour in BVT thin films is presented. The results provided an initial basis for a directed selection of the most promising BVT ternary systems applied as smart membrane precursors. In Chapter 4, BVT triblock terpolymer thin films of two different compositions are investigated. Moreover, the influence of the incorporated polybutadiene block on surface structure and domain spacing with regard to molecular weight and composition is discussed and compared to SVT. Subsequently, Chapter 5 focuses on distinctive tuning of the self-assembling properties of BVT triblock terpolymers in thin films by hydroxylation of the polybutadiene compartment. Both resulting hybrid and sponge-like morphologies are supposed to provide great potential as nanoporous membranes. Chapter 6 deals with a profound structure analysis investigating the influence of the chemical modification, presented in Chapter 5, by applying quasi *in-situ* (QIS) SFM nanotomography.

2.1 Study of ABC Triblock Terpolymer Thin Film Morphologies with regard to Membrane Properties

As an intitial step in the development of functional membrane precursors, methodical investigations concerning the effects of different volume ratios and molecular weights on the microphase separation behavior of BVT in thin films were performed. Table 3.1 summarizes

Table 2.1: *Molecular Characteristics of BVT Triblock Terpolymers*

Polymer [a]	M_w / M_n [b]	$\varphi_B : \varphi_V : \varphi_T$ [c]	Thin Film Morphology [d]
$\mathbf{B}_{30}\mathbf{V}_{14}\mathbf{T}_{56}{}^{141}$	1.02	1 : 0.4 : 1.8	L
$\mathbf{B}_{18}\mathbf{V}_{8}\mathbf{T}_{74}{}^{133}$	1.02	1 : 0.4 : 4.0	C [e]
$\mathbf{B}_{16}\mathbf{V}_{21}\mathbf{T}_{63}{}^{145}$	1.02	1 : 1.2 : 3.7	CSC
$\mathbf{B}_{58}\mathbf{V}_{27}\mathbf{T}_{15}{}^{78}$	1.03	1 : 0.4 : 0.2	L / C

[a] Subscripts represent weight fractions of the respective block (in weight %); the superscript denotes the total weight-average molecular weight M_w in kg/mol as determined by SEC in combination with ^{1}H-NMR; [b] Polydispersity determined via SEC. M_w=weight-average molecular weight; M_n=number-average molecular weight; [c] Relative volume fractions of blocks calculated with respect to polymer densities; [d] determined by SFM, SEM, GISAXS - L: lamellar morphology, C [e]: core-shell cylinders with a discontinuous shell, CSC: hexagonally packed core-shell cylinders

the molecular characteristics of the investigated BVT triblock terpolymers and their corresponding thin film morphologies by using scanning force microscopy (SFM), scanning electron microscopy (SEM) and grazing-incidence small-angle X-ray scattering (GISAXS).

Beside typical lamellar thin film structures, also an interesting non-regular thin film microphase separation was observed. PB cylinders oriented both normal and parallel to the substrate, were decorated with a non-continuous P2VP shell as shown in Figure 2.1 A. Concerning the interaction parameters, χ, of the single compartments, PB and P2VP show the largest incompatibility ($\chi_{PS,P2VP} = 0.325$). Thus, the decrease in the interfacial tension between these two blocks is energetically favored by minimising the contact areas resulting in a non-continuous spherical shell of P2VP.

Moreover, the most promising morphology for smart membrane precursors was a hexagonally ordered core-shell structure consisting of a soft PB core which is completely surrounded by the pH responsive P2VP as shown in Figure 2.1 B.

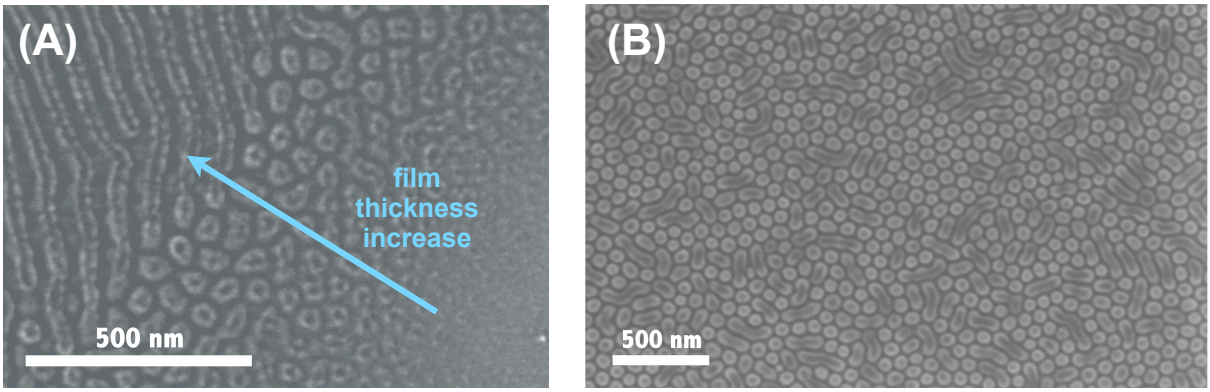

Figure 2.1: ***(A)*** *SEM image of a* $B_{18}V_8T_{74}{}^{133}$ *thin film morphology. The dark, electron poor PB core is non-regularly surrounded by the bright, electron rich P2VP. The direction of the arrow indicates a film thickness gradient.* ***(B)*** *SEM image of a* $B_{16}V_{21}T_{63}{}^{145}$ *thin film core-shell morphology.*

2.2 Towards Nanoporous Membranes based on ABC Triblock Terpolymers

As a second step, based on the investigations of the influence of volume ratio and molecular weight on BVT thin film morphologies, we focused here on two promising polymer compositions which self-assemble as core-shell cylinders and compared the investigated microphase separation behavior with the previous characterised SVT thin films.

All three triblock terpolymers show great potential for porous membranes due to the poly(*tert*-butyl methacrylate (P*t*BMA) what can be easily depolymerised by UV-light or electron beam exposure. Although, SVT and BVT triblock terpolymers show a comparable composition, it turned out that the microphase separation behavior in BVT thin films was significantly dominated by the PB block due to its low surface tension. Moreover, the BVT thin film long-range order was improved by increasing the solvent annealing times in chloroform vapor. Furthermore, the mechanical stability of the films was enhanced by crosslinking of the PB compartment not influencing the microphase separation.

In Figure 2.2, SVT and BVT thin films are exemplarily shown. Due to the depolymerisation of the P*t*BMA compartment, SVT thin films revealed a hexagonally ordered porous morphology whereas BVT thin films required further processing steps, for example ozonolysis, to destroy the PB core.

However, for the novel BVT terpolymers, several very useful features with respect to the membrane technology have been identified, namely a similar equilibrium morphology on substrates with different wettability, the feasibility of film transfer to another (porous)

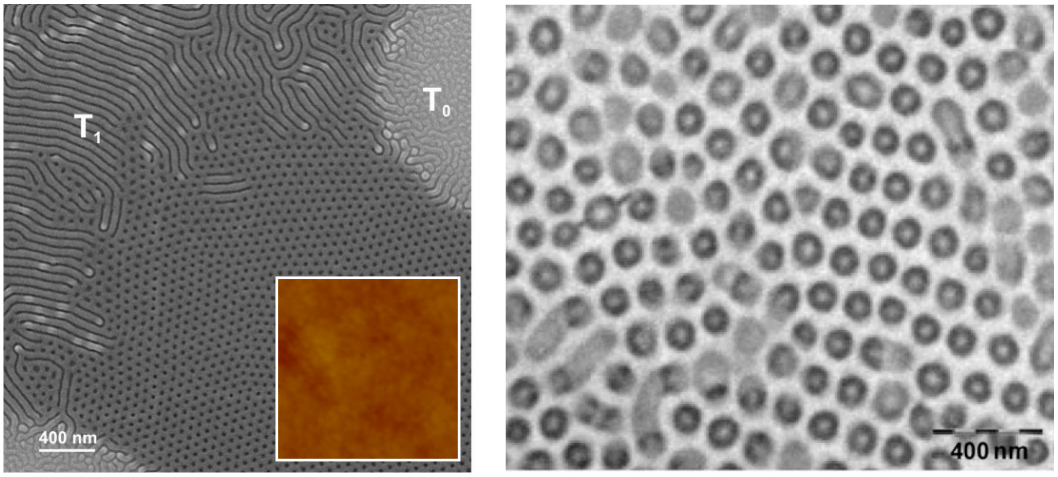

Figure 2.2: *SEM image of a $S_{16}V_{21}T_{63}{}^{140}$ thin film after annealing in chloroform vapor showing different morphologies in dependence of terrace height. Inset: SFM height image (size 1 x 1 μm^2; height scale Δz = 0-20 nm). The sample surface is covered with a smooth rigid layer of PtBMA (left image). Typical TEM image of a thin film of $B_{14}V_{18}T_{68}{}^{165}$ triblock terpolymer spin-cast onto a NaCl wafer and transferred onto a TEM grid, revealing hexagonally packed core-shell cylinders (right image).*

substrate and the stabilization of the films by internal UV crosslinking. Thin SVT films demonstrated membrane-suitable morphology and feasibility of their transfer to support membranes.

2.3 Chemical Modification for the Selective Control of Microphase Separation in ABC Triblock Terpolymer Thin Films

By recognising the strong effect of the PB surface tension on thin film morphologies, the next process step for generating functional membrane precursors focused on the directed chemical modification of the PB compartment to tune the microphase separation behavior in BVT thin films.

The selective, oxidative hydroboration (reaction scheme displayed in Figure 2.3) hydrophilised the polybutadiene block and increased its surface tension reducing the segregation to the free surface. Due to the high molecular weights, all investigated BVT triblock terpolymers proved to be stable towards dewetting during the solvent annealing procedure in chloroform vapor. By studying two non-modified BVT triblock terpolymers with inverse volume ratios and the corresponding hydroxylated ones, we observed structural changes

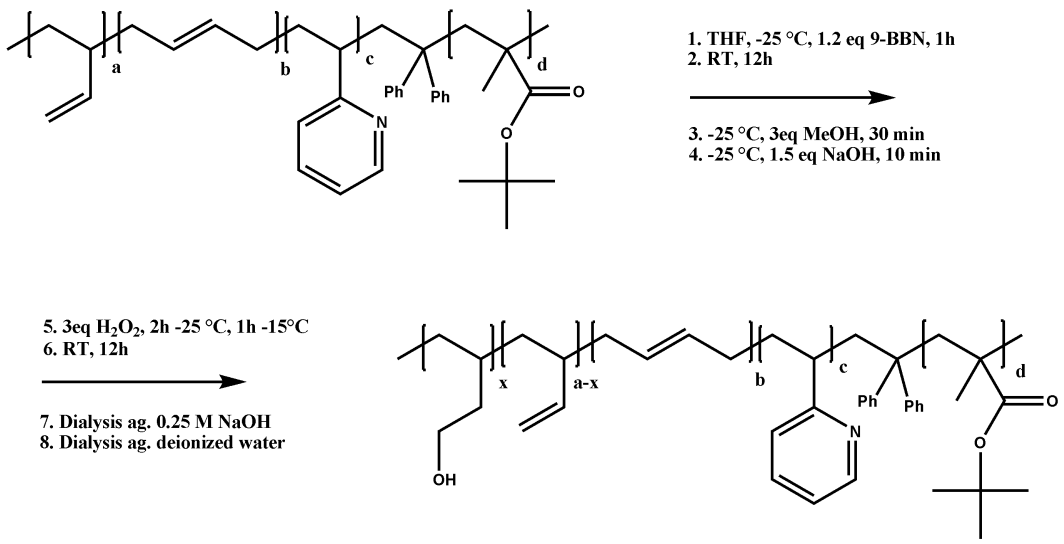

Figure 2.3: *Reaction scheme of the selective, oxidative hydroboration by use of 9-BBN.*

from previous core-shell cylinders into porous, hybrid morphologies and from former lamellae into a dense, sponge-like formation. These significant changes in the microphase separation behavior indicated the successful hydroxylation and, subsequently, highly promising, directed tuning options of BVT thin films for developing smart membrane precursors.

2.4 Going beyond the Surface: Revealing Complex Block Copolymer Morphologies with 3D SFM

After generating successfully two promising candidates for porous membrane precursors, we applied quasi *in situ* (QIS) SFM nanotomography for revealing the actual morphologies within the thin film volumes.

By using low-pressure plasma etching inside the SFM, the material was eroded in a controlled way without transferring the samples to a separate plasma source. The whole process ensured a constant high depth resolution down to 1.0 nm.

We analysed the microphase separation of a non-modifed $B_{14}V_{18}T_{68}$[165] triblock terpolymer and a hydroxylated one. For $B_{14}V_{18}T_{68}$[165], we enhanced our knowledge and enlarged former assumptions towards the fact that this triblock terpolymer self-assembles not in continuous core-shell cylinders but in a distorted perforated lamella (DPL) consisting of round-shaped objects with a soft intendation (PB) embedded in a glassy matrix (P2VP, P*t*BMA). With the hydroxylation, we introduced additional polarity via supplementary hydroxyl groups forming presumably intra- and intermolecular hydrogen bonds leading to

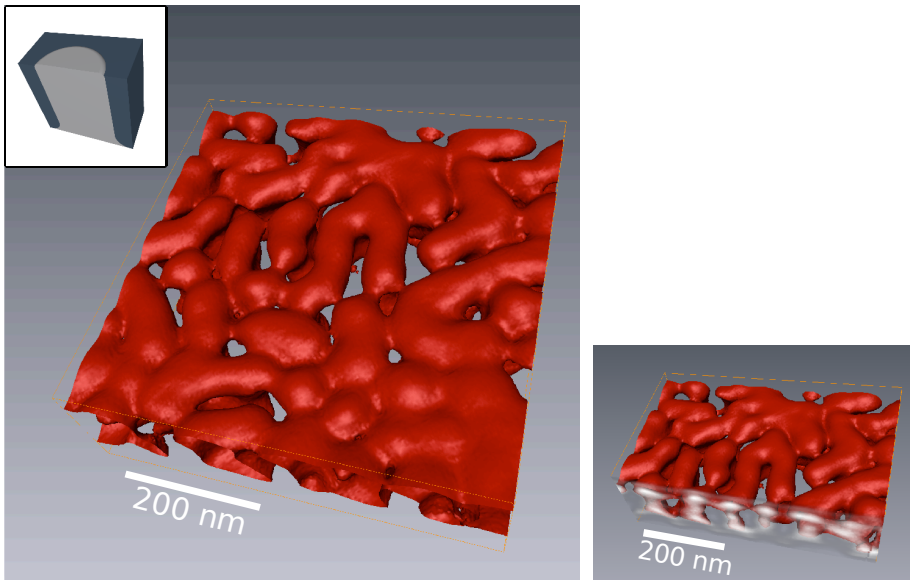

Figure 2.4: *3D reconstructions of a HO-$B_{14}V_{18}T_{68}$[165] thin film (200 × 200 × 36 voxels). The microphase coloured in red is composed of HO-PB and P2VP. Here, the matrix material PtBMA is transparent. Cross-section: clarifies the microphase separation and wetting behavior onto silicon substrate (right image). Inset: schematic drawing representing the microphase separated structure of a single round-shaped object embedded in a matrix.*

a reduced microphase separation. Furthermore, with a decrease of the C=C double bonds in the PB block, the glass transition temperature is expected to be shifted to higher values resulting in a glassy state at room temperature. Both effects cause a structural change that could be successfully demonstrated via 3D reconstruction of a HO-$B_{14}V_{18}T_{68}$[165] thin film as exemplarily shown in Figure 2.4. After the P*t*BMA degradation, the hydroxylated triblock terpolymer seemed just to wet partially the substrate resulting in a hybrid morphology with continuous pores.

2.5 Individual Contributions to joint Publications

The results presented in this thesis were obtained in collaboration with others, and published or submitted as indicated below. In the following, the contributions of all involved coauthors to the different publications are specified. The asterisk denotes the corresponding author(s).

Chapter 3

This work has been submitted to *Macromolecules* under the title '**Study of ABC Triblock Terpolymer Thin Film Morphologies with regard to Membrane Properties**' by A. Sperschneider, F. Schacher and A. H. E. Müller*.
I performed wrote the publication and performed most of the experiments.
F. Schacher synthesised most of the polymers .
Dr. K. Schmidt performed most of the GISAXS and SAXS mesurements.
F. Schacher and A. Müller were involved in the discussion whereas A. Müller corrected the manuscript.

Chapter 4

This work is published in *Small* **2007**, 3, No. 6, p. 1056–1063 under the title '**Towards Nanoporous Membranes based on ABC Triblock Terpolymers** ' by A. Sperschneider, F. Schacher, M. Gawenda, L. Tsarkova, M. Ulbricht, G. Krausch, J. Köhler, and A. H. E. Müller*.
F. Schacher and me wrote the publication.
F. Schacher synthesised most of the polymers and performed the TEM experiments.
I performed all SFM and SEM measurements as well as the optimization of the thin film transfer process and I was involved in all discussions.
M. Gawenda, L. Tsarkova, M. Ulbricht, G. Krausch, J. Köhler and A. Müller were involved in the discussions and corrected the manuscript.

Chapter 5

This work has been submitted to *Soft Matter* under the title '**Chemical Modification for the Selective Control of Microphase Separation in ABC Triblock Terpolymer Thin Films** ' by A. Sperschneider, F. Schacher, L. Tsarkova and A. H. E. Müller*.
I wrote the publication and performed most of the experiments and evaluated all data.
F. Schacher synthesised all polymers and was involved in discussions.
L. Tsarkova and A. Müller were involved in the discussions and corrected the manuscript.

Chapter 6

This work has been submitted to *Nano Letters* under the title '**Going beyond the Surface: Revealing Complex Block Copolymer Morphologies with 3D SFM**' by A. Sperschneider, M. Hund*, A. H. E. Müller and A. Böker*.
I wrote the publication, performed most of the experiments and evaluated most of the data.
M. Hund contributed to the quasi *in–situ* SFM nanotomography experiments and was involved in the discussions.
A. Böker was involved in the discussions and corrected the manuscript.

Chapter 3

Study of ABC Triblock Terpolymer Thin Film Morphologies with regard to Membrane Properties

ABSTRACT

We report on the microphase separation behavior and self-assembling properties in thin films of four poly<u>b</u>utadiene-block-*poly(2-<u>v</u>inylpyridine)*-block-*poly(<u>t</u>ert-butyl methacrylate) (BVT) triblock terpolymer compositions. With respect to their future application as smart membranes, the thin films were supposed to fulfull special conditions, e.g. homogenous film thickness, monodisperse porosity and controllable permeability by external stimuli (pH, light, temperature). By variation of the volume fractions,* $B_{30}V_{14}T_{56}{}^{141}$ *displayed a lamellar thin film morphology whereas* $B_{18}V_{8}T_{74}{}^{133}$ *thin films consisted of objects with a non-continuous P2VP shell. With further optimization of the block ratio,* $B_{16}V_{21}T_{63}{}^{145}$ *thin films revealed a highly promising core-shell cylindrical structure whereas* $B_{48}V_{27}T_{15}{}^{78}$ *thin films were covered with a continuous top layer.*

3.1 Introduction

The technological demand for miniaturization has increased significantly. A peculiar focus is placed on nanostructures based on block copolymers (BC) with respect to their large variety of chemical and physical properties [Li02, Ish03, Ols08]. BCs can be nowadays precisely tuned due to the permanent progress in polymer synthesis [Haw97, Had05]. A special field of interest represent ABC triblock terpolymers as basis for novel functional synthetic membranes with tailored properties. In contrast to simple AB diblock copolymers, ternary systems may provide sufficient mechanical stability in combination with an appropriate microstructure, for example with removable compartments. The selectivity of state-of-the-art membranes is often still limited due to their random pore size distribution. One quite frequently discussed application of such systems is the use as porous barriers for thin film composite membranes [Ulb06].

A commonly used technique for characterization of nanostructured thin films is scanning force microscopy (SFM), revealing both real-space topography informations and material properties of the surface. Moreover, scanning electron microscopy (SEM) images the top surface of the thin film in dependence of the electron contrast which is characteristic for each polymer compartment. However, with respect to the subsequent application as responsive membranes, it is indispensable to gain additionally structural information about the internal thin film morphologies.

To overcome limitations of the standard scattering techniques because of their transmission geometry, grazing-incident small-angle X-ray scattering (GISAXS) has been recognized as a powerful tool combining small-angle X-ray scattering (SAXS) revealing lateral structures with grazing incidence diffraction (GID) using reflection geometry [Lev89]. As a nondestructive method, GISAXS has been applied in particular for characterization of BC thin films to gain detailed understanding of lateral structure formation and internal ordering [MB03, Bus07, Smi02, Pap04, Li04, Par05, Xu04, Kim04]. The resulting data can be described theoretically by the model of the Distorted Wave Born Approximation (DWBA) [Sin88, Rau95, Bus06, Laz02, Lee05].

Previous thin film studies of Ludwigs et *al.* dealing with a triblock terpolymer system consisting of poly<u>s</u>tyrene-*block*-poly(2-<u>v</u>inylpyridine)-*block*-poly(<u>*t*</u>*ert*-butyl methacrylate) (SVT), revealed a promising perforated lamella (PL) morphology which could be stimulated by changing the pH [Lud05a, Lud05b, Lud03a]. However, with respect to the glass transition temperatures of the three compartments, the resulting thin films were brittle and the transfer to other substrates was complicated. Thus, this study focuses on the intital steps for creating smart synthetic membranes by using a novel triblock terpoly-

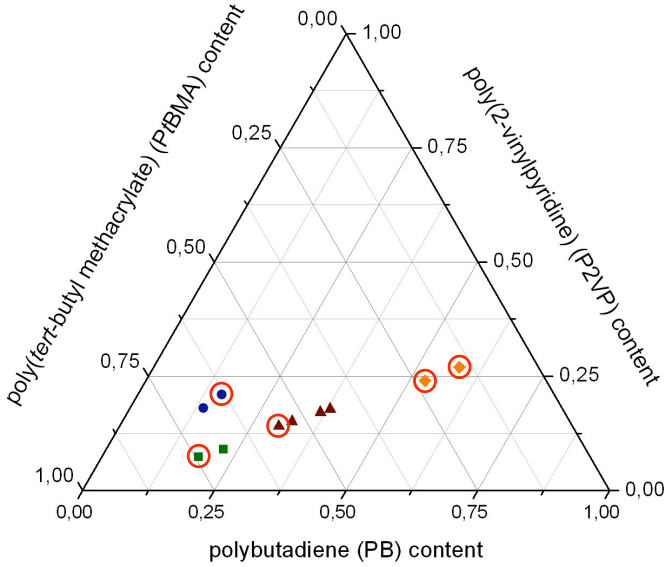

Figure 3.1: *Ternary compositional diagram of all synthesised BVT triblock terpolymers with respect to different block ratios and molecular weights. The different symbols represent the four synthesis series (▲ series 1; ■ series 2; ● series 3; ♦ series 4). The ○-markers indicate the investigated polymer compostions.*

mer system consisting of polybutadiene-*block*-poly(2-vinylpyridine)-*block*-poly(*tert*-butyl methacrylate) (BVT). The former rigid polystyrene block was replaced by the soft, rubber-like polybutadiene providing an increase in the flexibility of the material.

As a preliminary step, BVT triblock terpolymers with various block ratios (Table 3.1) and narrow molecular weight distributions (1.02 - 1.03) were synthesised via sequential living anionic polymerization (see also Figure 3.1).

To gain an overview about microphase separation and self-assembling properties of these BVT triblock terpolymers in thin films, four distinct polymer compositions were investigated in various film thicknesses. After a controlled solvent annealing procedure, the real-space topographies were analysed by scanning force microscopy. Moreover, GISAXS as a noninvasive technique was used to gain information about the internal ordering of the terpolymer thin films. As a pre-stage for developing intelligent thin film composite membranes, scanning electron microscopy was used to remove the electron sensitive poly(*tert*-butyl methacrylate) compartment for detailed morphological investigations.

3.2 Experimental

Polymer Characteristics. All four block terpolymer systems presented in this study were synthesized via sequential living anionic polymerization [Sch09]. Further details about a

first bulk characterization in THF may be found elsewhere [Sch09a].

Table 3.1: *Molecular Characteristics of BVT Triblock Terpolymers*

Polymer [a]	M_w / M_n [b]	$\varphi_B : \varphi_V : \varphi_T$ [c]	Thin Film Morphology [d]
$\mathbf{B}_{30}\mathbf{V}_{14}\mathbf{T}_{56}{}^{141}$	1.02	1 : 0.4 : 1.8	L
$\mathbf{B}_{18}\mathbf{V}_{8}\mathbf{T}_{74}{}^{133}$	1.02	1 : 0.4 : 4.0	C [e]
$\mathbf{B}_{16}\mathbf{V}_{21}\mathbf{T}_{63}{}^{145}$	1.02	1 : 1.2 : 3.7	CSC
$\mathbf{B}_{58}\mathbf{V}_{27}\mathbf{T}_{15}{}^{78}$	1.03	1 : 0.4 : 0.2	L / C

[a] Subscripts represent weight fractions of the respective block (in weight %); the superscript denotes the total weight-average molecular weight M_w in kg/mol as determined by SEC in combination with ^{1}H-NMR; [b] Polydispersity determined via SEC. M_w=weight-average molecular weight; M_n=number-average molecular weight; [c] Relative volume fractions of blocks calculated with respect to polymer densities; [d] determined by SFM, SEM, GISAXS - L: lamellar morphology, C [e]: core-shell cylinders with a discontinuous shell, CSC: hexagonally packed core-shell cylinders

Thin film preparation. Polymer thin films were prepared via spin-casting from 5 g/L and 10 g/L chloroform solutions, respectively, on polished silicon wafers (5 mm × 5 mm). In order to be consistent with the requirements of GISAXS measurements, silicon wafers of 3 cm × 3 cm were prepared. For equilibration of the microdomain structures, the chain mobility was significantly improved by controlled solvent vapor treatment at a solvent vapor saturation of 80 %. All experiments were realized in chloroform atmosphere. Moreover, during the annealing process, the temperature of the reaction chamber was kept constant at 25 °C. To ensure reproducibility, the developed morphologies were quenched with a constant flow of pure dried air.

Scanning Force Microscopy (SFM). Microdomain structures and film thicknesses were investigated by using a commercial SFM (DimensionTM 3100 equipped with a hybrid XY closed-loop scanner and a NanoScope®IV SPM controller, all from Vecco Instruments Inc.) operated in Tapping Mode. The spring constant of the silicon cantilevers (OMCL-AC160TS, Olympus, Japan) was in the range between 35-92 nN/m. The corresponding resonance frequency varies between 285 and 385 kHz. For determination of the film thickness, the polymer films was scratched with a scalpel. Subsequently, the height difference was measured between polymer surface with respect to the underlying substrate. The phase contrast was resolved due to the different physical properties of the components. Polybutadiene is liquid at room temperature whereas poly(*tert*-butyl methacrylate) and

poly(2-vinylpyridine) are in a glassy state at temperatures below 100 °C.

Scanning Electron Microscopy (SEM). We used SEM (LEO 1530, Zeiss) for further characterization of the polymer thin films. For the evaluation of the electron microscopy data, it is essential to consider the depolymerization process of the P*t*BMA compartment caused by the electron beam. Thus, these microdomains are supposed to shrink significantly distorting the analysis data sets [Saw96]. Applying the InLens detector with a slow acceleration voltage of 0.5 kV, we received a sufficient material contrast between polybutadiene and poly(2-vinylpyridine) without staining or sputtering.

Grazing-Incidence Small-Angle X-ray Scattering (GISAXS). The GISAXS experiments were performed at the XOR sector 8-ID at the Advanced Photon Source at Argonne National Laboratory using monochromatic X-rays with a wavelength of 0.16868 nm. The distance of the detector was adjusted to 1991 mm. The incident angle α_i of the X-ray beam was aligned to 0.18° what is between the critical angles of the single homopolymers (see Table 3.2) and the SiO_x substrate ($\alpha_{c_{Si}} = 0.22°$). This configuration implies both full penetration of the polymer thin film and total reflection at the silicon interface [Tol99, Bus06, Par09]. The exposure time was varied in the range of 5 to 120 s per frame. In order to block the strong specular reflection of the X-ray beam at $q_y = 0$ and the diffuse scattering, a beam-stop consisting of aluminium foil was adjusted in front of the detector.

Table 3.2: *Homopolymer Characteristics*

Polymer	α_c[°]	electron density [cm^{-3}]	γ [mN/m]	T_g [°C] [Gol99]
PB	0.16	$3.2 \times 10^{23}/cm^3$ [a]	24.5 - 32.0 [Lee67, Tur95]	-16
P2VP	0.17	$3.7 \times 10^{23}/cm^3$ [a]	40.0 [Ish90]	104
P*t*BMA	0.17	$3.4 \times 10^{23}/cm^3$ [b]	30.5 [Mar96]	125 - 130

[a] from Ref. [Hüc00]; [b] from Ref. [Lud03]

Small-Angle X-ray Scattering (SAXS). For studies of the microdomain orientation in bulk samples (dried slowly from chloroform solution at room temperature without strirring), in-situ synchrotron SAXS at the ID2 beamline at the European Synchrotron Radiation Facility (ESRF) was used. The X-ray beam had a diameter of 100 mm. The photon energy was set to 12.5 keV implying 0.1 nm wave length for the X-rays. For the image recording, a two-dimensional CCD camera was installed with a sample distance of 10 m within an evacuated flight tube. In dependence of the bulk sample, background,

cuvettes, solvent, air and beamp stop scattering was subtracted from the received data sets.

3.3 GISAXS Data Analysis

A schematic set-up for GISAXS experiments is illustrated in Figure 3.2. Monochromatic X-rays strike the polymer film surface in x-direction, along k_i with a very small incident angle α_i, typically in the range of 0.1 - 0.3° [Bus07]. The resulting scattering distribution of the horizontal exit angle θ_f (detected as $2\theta_f$) and the vertical exit angle α_f is collected by a two-dimensional detector. Scattering effects resulting from a momentum change can

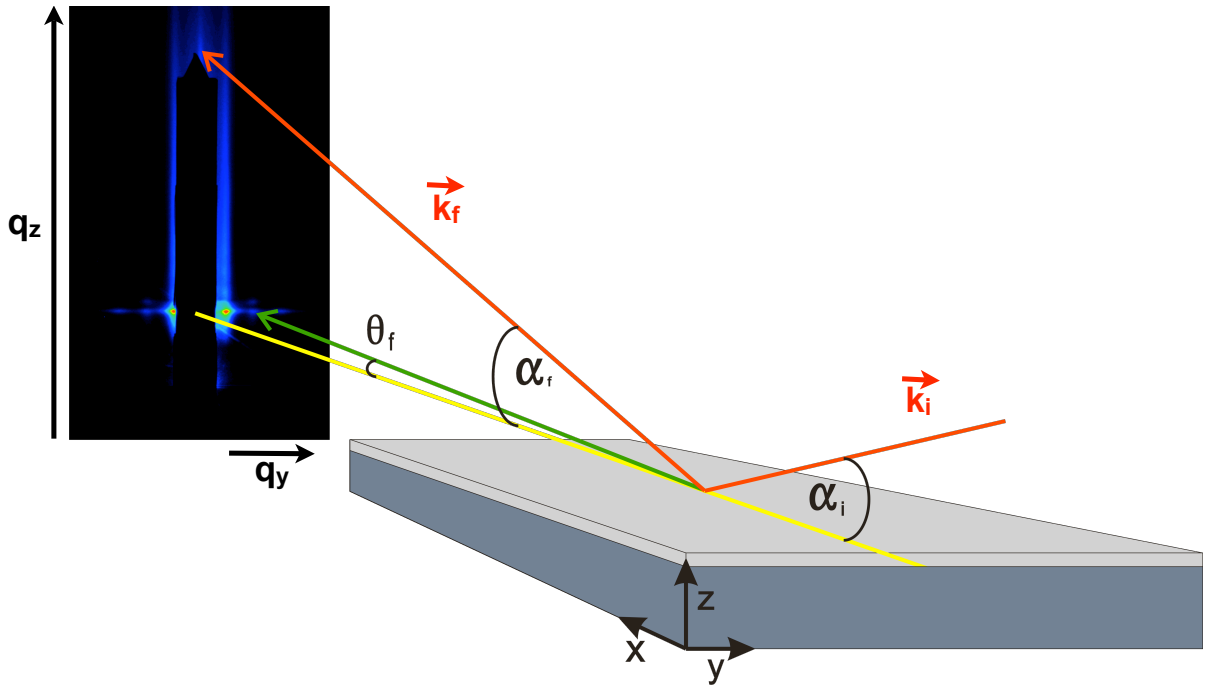

Figure 3.2: *Schematic of GISAXS experimental set-up. The X-ray beam aligned in x-direction strikes the sample surface with a wave angle α_i typically in the range of 0.1 - 0.3 ° which is in close proximity to the critical angles of both substrate and polymer thin film [Bus07]. A two-dimensional detector in the y - z plane, protected by a beam stop, collects the scattering intensities of the vertical exit angle α_f and the horizontal exit angle θ_f. Here, the horizontal signals in the GISAXS map result from Bragg rods caused by a lamellar morphology. The strong vertical reflections beside the beam stop indicate a microdomain orientation perpendicular to the silicon substrate.*

be described by the scattering vector $\overrightarrow{q}$ according to

$$\vec{q} = \frac{2\pi}{\lambda} \begin{pmatrix} \cos(\alpha_f)\cos(2\theta_f) - cos(\alpha_i) \\ \cos(\alpha_f)\sin(2\theta_f) \\ \sin(\alpha_f) + \sin(\alpha_i) \end{pmatrix} \tag{3.1}$$

A beam-stop blocks both the strong specular reflection of the X-ray beam and the diffuse scattering. Thus, the analysis of the weak off-specular scattering is facilitated [Kim04, Lee05].

For successful morphological investigations of polymer thin films, the critical angle α_c of the soft matter has to be determined. In case of $\alpha_i = \alpha_c$, total external reflection occurs resulting in an increase of the reflected scattering intensities also referred to as Yoneda peak [Yon63] or Vineyard effect [Vin82]. Under these conditions, the X-ray beam penetrates the sample just a few nanometers biasing the results. In order to gain structural informations about the complete volume, the incident angle of the X-rays α_i has to be larger than the critical angle of the sample material [MB03, Rot04] and smaller than the critical angle of the substrate revealing characteristic scattering profiles. For further analysis, the vertical exit angle α_f provides information about the kind of scattering. Specular scattering is observed, if $\alpha_i = \alpha_f$ disclosing the electron density distribution normal to the surface. For $\alpha_i \neq \alpha_f$ diffuse scattering reveals information about lateral correlations and surface roughness [Sin88, Laz02, MB03, Rot04].

Moreover, the scattering data evaluation is facilitated by cutting the two-dimensional maps into slices. Horizontal sections with a constant q_z reveal the typical small-angle X-ray scattering (SAXS) signals indicating structural characteristics like lamella or cylinders including their long period L_0. From vertical cuts, with q_y = constant, the grazing incidence diffraction (GID) provides information about film thickness and surface roughness.

3.4 Results and Discussion

Considering the future application of the presented thin BVT triblock terpolymer films as 'skin' top layers of composite membranes, it is indispensable to develop reproducible, thermodynamically equilibrated and homogenous membrane-like morphologies. As a pre-stage, we extended the standard solvent annealing procedure with an additional temperature set-up for controlling the sample chamber separately.

Moreover, the synthesized BVT triblock terpolymers possess high molecular weights retarding surface roughening on the micro- and macroscale (terrace formation) during the

solvent annealing process. In order to investigate basic microphase separation and self-assembling properties, the discussion of all BVT triblock terpolymer compositions will go far beyond the scope of this work. Thus, one BVT system of each synthesis series is presented in detail.

The BVT triblock terpolymer films were prepared in various film thicknesses to gain fundamental information about their self-assembling behavior. Our aim was the development of a thermodynamically stable phase-separated monolayer since thicker films often provide significant morphological discontinuities. This may result in the failure of the membrane scope of application. Table 3.3 summarizes the long periods L_0 of all investigated thin film morphologies.

Table 3.3: *Overview of characteristic long periods L_0 of BVT thin films*

series - polymer	film thickness [nm]	characteristic long period [nm]			
		SFM	REM	GISAXS	SAXS (bulk)
1 - $\mathbf{B_{30}V_{14}T_{56}}^{141}$	46 ± 4 [a]	78 ± 4	×	81 ± 2	84
2 - $\mathbf{B_{18}V_{8}T_{74}}^{133}$	31 ± 2	58 ± 4	58 ± 4	58 ± 2	×
3 - $\mathbf{B_{16}V_{21}T_{63}}^{145}$	43 ± 4	80 ± 5	×	80 ± 2	74
4 - $\mathbf{B_{58}V_{27}T_{15}}^{78}$	63 ± 3	top layer	top layer	48 ± 2	70

[a] comparable long periods obtained for a film thickness of 77 ± 2 nm

Thin film characterization of $\mathbf{B_{30}V_{14}T_{56}}^{141}$. This triblock terpolymer system possess a block ratio of PB : P2VP : P*t*BMA of 1 : 0.4 : 1.8 and a polydispersity of 1.02. The phase separation behavior was investigated for two different film thicknesses.

After the controlled solvent annealing procedure, a 46 ± 3 nm thin film was analysed by SFM for gaining information about the topographic properties. The corresponding height image in Figure 3.3 A displays a bright, stripe-like pattern. Regarding the glass transition temperatures of the homopolymers (see also Table 3.2), poly(2-vinylpyridine) (P2VP) and poly(*tert*-butyl methacrylate) (P*t*BMA) are in a glassy state at room temperature. Polybutadiene (PB), however, is liquid at the same time and, thus, can be easily distorted during the scanning process due to tip interactions.

Moreover, previous studies of Böker et *al.* supposed P2VP to wet the silicon substrate and act as an anchor due to its polar properties facilitating the aspired phase separation of PB and P*t*BMA [Bök01]. Additional driving forces, supporting this process, originate

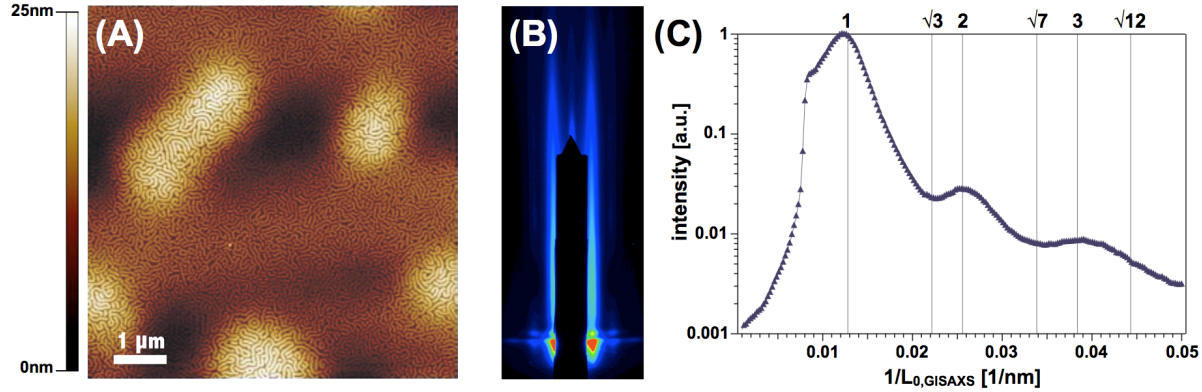

Figure 3.3: *Morphological investigations of a 45 ± 3 nm* $B_{30}V_{14}T_{56}{}^{141}$ *thin film.* ***(A)*** *SFM height image showing a stripe-like pattern;* ***(B)*** *two-dimensional GISAXS data map revealing straight, vertical Bragg rods indicating an orientation of the morphology normal to the substrate (the black area corresponds to the beam stop,* $\alpha_i = 0.18\,°$*);* ***(C)*** *horizontal cut of the 2D GISAXS data map at highest intensity gives information about lateral SAXS patterns. Here, typical reflexes for a lamellar morphology were observed.*

from the surface tensions. Both PB and P*t*BMA have similar low surface tensions in the range of 24.5 - 32.0 mN/m (for details see Table 3.2) causing a competition between both at the free air interface. Thus, the stripe-like pattern is supposed to consist of the rigid P*t*BMA whereas the darker, softer material is assumed to be composed of polybutadiene. We determined an average long period, $L_{0,SFM}$ of 78 ± 4 nm.

Due to regional limitations of the SFM technique, GISAXS was applied for large areas to obtain a random average of the morphology and the orientation towards the silicon substrate. The two-dimensional (2D) GISAXS data set is displayed in Figure 3.3 B. The black area in the center is caused by the beam stop as mentioned before. Straight, vertical Bragg rods at q_y of 0.08 nm^{-1} indicate a self-assembled structure oriented perpendicular to the substrate. Performing a horizontal cut by a constant q_z value, the typical SAXS reflections revealing that a lateral morphology is obtained (Figure 3.3 C). Based on the first order peak (n = 1) corresponding to the [100]-reflection at 0.08 nm^{-1}, the long period $L_{0,GISAXS}$ can be calculated by Eq. (3.2)

$$L_0 = \frac{2\pi n}{q_y} \tag{3.2}$$

with the peak order n and the scattering vector q_y. Here, we determined $L_{0,GISAXS}$ to be 78 ± 2 nm what is in good accordance with the results from SFM. Concerning the morphology, the distinct reflections at [100] : [200] : [300] (ratio of the reflex positions 1 : 2 :3) indicate a lamellar structure. The typical cylindrical reflex positions at $\sqrt{3}$, $\sqrt{7}$

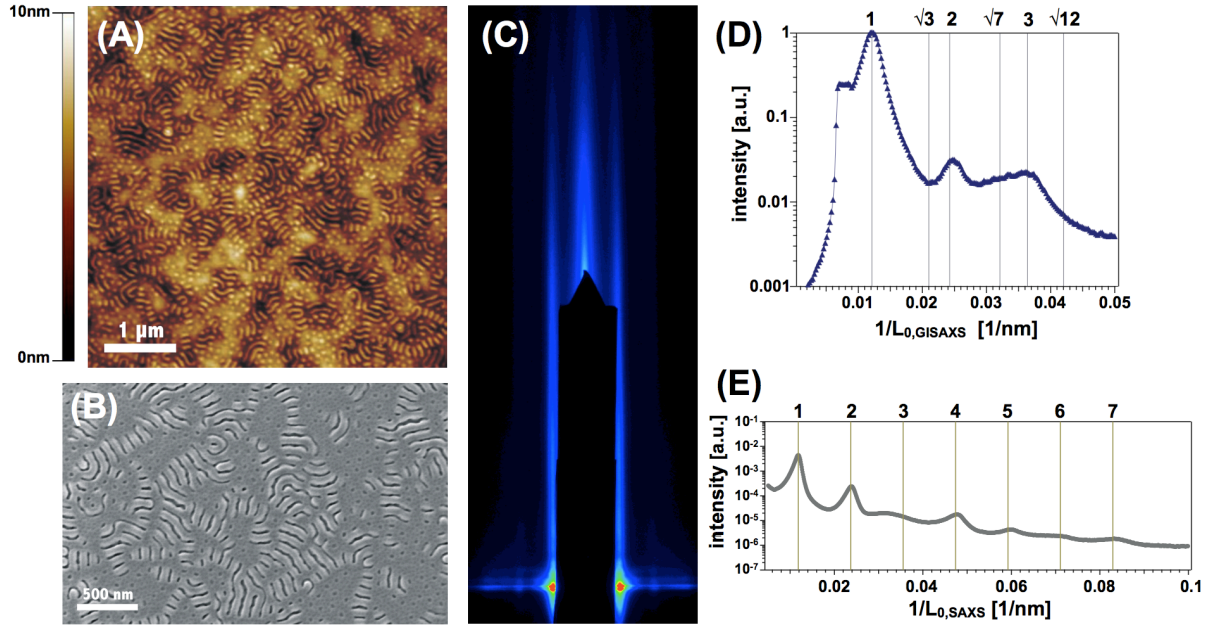

Figure 3.4: *Morphological investigations of a 77 ± 2 nm* $B_{30}V_{14}T_{56}{}^{141}$ *thin film.* ***(A)*** *SFM height image showing both a stripe-like pattern and partially covered areas;* ***(B)*** *two-dimensional GISAXS data map revealing a straight, centered Bragg rod indicating a parallel orientation of the morphology to the substrate (black area corresponds to the beam stop,* $\alpha_i = 0.18\,°$*);* ***(C)*** *horizontal cut of the 2D GISAXS data map at highest intensity gives information about lateral SAXS patterns;* ***(E)*** *SAXS patterns from* $B_{30}V_{14}T_{56}{}^{141}$ *bulk samples cast from chloroform solution.*

and $\sqrt{12}$ are missing completely.

By increasing the film thickness to 77 ± 2 nm, the topography is altered. The dark, low areas in the SFM height image in Figure 3.4 A yet exhibit the stripe-like pattern. However, the film surface seemed to roughen on the nanoscale by forming additional higher regions protruded by round, bright objects.

Further SEM investigations show the $B_{30}V_{14}T_{56}{}^{141}$ thin film surface after the destruction of the P*t*BMA compartment (Figure 3.4 B). The round objects, imaged by SFM, disappeared completely revealing dark holes indicating the decomposition of the irradiation sensitive P*t*BMA [Saw96]. Moreover, focusing on the stripe-like pattern, the mechanism of the structural formation was revealed. Based on the initial structure of lamellae oriented normal to the substrate, the increase of the film thickness initiated the coalescence with a preferential direction from the substrate to the free air interface. As a result, the lamellar orientation shifted from perpendicular to parallel with respect to the substrate.

GISAXS measurements confirmed this assumption. Regarding the 2D data map in Figure 3.4 C, the intensity of the former vertical, significant Bragg rods decreased whereas

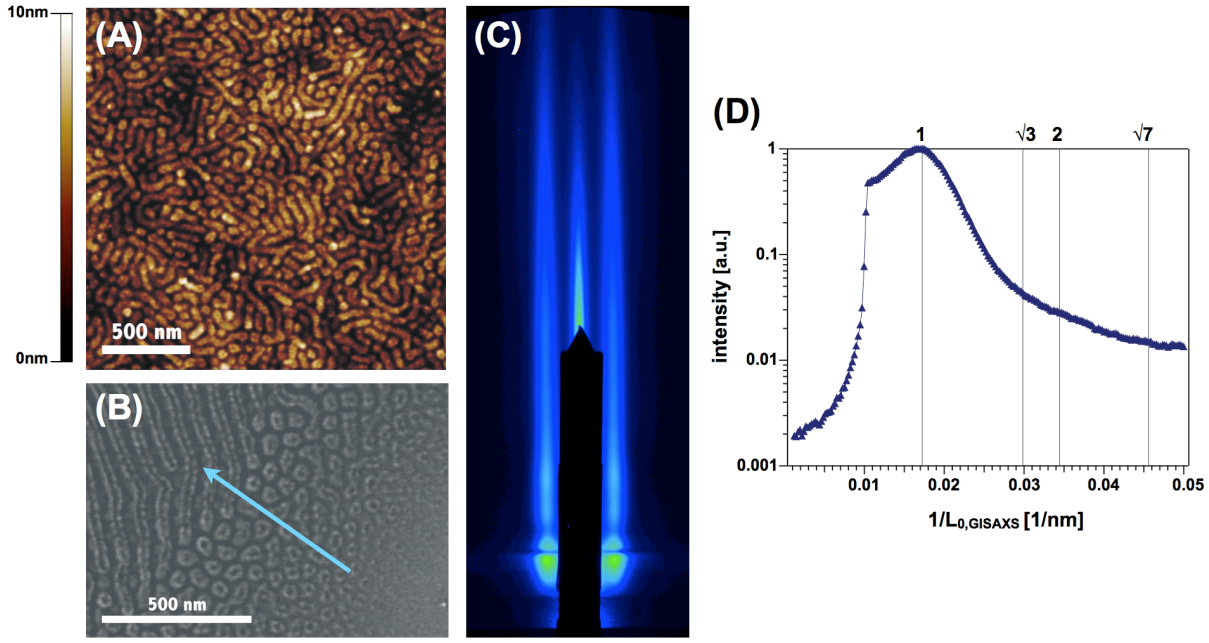

Figure 3.5: *Morphological investigations of a 31 ± 2 nm* $B_{18}V_8T_{74}{}^{133}$ *thin film.* ***(A)*** *SFM height image show a stripe-like pattern with undulated shapes;* ***(B)*** *thin film thickness gradient in arrow direction revealing the changing morphologies;* ***(C)*** *two-dimensional GISAXS data map revealing both straight, vertical Bragg rods and a centered reflex indicating an orientation normal and parallel to the substrate (the black area corresponds to the beam stop,* $\alpha_i = 0.18\,°$*);* ***(D)*** *horizontal cut of the 2D GISAXS data map at the highest intensity. Here, no reflections at all have been observed.*

an additional straight reflex in the center intensified. This reflex indicates a parallel orientation of the morphology regarding the substrate. Thus, both alignments are found for this film thickness of 77 ± 2 nm over large areas. Regarding the horizontal cut in Figure 3.4 D, the lamellar morphology with distinct reflex positions at 1 : 2 : 3 is confirmed and a long period of 82 ± 4 nm is determined.

For additional validation, SAXS bulk investigations were performed. Figure 3.4 E displays the characteristic SAXS pattern with reflex ratios of 1 : 2 : 3 : 4 : 5 : 6 : 7 indicating a highly ordered lamellar morphology with a bulk long period of 84 nm.

Thin film characterization of $\mathbf{B_{18}V_8T_{74}}^{133}$. Here, the P*t*BMA content was significantly increased whilst the ratio of the other two polymer compartments remained constant. A block ratio of 1 : 0.4 : 4.0 and a polydispersity of 1.02 was obtained. Due to solubility effects, very thin films in the range of 31 ± 2 nm were equilibrated by the controlled solvent annealing process. The self-assembling properties of this polymer were initially investigated by SFM.

In Figure 3.5 A, a typical SFM height image displays both round and stripe-like patterns

with undulated shapes and a long period of 58 ± 6 nm. However, the SFM resolution is limited by the tip radius preventing further detailed imaging. Thus, SEM was used as an additional characterization procedure. Figure 3.5 B shows a $B_{18}V_8T_{74}$[133] thickness gradient with increasing thickness in arrow direction. Starting at a film thickness of 20 ± 4 nm, a disordered phase was observed. By increasing the film thickness, irregular, distorted objects with a dark core appeared. The corresponding shell, however, was difficult to focus. Due to the high contrast, the half-spherical objects indicate their composition of the electron rich P2VP. By further enlarging the film thickness to 55 ± 3 nm, the objects appeared as a cylindrical morphology with a dark PB core decorated with a non-continuous P2VP shell oriented parallel towards the silicon substrate. A comparable morphology was found in bulk investigations by Schacher et *al.* [Sch09a]. The exisiting phase separation can be explained by the the interaction parameters, χ, of the three polymer compartments. The largest incompatibility is found between PB and P2VP with an interaction parameter $\chi_{PS,P2VP} = 0.325$ [Sch09a]. Thus, the decrease in the interfacial tension between these two blocks is energetically favored by minimising the contact areas resulting in a non-continuous shell of P2VP.

The corresponding GISAXS measurements (Figure 3.5 C) revealed a two-dimensional data set with Bragg rods oriented both normal and parallel to the substrate. For gaining lateral scattering information, a horizontal cut depicted a permanent decreasing signal without any characteristic reflections. However, by evaluating the first order peak position, a long period $L_{0,GISAXS}$ was determined to be 58 ± 2 nm which is in good agreement with previous SFM results.

With the directed increase of the P*t*BMA volume fraction, a morphological shift from lamellae towards core-shell cylinders was obtained. This special composition seemed not applicable as functional membranes.

Thin film characterization of $\mathbf{B_{16}V_{21}T_{63}}$[145]. Further synthetic efforts focused on an optimization of the block ratio facilitating the self-assembly of hexagonally packed core-shell cylinders with a P2VP-shell. By selective destruction of the core, we expected to generate stable perforations and channels, respectively, which may be externally stimulated by changing the pH.

The phase behavior of the resulting $B_{16}V_{21}T_{63}$[145] triblock terpolymer with a block ratio of 1 : 1.2 : 3.7 and a polydispersity of 1.02 was investigated by preparing three different film thicknesses for a general survey. The samples were annealed by controlled solvent vapor and investigated by SFM. It is remarkable that for all three thickness ranges (30 ± 2 nm; 43 ± 4 nm; 57 ± 3 nm), similar topographic morphologies (SFM) and Bragg

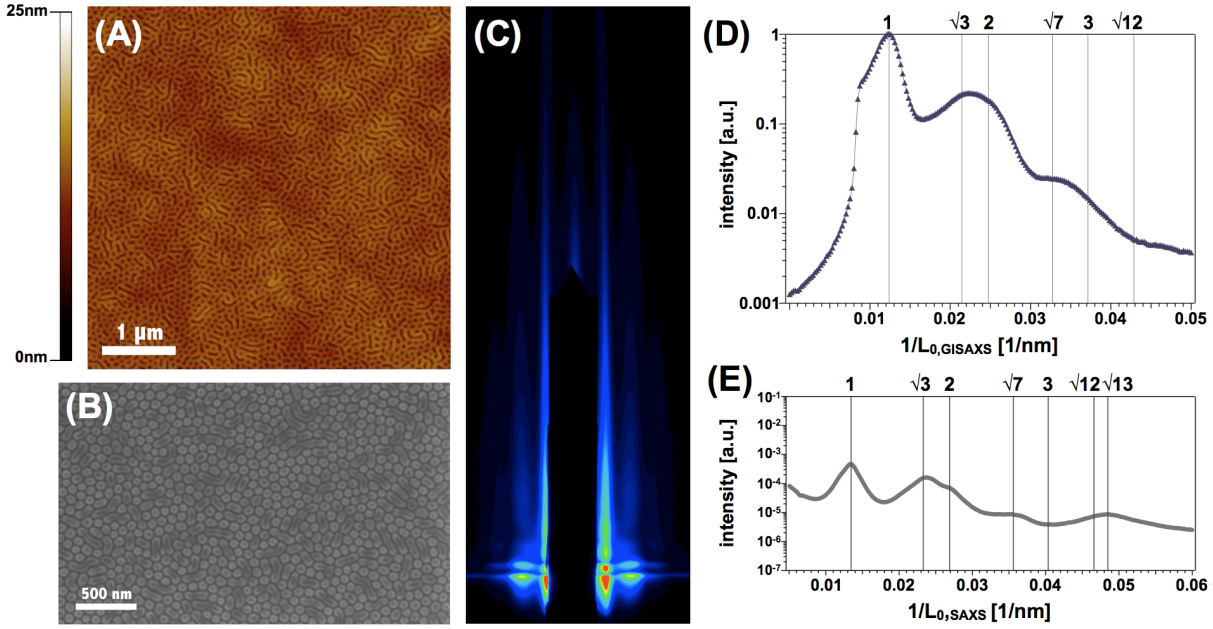

Figure 3.6: *Morphological investigations of a 43 ± 4 nm* $B_{16}V_{21}T_{63}{}^{145}$ *thin film.* ***(A)*** *SFM height image showing a mesh-like morphology which is partially hexagonally ordered;* ***(B)*** *SEM image after degradation of the PtBMA matrix phase revealing core-shell cylinders;* ***(C)*** *two-dimensional GISAXS data map revealing three straight, vertical Bragg rods indicating an orientation of the morphology normal to the substrate (the black area corresponds to the beam stop,* $\alpha_i = 0.18\,°$*);* ***(D)*** *horizontal cut of the 2D GISAXS data map at the highest intensity. Here, the peaks are broadened including both typical reflex ratios for cylinders or lamellae;* ***(E)*** *standard SAXS pattern of bulk samples indication a cylindrical morphology.*

rods (GISAXS) were found. This investigation may originate from the higher content of P2VP block stabilizing the self-assembly of the single compartments. In order to simplify matters, we present here just one representative film thickness. The height image in Figure 3.6 A shows the topographic characteristics of a 43 ± 4 nm thin film.

The surface is determined by a bright, mesh-like pattern consisting of the two glassy polymer compartments (P2VP and P*t*BMA). The lower, darker and coincidental soft objects are composed of PB. The partially hexagonally oriented structure resembles a membrane-like structure to some extend. By SFM, we determined a long period of 80 ± 5 nm.

Additional SEM investigations (Figure 3.6 B) revealed considerable structural changes. By depolymerization of the P*t*BMA matrix phase caused by the electron beam, PB and P2VP compartments remain. The previously found mesh-like pattern disappeared completey revealing objects consisting of a dark core surrounded by a brighter shell with a preferred orientation perpendicular to the substrate. Regarding the electron densities in

Table 3.2, the dark, electron-poor core is assigned to PB surrounded by the electron-rich P2VP compartment. The appearance of the polar P2VP block on the surface is explained by the tendency of polybutadiene to segregate to the free air interface. The resulting driving forces seemed to be much stronger than the tendency of P2VP to wet the polar silicon substrate. Due to the interconnectivity of both block, P2VP is assumed to be pulled away from the substrate resulting in a core-shell morphology.

Further GISAXS measurements reveal three significant vertical Bragg rods indicating a considerable orientation of the morphology perpendicular to the substrate (Figure 3.6 C). By preparing a horizontal cut, broadened peaks appear as shown in Figure 3.6 D. The first order peak at 0.079 nm^{-1} represents the [100] reflection and indicates a long period of 80 ± 2 nm. Further reflexes, however, could not be resolved due to the broadened peak areas including both cylindrical and lamellar features.

The performed bulk analysis in Figure 3.6 E shows cylindrical reflections with a ratio of $1 : \sqrt{3} : 2 : \sqrt{7} : \sqrt{12} : \sqrt{13}$ revealing a bulk long period of 74 nm.

Thin film characterization of $\mathbf{B_{48}V_{27}T_{15}}^{78}$. Within the last synthesis series, the block ratios have been inverted compared to $B_{16}V_{21}T_{63}{}^{145}$. Hence, we expect core-shell cylinders consisting of a P*t*BMA core and a P2VP shell which are embedded in a flexible PB matrix.

After the controlled solvent annealing procedure, a 63 ± 3 nm thin film was characterised by SFM revealing a nonspectacular, homogenous top layer. Even by variation of the tapping conditions, no informations about topography or phase contrast could be obtained (Figure 3.7 A). Additional SEM measurements (not shown here), displayed the same top layer without any features. Even an increase in the acceleration voltage showed no improvement. Due to the stability of this top layer while scanning in SEM and the large PB content in the polymer system, it is reasonable to assume that the top layer consists of polybutadiene.

To obtain more details about the phase separation behavior below this top layer, we applied GISAXS. The 2D data map (Figure 3.7 B) revealed a predominant structural orientation parallel to the substrate (centered Bragg rod). However, also a clear vertical Bragg rod at $q_y = 0.13$ nm^{-1} indicating an orientation perpendicular to the substrate is displayed. By cutting in the horizontal direction (Figure 3.7 C), the lateral SAXS patterns are shown. In this case, three peaks appeared with a reflex ratio of $1 : \sqrt{3} : 2$ which is characteristic for a cylindrical morphology. The first order peak revealed a long period of 48 ± 2 nm. Due to the reduced solubility in chloroform, no bulk samples could be analysed.

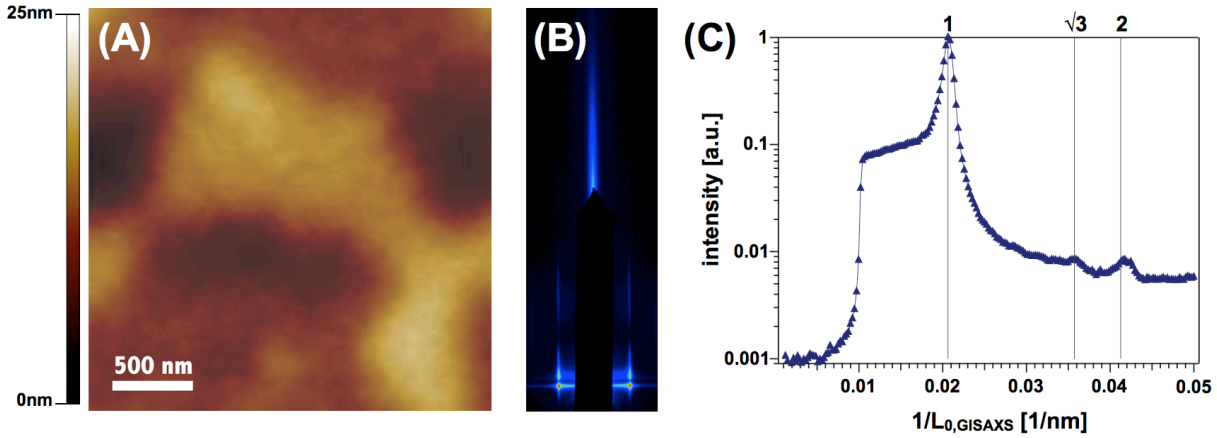

Figure 3.7: *Morphological investigations of a 63 ± 3 nm* $B_{48}V_{27}T_{15}{}^{78}$ *thin film.* ***(A)*** *SFM height image show a smooth, homogenous top layer;* ***(B)*** *two-dimensional GISAXS data map revealing one straight, vertical Bragg rod in the center indicating an orientation of the morphology parallel to the substrate but also one clear straight, vertical Bragg rod indicating a perpendicular orientation (the black area corresponds to the beam stop,* $\alpha_i = 0.18\,°$*);* ***(C)*** *horizontal cut of the 2D GISAXS data map at the highest intensity revealing cylindrical signals.*

3.5 Conclusion

We investigated four different BVT triblock terpolymer compositions and their microphase separation properties in thin films with respect to the future application as functional synthetic membranes. Thus, the thin films were supposed to consist of a self-assembled, flexible monolayer providing a homogenous film thickness and a monodisperse porosity which could be adjusted by external stimuli such as pH, light or temperature.

For the $B_{30}V_{14}T_{56}{}^{141}$ triblock terpolymer, a lamellar thin film morphology was detected which did not appear suitable for further investigations. By increasing the content of the P*t*BMA matrix, $B_{18}V_{8}T_{74}{}^{133}$ revealed objects with a non-continuous P2VP shell which were not appropriate as porous thin films. Further optimization in the synthesis, $B_{16}V_{21}T_{63}{}^{145}$ fulfilled the conditions by self-assembling in a cylindrical core-shell morphology with a P2VP-shell surrounding a PB core. Hence, this polymer composition shows a large potential for the desired membrane application. Further emphasis will be put on the removement of the core in order to establish filtration properties and improving flux conditions. Finally, $B_{48}V_{27}T_{15}{}^{78}$ thin films were expected to microphase separate as core-shell cylinders consisting of a P*t*BMA core and a P2VP shell which are embedded in a flexible PB matrix. During the experimental procedures, a flexible top layer covering cylindrical morphologies was investigated. Thus, the microphase separation behavior of this thin film

series deserves further studies in order to decide its relevance for the membrane applications. Future steps will focus on the deeper understanding of the formation mechanism and the structural extension over large areas.

3.6 Acknowledgement

The authors thank Dr. Kristin Schmidt, Clemens Liedel and Heiko Schoberth for the GISAXS measurements at APS and SAXS measurements at ID2 beamline at Grenoble. Moreover, we gratefully acknowledge the fruitful discussions with Professor Alexander Böker.

References

[Bök01] A. Böker, A. H. E. Müller, and G. Krausch. *Macromolecules*, **34**, 7477–7488 (2001)

[Bus06] P. Busch, R. M., D.-M. Smilgies, D. Posselt, and C. M. Papadakis. *Journal of Applied Crystallography*, **39**, 433–442 (2006)

[Bus07] P. Busch, D. Posselt, D.-M. Smilgies, R. M., and C. M. Papadakis. *Macromolecules*, **40**(3), 630–640 (2007)

[Gol99] T. Goldacker. *Dissertation - Überstrukturen in Mischungen aus Blockcopolymeren*. Bayreuth (1999)

[Had05] N. Hadjichristidis, M. Pitsikalis, and H. Iatrou. *Advances in Polymer Science*, **189**, 1–124 (2005)

[Haw97] C. Hawker. *Accounts of Chemical Research*, **30**(9), 373–382 (1997)

[Hüc00] H. Hückstädt, A. Göpfert, and V. Abetz. *Macromolecular Chemistry and Physics*, **201**(3), 296–307 (2000)

[Ish90] K. Ishizu, Y. Yamada, and T. Fukutomi. *Polymer*, **31**(11), 2047–2052 (1990)

[Ish03] K. Ishizu, K. Tsubaki, A. Mori, and S. Uchida. *Progress in Polymer Science*, **28**(1), 27–54 (2003)

[Kim04] S. Kim, M. Misner, T. Xu, M. Kimura, and T. Russell. *Advanced Materials*, **16**(3), 226–231 (2004)

[Laz02] R. Lazzari. *Journal of Applied Crystallography*, **35**, 406–421 (2002)

[Lee67] L. H. Lee. *Journal of Polymer Science Part a-2-Polymer Physics*, **5**(6PA2), 1103 (1967)

[Lee05] B. Lee, I. Park, J. Yoon, S. Park, J. Kim, K. W. Kim, T. Chang, and M. Ree. *Macromolecules*, **38**(10), 4311–4323 (2005)

[Lev89] J. R. Levine, J. B. Cohen, Y. W. Chung, and P. Georgopoulos. *Journal of Applied Crystallography*, **22**(6), 528–532 (1989)

[Li02] H. Li and W. Huck. *Current Opinion in Solid State and Materials Science*, **6**(1), 3–8 (2002)

[Li04] M. Li, K. Douki, K. Goto, C. Coenjarts, D.-M. Smilgies, and C. K. Ober. *Chemistry of Materials*, **16**(20), 3800–3808 (2004)

[Lud03] S. Ludwigs, A. Böker, V. Abetz, A. H. E. Müller, and G. Krausch. *Polymer*, **44**(22), 6815–6823 (2003)

[Lud03a] S. Ludwigs, A. Böker, A. Voronov, N. Rehse, R. Magerle, and G. Krausch. *Nature Materials*, **2**, 744 (2003)

[Lud05] S. Ludwigs, K. Schmidt, and G. Krausch. *Macromolecules*, **38**(6), 2376–2382 (2005)

[Lud05a] S. Ludwigs, K. Schmidt, C. Stafford, E. Amis, M. Fasolka, A. Karim, R. Magerle, and G. Krausch. *Macromolecules*, **38**(5), 1850–1858 (2005)

[Mar96] J. E. Mark. *Physical Properties of Polymers Handbook*. AIP Press, New York (1996)

[MB03] P. Müller-Buschbaum. *Analytical and Bioanalytical Chemistry*, **376**(1), 3–10 (2003)

[Ols08] D. Olson, L. Chen, and M. Hillmyer. *Chemistry of Materials*, **20**, 869–890 (2008)

[Pap04] C. M. Papadakis, P. Busch, D. Posselt, and D.-M. Smilgies. *Advances in Solid State Physics (Vol. 44) - Morphological Transition in Thin Lamellar Diblock Copolymer Films as Revealed by Combined GISAXS and AFM Studies*. Springer Verlag, Heidelberg (2004)

[Par05] I. Park, B. Lee, J. Ryu, K. Im, J. Yoon, M. Ree, and T. Chang. *Macromolecules*, **38**(25), 10532–10536 (2005)

[Par09] S. Park, B. Kim, J. Xu, T. Hofmann, B. M. Ocko, and T. P. Russell. *Macromolecules*, **42**(4), 1278–1284 (2009)

[Rau95] M. Rauscher, T. Salditt, and H. Spohn. *Physical Review B*, **52**(23), 16855–16863 (1995)

[Rot04] S. V. Roth, P. Müller-Buschbaum, M. Burghammer, H. Walter, P. Panagiotou, A. Diethert, and C. Riekel. *Spectrochimica Acta Part B: Atomic Spectroscopy*, **59**(10-11), 1765–1773 (2004)

[Saw96] L. C. Sawyer and D. T. Grubb. *Polymer microscopy*. Chapman & Hall, London, 2nd edition (1996)

[Sch09] F. Schacher, A. Walther, M. Ruppel, M. Drechsler, and A. H. E. Müller. *Macromolecules*, **42**(10), 3540–3548 (2009)

[Sch09a] F. Schacher, J. Yuan, and A. H. E. Müller. *unpublished* (2009)

[Sin88] S. K. Sinha, E. B. Sirota, S. Garoff, and H. B. Stanley. *Physical Review B*, **38**(4), 2297–2311 (1988)

[Smi02] D.-M. Smilgies, P. Busch, D. Posselt, and C. M. Papadakis. *Synchroton Radiation News*, **15**(5), 35–42 (2002)

[Tol99] M. Tolan. *X-Ray Scattering from Soft-Matter Thin Films* (1999)

[Tur95] A. Turturro, E. Gattglia, P. Vacca, and G. T. Viola. *Polymer*, **36**(21), 3987–3996 (1995)

[Ulb06] M. Ulbricht. *Polymer*, **47**, 2217–2262 (2006)

[Vin82] G. H. Vineyard. *Physical Review B*, **26**(8), 4146–4159 (1982)

[Xu04] T. Xu, J. T. Goldbach, M. J. Misner, S. Kin, A. Gibaud, O. Gang, B. Ocko, K. W. Guarini, C. T. Black, C. J. Hawker, and T. P. Russell. *Macromolecules*, **37**(8), 2972–2977 (2004)

[Yon63] Y. Yoneda. *Physical Reviews*, **131**(5), 2010–2013 (1963)

Chapter 4

Towards Nanoporous Membranes based on ABC Triblock Terpolymers

ABSTRACT

Block copolymers represent an exciting class of complex materials as they self-assemble into highly regular structures of nanoscopic dimensions. When prepared as thin films, such structures can be used for a variety of applications including lithographic masks or nanoporous membranes. Reported here are nanostructures in thin films of structurally analogous polybutadiene-block-*poly(2-vinylpyridine)*-block-*poly(*tert-*butyl methacrylate) (BVT) and polystyrene*-block-*poly(2-vinylpyridine)*-block-*poly(tert-butyl methacrylate) (SVT) triblock terpolymers which are synthesized via sequential living anionic polymerization. The morphological behavior of annealed SVT and BVT films is investigated by scanning force and electron microscopies. The difference in the terpolymer composition results in the formation of an ordered perforated lamella phase in SVT films and hexagonally packed core/shell cylinders in BVT films. Further, the BVT films show high potential for the fabrication of composite membranes using track-etched poly(ethylene terephthalate) macroporous filters as a support.*

4.1 Introduction

The development of synthetic membranes has always been inspired by nature, in particular by the fact that the selective transport through biological membranes is enabled by highly specialized macro- and supramolecular assemblies based on and involved in molecular recognition. The success of membrane technology has already been impressively demonstrated for the first large-scale industrial processes, water purification by reverse osmosis, and blood detoxification by dialysis or ultrafiltration. The search for novel synthetic membranes, in particular those with higher transport selectivity, is still a significant challenge in this field.

Currently, most of the membranes used are produced from organic polymers via phase inversion methods, that is, a controlled phase separation of polymer solutions induced by nonsolvent addition, solvent evaporation or temperature change [Mul96, vdW96]. Many scientifically interesting, technically challenging, and commercially attractive separation problems cannot be solved with membranes using current techniques. Novel membranes with a higher chemical selectivity, for example, for isomers, enantiomers or larger biomolecules, or with a selectivity that can be switched by an external stimulus or that can adapt to the environment and process conditions are required. In addition, minimizing the thickness of the membrane barrier layer is essential. Approaches to develop synthetic 'next generation' membranes have been recently reviewed [Ulb06].

The potential of block copolymers with incompatible blocks for nanotechnology applications has been realized in the past decade and a considerable number of examples has been described in the literature [Hil05]. Nanoporous materials may be generated by the selective removal of one of the components from a self-assembled block copolymer. Through adjusting chain length, composition, and molecular architecture, these materials are able to exhibit pore sizes and topology of parent structures and they can therefore be employed as nanolithographic masks, templates or even separation membranes. Lee et *al.* first reported a porous membrane-like structure from an ordered block copolymer precursor [Lee88]. The generated porous films were characterized by using adsorption measurements as well as gravimetric and spectroscopic measurements. Three years later, Smith and Meier showed that ozonolysis can effectively remove the polydiene component in polystyrene-*block*-polybutadiene (PS-BB) or polystyrene-*block*-polyisoprene (PS-PI) diblock copolymers without altering the structure of the uncrosslinked PS domains [Smi92]. In 2003, Sidorenko et *al.* used a mixture of a polystyrene-*block*-poly(4-vinylpyridine) (PS-P4VP) diblock copolymer and 2-(4-hydroxybenzene-azo)benzoic acid (HABA). Depending on the casting conditions, the annealing solvent, and polymer-analogous reactions, thin films with pores perpendicular to the surface could be generated [Sid03]. An elegant way

to nanoporous materials without the need of crosslinking or degradation steps was shown by Zalusky et *al.* [Zal01]. Mesoporous polystyrene monoliths were prepared by hydrolytical removal of the polylactide block from a polystyrene-*block*-polylactide (PS-PLA) diblock copolymer. Pore sizes within this system were adjustable via the molecular weight of the diblock copolymer. Rather simple methods for alignment of PLA cylinders were also presented [Zal02]. Nanoporous PS generated in this way has the solubility and thermal characteristics of bulk polystyrene homopolymer and any potential application of these materials that requires pore structure stability must work within these limitations.

A different approach was published by Ndoni et *al.* in 2003 [Ndo03]. Here the polydiene component of a diblock copolymer was not removed through ozonolysis but kept as matrix material. They report on the synthesis and radical crosslinking of polybutadiene-*block*-poly(dimethylsilane) (PB-PDMS) followed by removal of the silane compound through HF etching. Unfortunately, the morphology was strongly affected by the rather rigorous crosslinking conditions. When replacing polybutadiene by polyisoprene and performing the etching step with tetrabutylammonium fluoride (TBAF) instead of HF, Cavicchi et *al.* obtained better results [Cav04]. They report on the formation of porous PI monoliths from ordered, aligned and crosslinked PI-PDMS. Structures and porosity were investigated with scanning electron microscopy (SEM) and small-angle X-ray scattering (SAXS) measurements after removal of the silyl component with TBAF in THF. These experiments showed that nanoporous rubbers may be generated, having potential as functionalizable porous materials through the remaining double bonds.

It was shown earlier that the microdomain structures in thin films of SVT triblock terpolymer show pronounced dependence on the film thickness [Lud05]. [12]. Among those, the perforated lamella morphology (PL) is the most suitable for the fabrication of novel composite membranes. It was demonstrated in experiments [Lud03a, Tsa06, Par06, Kno02], and in computational simulation [Haj97] that in thin films of cylinder-forming block copolymers the PL phase is stabilized by the strong surface fields. Moreover, the PL structure was successfully converted into a pH-responsive layer through the hydrolysis of the ester moiety of the P*t*BMA component [Lud05a]. Furthermore, additional morphologies such as short standing cylinders or complex gyroid structures, which provide a complex but regular channel geometry, are potentially of great interest.

Despite the impressive microscopic, spectroscopic and other characterization studies of the ordered porous morphologies based on di- or triblock copolymers, a direct demonstration of the membrane function, i.e. permeability measurements or even a selective permeation controlled by the nanoporosity of the polymer film, is yet to be accomplished.

Here we demonstrate the effect of the triblock terpolymer composition on the resulting complex morphology in thin films of polystyrene-*block*-poly(2-vinylpyridine)-*block*-poly(tert-butyl methacrylate) (SVT) and of polybutadiene-*block*-poly(2-vinylpyridine)-*block*-poly(*tert*-butyl methacrylate) (BVT) triblock terpolymers. Additionally, we varied the nature of the substrate, the molecular weight of the BVT terpolymer and the annealing conditions. By replacing the rather brittle polystyrene block in the SVT terpolymer through rubbery polybutadiene, we optimize the matrix properties, yielding a more flexible system. Furthermore, crosslinking of the polybutadiene compartment enhances the thin film stability. The morphological behavior of annealed SVT and BVT films was investigated by scanning force microscopy (SFM), transmission electron microscopy (TEM) and SEM. The strategic aim of this work is to explore the potential of the fabrication of composite membranes from nanoporous block copolymer thin films on macroporous filters as supports.

4.2 Experimental Part

Synthesis of Block Terpolymers: The synthesis and characterization of the linear SVT triblock terpolymers have already been described [Lud03]. The BVT triblock terpolymers were synthesized via sequential living anionic polymerization in THF using sec-butyl lithium as initiator. After polymerization of butadiene and 2-vinylpyridine at -10°C and -70°C respectively, 1,1-diphenylethylene was added to reduce the nucleophilicity of the living chain ends. During the polymerization of the P*t*BMA block at -35°C, samples were taken from the reactor after different polymerization times and were precipitated into degassed methanol.

Table 4.1: *Molecular Characteristics of Triblock Terpolymers*

Polymer [a]	M_w / M_n [b]	$\varphi_B : \varphi_V : \varphi_T$ [c]
$\mathbf{S}_{16}\mathbf{V}_{21}\mathbf{T}_{63}{}^{140}$	1.03	1 : 1.3 : 3.90
$\mathbf{B}_{16}\mathbf{V}_{21}\mathbf{T}_{63}{}^{145}$	1.02	1 : 1.3 : 3.90
$\mathbf{B}_{14}\mathbf{V}_{18}\mathbf{T}_{68}{}^{165}$	1.02	1 : 1.2 : 4.85

[a] Subscripts represent weight fractions of the respective block (in weight %); the superscript denotes the total weight-average molecular weight M_w in kg/mol; [b] Polydispersity determined by GPC. M_w=weight-average molecular weight; M_n=number-average molecular weight; [c] Relative volume fractions of blocks

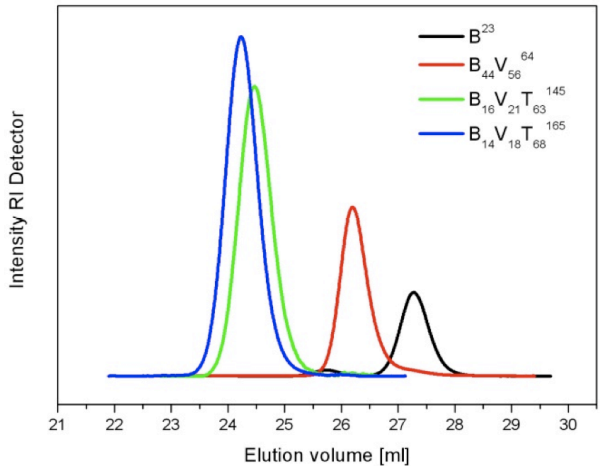

Figure 4.1: *Gel-permeation chromatography (GPC) eluograms of polybutadiene, polybutadiene*-b-*poly(2-vinylpyridine), and two BVT triblock terpolymers.*

The number-average molecular weight of the polybutadiene precursor and the molecular weight distributions of the triblock terpolymers were determined by gel permeation chromatography (GPC). All polymers exhibit a narrow molecular weight distribution characterized by polydispersity indices between 1.01 and 1.05.

Additionally, ^{1}H-NMR spectra were acquired using $CDCl_3$ as solvent and tetramethylsilane (TMS) as internal standard. The molecular weights of the P2VP and the PtBMA blocks were calculated using the terpolymer composition determined by NMR and the polystyrene molecular weights from GPC. The molecular parameters of the triblock terpolymers are listed in Table 4.1 and GPC eluograms of BVT are shown in Figure 4.1.

Size-Exclusion Chromatography (SEC): SEC measurements were performed on a set of 30 cm SDV-gel columns of 5 μm particle size having nominal pore sizes of 10^5, 10^4, 10^3 and 10^2 Å with refractive index and UV (λ = 254 nm) detection. An elution rate of 1 mL/min with THF as solvent was used.

^{1}H-Nuclear Magnetic Resonance Spectroscopy (NMR): ^{1}H-NMR spectra were recorded on a Bruker 250 AC spectrometer using either $CDCl_3$ or THF-d_8 as solvent and tetramethylsilane (TMS) as internal standard.

Thin Film Preparation: SVT and BVT polymer thin films were prepared by spin-casting 5 g/L solutions in chloroform onto polished silicon wafers and NaCl surfaces, respectively. In order to improve the chain mobility and equilibrate the microdomains, the thin films were annealed under controlled solvent vapor pressure. The samples were subsequently quenched by a flow of pure dried air in order to freeze the developed morphologies. The fast quenching procedure ensures reproducibility.

For crosslinking of the polybutadiene block in BVT thin films, 3 wt.% of the photoinitiator Lucirin-TPO (BASF) was added to a 5 g/L polymer solution. After spin-casting onto NaCl (crysTec GmbH, Germany) and annealing in controlled solvent vapor, the samples were subsequently exposed to UV light for 60 min with a cutoff at 300 nm, leaving the PtBMA block undamaged.

SFM: Microdomain structures and film thickness were investigated with SFM (Dimension 3100, Veeco Metrology) operated in Tapping Mode. The spring constant of the silicon cantilevers was in the range between 35-92 nN/m. The corresponding resonance frequency varies between 285 and 385 kHz. Phase images were recorded at free amplitudes of about 30-50 nm at a setpoint of 90% of the free cantilever amplitude. Height measurements were performed by scratching the polymer films with a scalpel (see Ref. [Tsa06]) and measuring the height of the polymer film surface with respect to the underlying substrate. The phase contrast was resolved due to the different physical properties of the components. Polybutadiene is liquid at room temperature whereas poly(*tert*-butyl methacrylate) and poly(2-vinylpyridine) are in a glassy state at temperatures below 100°C.

Field-Emission SEM: We used SEM (LEO 1530, Zeiss) for further characterization of the polymer thin films. Due to the depolymerization of the PtBMA matrix phase by the electron beam, new insights into the morphology were gained [Saw96]. Applying the InLens detector with a slow acceleration voltage of 0.5 kV, we received a sufficient material contrast between the two remaining polymer phases without staining or sputtering.

TEM: For creating new polymer composite membranes, it is essential to remove the triblock terpolymers from the substrates, enabling the transfer to template membranes. To this end we prepared thin films of $B_{14}V_{18}T_{68}{}^{165}$ on NaCl substrates (as explained above). After solvent annealing, the NaCl plates were dissolved in bidestilled water and the free-floating film was picked up with carbon-coated copper grids (Plano, Wetzlar). Subsequently, the samples were checked with TEM (CEM 902, Zeiss, 80 kV) for defects caused by the transfer.

4.3 Results and Discussion

In order to induce long-range order of microstructures of block copolymer thin films, thermal or solvent annealing procedures are typically applied. The assembly of microdomains at the microscale is accompanied by macroscale surface roughening, that is, the formation of terraces (coexisting flat regions with equilibrium film thickness) and of dewetting patterns. These two other dynamic processes are considered to pronouncedly and destructively

affect (in case of dewetting) thin films from block copolymers with a relatively low total molecular weight. Thin polymer films consisting of comparatively long chains (with a total molecular weight of above 100 kg/mol) are relatively stable towards dewetting [Geo02] on an experimental timescale. In addition, in thin films of high molecular weight block copolymers, such as presented in this study, the terrace formation is considerably retarded due to the high viscostity of the polymers [Tsa07].

Thin Film Phase Behavior of $\mathbf{S_{16}V_{21}T_{63}}^{140}$. After spin-casting from a chloroform solution, the samples were annealed for 100 h in chloroform vapor ($p_{CHCl_3} = 0.8\ p_0$, with p_0 representing the vapor pressure of chloroform at 295 K). Under these annealing conditions the polymer volume fraction in swollen films is $\varphi = 0.36 \pm 0.04$. Due to the polymer swelling, the chain mobility is considerably increased, facilitating the diffusion-driven transport and the development of the equilibrium macro- and microstructures.

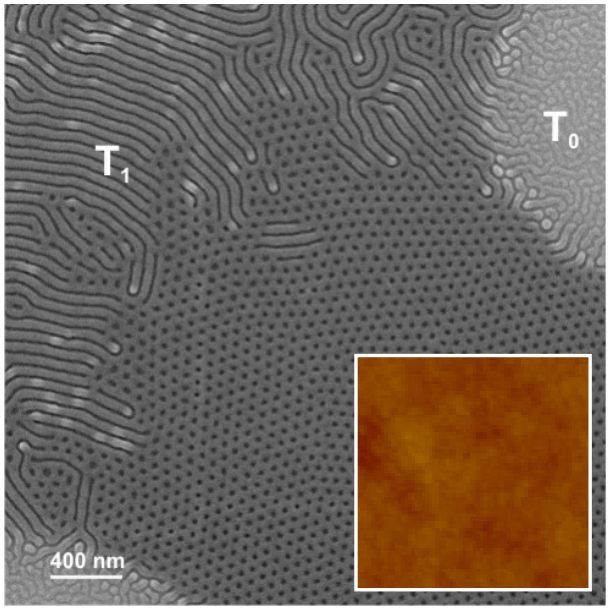

Figure 4.2: *SEM image of a $S_{16}V_{21}T_{63}{}^{140}$ thin film after annealing in chloroform vapor ($p_{CHCl_3} = 0.8\ p_0$; $t = 100$ h) with an acceleration voltage of 1.0 kV showing different morphologies dependent on terrace height. Scale bar: 400 nm. Inset: SFM height image (size 1 x 1 μm^2; height scale Δz = 0-20 nm). The sample surface is covered with a smooth rigid layer of PtBMA.*

The annealed $S_{16}V_{21}T_{63}{}^{140}$ samples show macrostructures (terraces) on a scale of tens of micrometers (visible in optical microscopy). Large-scan SFM height images (not shown here) reveal coexisting terraces with the heights of $T_0 = 16\pm3$ nm and $T_1 = 36\pm2$ nm with characteristic microstructures in each terrace, which can only be visualized in SEM (Figure 4.2). On a microscale the SFM height and phase images show no lateral structure

(inset in Figure 4.2 A). The whole polymer surface is covered with a smooth, stiff layer of one component. In contrast, SEM measurements show the surface layer to be unstable during the electron beam exposure despite a low acceleration voltage of 0.5 kV. Comparing all three polymer components, poly(*tert*-butyl methacrylate) (P*t*BMA) is the only block that is depolymerized via photolysis during UV or electron beam exposure [Gra88].

In addition, P*t*BMA represents the phase with the lowest surface tension (see Table 4.2) which is expected to form a glassy (glass transition temperature $T_{g(PtBMA)}$= 135°C) continuous cover layer which then minimizes the interfacial tension between the polymer film and air [Has85, Ana89]. The other two components, polystyrene (γ_{PS} = 41 mN/m [Mar96]) and poly(2-vinylpyridine) (γ_{P2VP} = 40 mN/m [Ish90]), remain underneath this surface layer independent of the resulting morphology.

Table 4.2: *Surface Tensions of used Polymer Components*

Polymer	Surface tension [mN/m]
polystyrene (PS)	41.0 [Mar96]
polybutadiene (PB)	24.5 - 32.0 [Lee67, Tur95]
poly(2-vinylpyridine) (P2VP)	40.0 [Ish90]
poly(*tert*-butyl methacrylate) (P*t*BMA)	20.7 [Mar96]

We now describe in more detail the microdomain structures as revealed by the SEM measurements. The thinnest part of the film (T_0 in Figure 4.2) is often referred to as a disordered phase or wetting layer. With increasing film thickness, T_0 transforms into cylinders orientated parallel to the substrate which form the first terrace, T_1. Moreover, with further increase of the film thickness to 47 ± 2 nm the cylindrical structure changes to PL morphology, resembling a typical filter or membrane surface. The associated changes in height within one terrace may be due to different characteristic spacings of cylinder and PL morphology [Tsa06].

The molecular architecture of SVT suggests that a PL unit cell consists of a polystyrene core surrounded by a poly(2-vinylpyridine) shell and penetrated by well-defined P*t*BMA pores (for further information see Refs. [Lud03a, Lud05b, Lud05]).

The SEM image of a $S_{16}V_{21}T_{63}{}^{140}$ thin film in Figure 4.3 indicates the formation of the PL phase over macroscopically large areas. The hexagonal order of perforations (pores) with an average diameter of 35 ± 3 nm is confirmed by the Fourier transformation (inset in Figure 4.3 B). The estimated porosity of such nanostructures is about 21%.

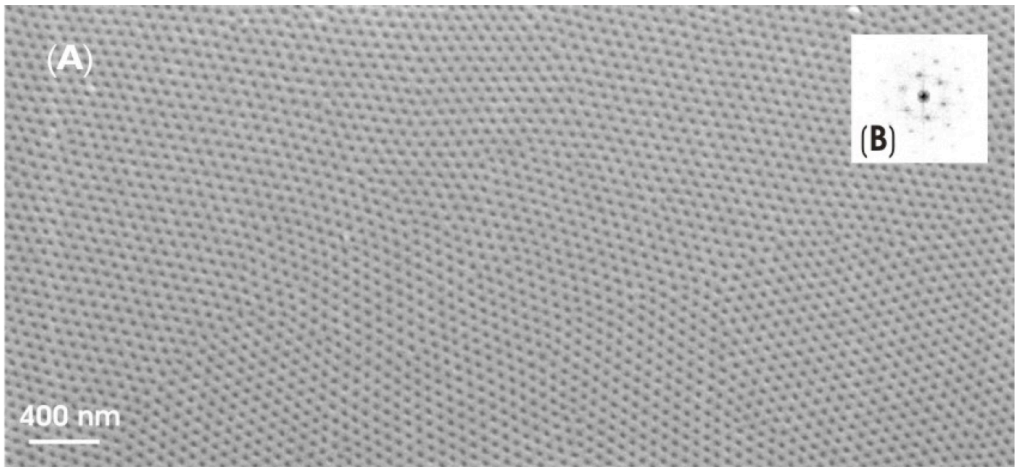

Figure 4.3: ***(A)*** *Typical SEM image of a* $S_{16}V_{21}T_{63}{}^{140}$ *triblock terpolymer thin film after spin-casting from chloroform solution and solvent annealing for 100 h; acceleration voltage 1.0 kV. Scale bar: 400 nm;* ***(B)*** *Fourier transformation confirms the hexagonally arranged PL structure.*

We note that the observed microstructures and terrace heights are in agreement with the combinatorial studies of Ludwigs et *al.* [Lud05b].

Thin Film Phase Behavior of $\mathbf{B_{16}V_{21}T_{63}}^{145}$. Spin-casted 30 ± 2 nm thick films were annealed in chloroform vapor under the same conditions as described for $S_{16}V_{21}T_{63}{}^{140}$. SFM height measurements reveal a macroscopically smooth surface of the film with no terraces formed upon the annealing procedure. On a smaller scale, the lateral nanostructures become visible. The SFM height image in Figure 4.4 A reveals coexisting morphology represented by channels (dark and white stripes) and by wells (dark dots) surrounded by mesh-like walls (bright area). In the corresponding phase image (4.4 B), two phases with different mechanical properties are clearly distinguished.

The dark color in the phase image corresponds to the PB block, which is the only soft component in the presented system. The mesh-like hard matrix is presumably composed of the two other glassy components, that is, P2VP and P*t*BMA. We note that, in contrast to the $S_{16}V_{21}T_{63}{}^{140}$ films, the PL morphology was not observed. The nanostructured, free surface of $B_{16}V_{21}T_{63}{}^{145}$ films, as revealed by SFM measurements, indicates that P*t*BMA does not form the continuous surface layer that was detected for $S_{16}V_{21}T_{63}{}^{140}$ films (inset to Figure 4.2). This effect can be explained by the modified polymer composition, the consequential changes in T_g and the surface tension (Table 4.2) of the BVT components. Both, PB and PtBMA blocks show comparable surface tension enabling both components to segregate to the free surface. Therefore, the lateral nanopattern can be resolved in solvent annealed films by SFM measurements.

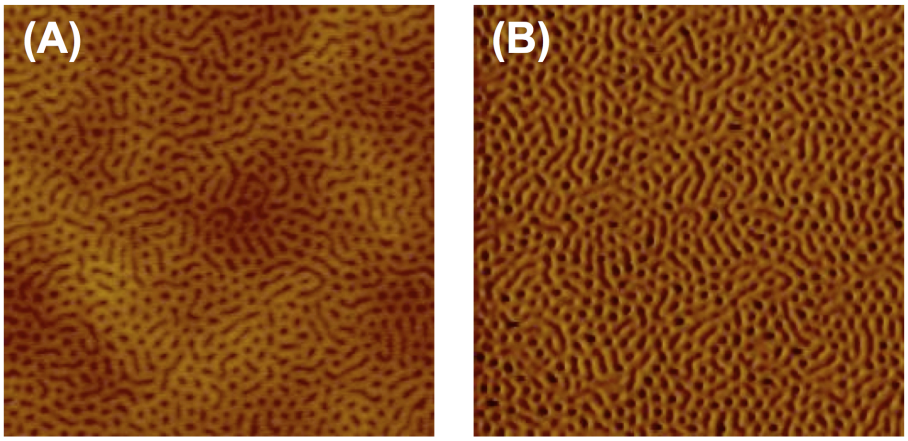

Figure 4.4: ***(A)*** *Typical SFM height image of a* $B_{16}V_{21}T_{63}{}^{145}$ *triblock terpolymer thin film spin-cast from chloroform solution after annealing for 100 h in chloroform vapor (image size 2.5 x 2.5* μm^2*; height scale* Δz *= 0-20 nm) showing coexisting morphologies. The low, dark areas correspond to the soft PB compartment, which is distorted due to strong SFM tapping conditions. The higher, brighter mesh-like matrix is presumably composed of the other two rigid polymer compartments P2VP and P*t*BMA. The contrast differences in the corresponding phase image* ***(B)*** *confirm this observation (image size 2.5 x 2.5* μm^2*; phase contrast 30 °).*

Additional information concerning the composition of the mesh-like hard matrix was obtained by SEM. Figure 4.5 displays the microdomain pattern in the $B_{16}V_{21}T_{63}{}^{145}$ film, which was described above (Figure 4.4). The structure is represented by core-shell stripes and dots, which we identify with the core-shell cylinders oriented parallel and perpendicular to the film surface, respectively, with an average diameter of 67.8 ± 9.0 nm (Figure 4.5). The mesh-like hard matrix, which was clearly visualized in SFM images (Figure 4.4), is decomposed upon electron-beam-exposure, which implies that it is composed of P*t*BMA.

The stripes and distorted dots, which appear as defects in the hexagonally ordered structure of perpendicular cylinders, annihilate upon increasing the time of equilibration. Using step-wise annealing process, we followed the evolution of cylinders lying parallel to the substrate into cylinders oriented perpendicular to the substrate. The TEM image in Figure 4.6 displays the mechanism of such transformation via interfacial undulations along the parallel cylinder axis and the resulting break-up into spherical domains [Tsa06a].

Thin Film Phase Behavior of $B_{14}V_{18}T_{68}{}^{165}$. To further investigate of the molecular architecture effects on the resulting morphology and long-range order, we studied a BVT terpolymer with increased total molecular weight. A 39 ± 3 nm thick film was prepared under the conditions described above. SFM height measurements revealed a smooth, macroscale film surface (no terrace development).

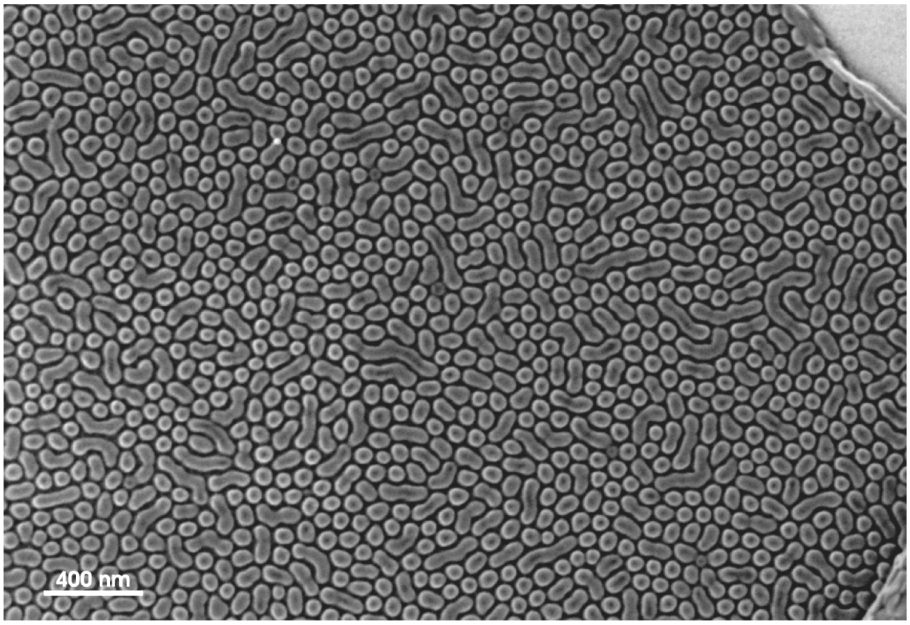

Figure 4.5: *SEM image of the $B_{16}V_{21}T_{63}{}^{145}$ film shown in Figure 4.4 (acceleration voltage 0.5 kV). Solely cylinders oriented perpendicular and parallel to the substrate surface are found whereas the surrounding matrix phase, which was clearly resolved in the SFM height measurements, is depolymerized by the electron beam. The scalebar corresponds to 400 nm.*

SEM measurements (not shown) reveal vertically oriented core-shell cylinders with an average diameter of 64 ± 5 nm which look similar to the structures described above for $B_{16}V_{21}T_{63}{}^{145}$ (Figure 4.5). In order to obtain further insight into microdomain structure, we performed SFM measurements of the BVT films after exposure to the electron beam in SEM. SFM height and phase images in Figure 4.7 clearly confirm the core-shell morphology.

We note that due to removal of the P*t*BMA block, in the height image the film surface appears to be rough with an averaged roughness of 6 ± 1 nm as calculated by the Nanoscope software. In order to probe the potential of BVT nanostructures in membrane technology, we replaced the silicon oxide substrate by th crystalline sodium chloride (NaCl) surface, which makes the transformation of the polymer film from the solid substrate for further analysis and usage more feasible. Immediately after annealing on NaCl substrate, BVT films were transferred onto carbon-coated TEM grids. Carbon coating enhances film stability during the electron beam exposure.

The TEM image in Figure 4.8 A clearly reveals the core-shell morphology, which confirms the successful film transfer. A further step towards optimization of the mechanical properties and chemical stability of the membrane prototypes was achieved by selective crosslinking of the PB component via UV-initiator. The above procedure considerably im-

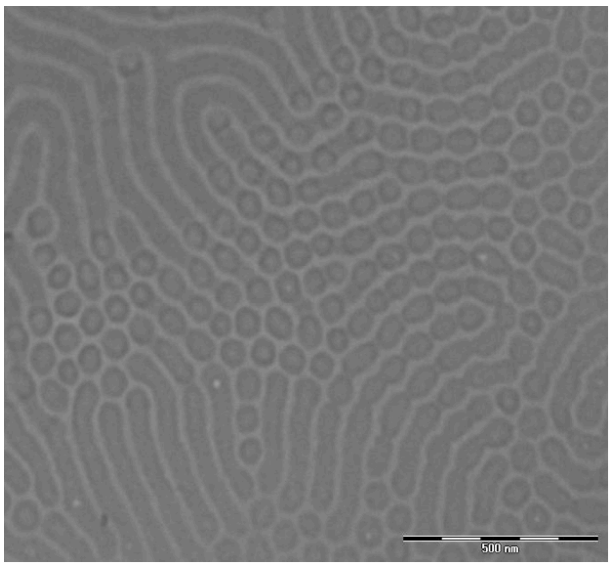

Figure 4.6: *TEM image of a $B_{16}V_{21}T_{63}{}^{145}$ thin film successfully transferred after controlled solvent annealing for two hours reveals an intermediate stage in the cylinder transformation mechanism. The cylinders orientated parallel to the substrate show a rather undulated shape resulting in a break-up into spherical domains. Scale bar: 500 nm.*

proves physical properties of the liquid polybutadiene segments, leading to a rubbery material and therefore facilitates the film transfer to the technologically approved substrates. Importantly, the desired film nanostructure is perfectly preserved after crosslinking (Figure 4.8 B).

In order to characterize and probe the size/charge-based permeation selectivity of block copolymer nanostructures, thin polymer films must be transformed onto suitable substrates providing sufficient mechanical stability of a potential membrane. Considering the diameters of the pore precursors identified in this work ($\approx$ 35 nm; SVT) moderately thick (membrane) filters with pore diameters of between $\approx$ 0.2 and $\approx$ 5 μm are suitable base materials for the fabrication of block copolymer thin-film composite membranes. Surface-functionalized track-etched poly(ethylene terephthalate) (PET) membranes, which have already been well established as model systems for selective and stimuli-responsive transport through well-defined pores in the nano- and micrometer range [Ulb06, Gei07], are the first choice.

The transfer to other supports, for example to silicon nitride-based microsieves [vR04], is another perspective. The results of our study demonstrate that upon annealing under sufficient solvent vapour pressure, the resulting microdomain structure is not sensitive to the chemical nature of the substrate (NaCl or silicon oxide) due to the strong screening effect of the solvent. On the other hand, the transfer of the polymer films to the supporting

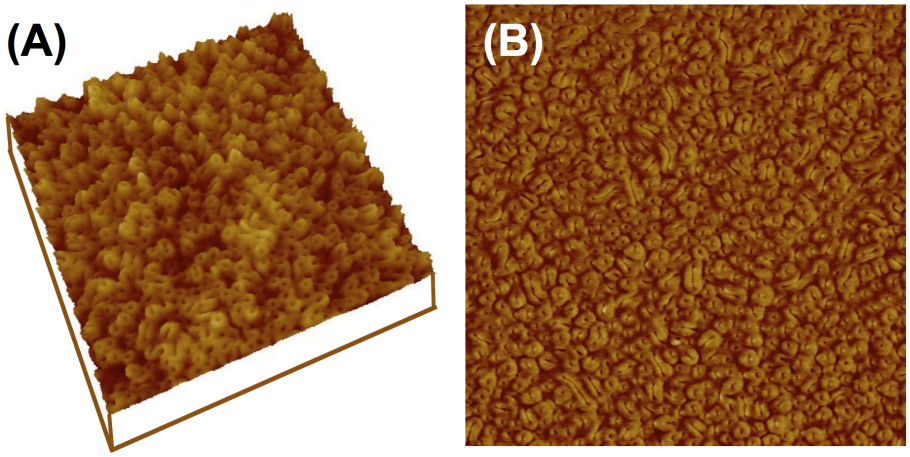

Figure 4.7: ***(A)*** *Typical three-dimensional SFM height image (image size 2.5 x 2.5 μm^2; height scale Δz = 0-20 nm) of a $B_{14}V_{18}T_{68}{}^{165}$ triblock terpolymer (spin-cast from chloroform solution, solvent annealed for 100 h) after electron-beam exposure. The resulting morphology of vertical cylinders can be easily observed. The corresponding phase image* ***(B)*** *confirms the structure of core-shell cylinders whereas the soft PB compartment forms the core (black area) and the stiff P2VP compartment equals the surrounding shell (bright area) (image size 2.5 x 2.5 μm^2; phase contrast = 20°).*

membranes is considerably facilitated by the improved mechanical properties of the films.

4.4 Conclusion

SFM, TEM and SEM reveal the nanostructures in thin films of structurally analogous polybutadiene-*block*-poly(2-vinylpyridine)-*block*-poly(tert-butyl methacrylate) (BVT) and polystyrene-*block*-poly(2-vinylpyridine)-*block*-poly(*tert*-butyl methacrylate) (SVT) triblock terpolymers. The difference in the terpolymer composition results in the formation of an ordered perforated lamella phase in SVT films and hexagonally packed core-shell cylinders in BVT films. Both morphologies are considered to be attractive precursors for nanoporous separation membranes. This requires further processing of the films via selective degradation of one component in order to 'open' the pores.

For the novel BVT terpolymers, several very useful features with respect to the membrane technology have been identified, namely a similar equilibrium morphology on substrates with different wettability, the feasibility of film transfer to another (porous) substrate, and the stabilization of the films by internal crosslinking. Thin SVT films demonstrated membrane-suitable morphology and feasibility of their transfer onto support membranes. Further processing of terpolymers microstructures towards nanoporous separation membranes is currently under investigation.

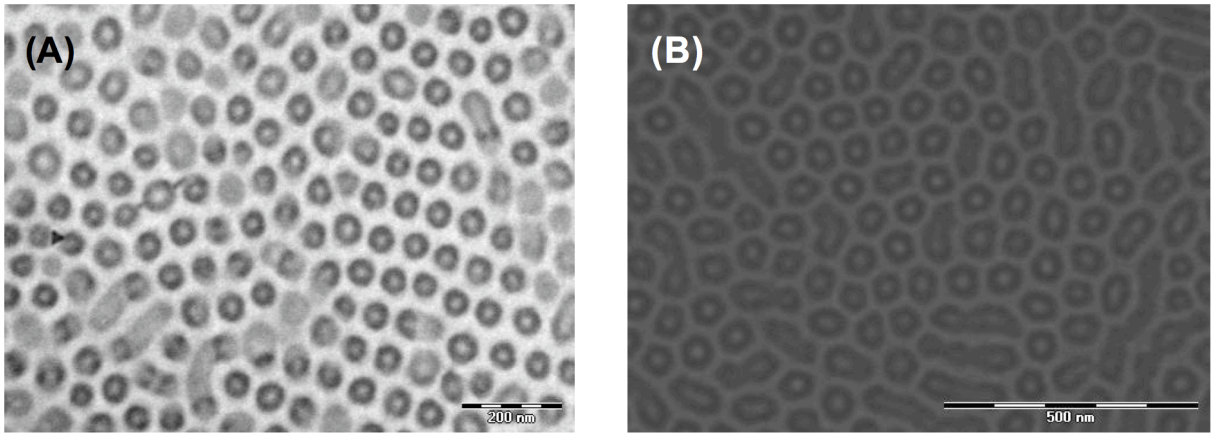

Figure 4.8: ***(A)*** *TEM image of a thin film of* $B_{14}V_{18}T_{68}{}^{165}$ *triblock terpolymer spin-cast onto a NaCl wafer from chloroform solution and transferred onto a TEM grid, revealing hexagonally packed core-shell cylinders: polybutadiene core and poly(2-vinylpyridine) shell in a poly(*tert*-butyl methacrylate) matrix. Scale bar: 200 nm.* ***(B)*** *TEM image of a crosslinked* $B_{14}V_{18}T_{68}{}^{165}$ *thin film displaying comparable structures as shown in* ***(A)****. Scale bar: 500 nm.*

4.5 Acknowledgement

This research is supported by the VolkswagenStiftung. We thank Carmen Kunert for the TEM measurements.

References

[Ana89] S. H. Anastasiadis, T. P. Russell, S. K. Staija, and C. F. Majkrzak. *Physical Review Letters*, **62**(16), 1852–1855 (1989)

[Cav04] K. A. Cavicchi, A. S. Zalusky, M. A. Hillmyer, and T. P. Lodge. *Macromolecular Rapid Communications*, **25**(6), 704–709 (2004)

[Gei07] C. Geismann, A. Yaroshchuk, and M. Ulbricht. *Langmuir*, **23**(1), 76–83 (2007)

[Geo02] M. Geoghegan and G. Krausch. *Progress in Polymer Science*, **28**(2), 261–302 (2002)

[Gra88] N. Grassie and G. Scott. *Polymer Degradation and Stabilisation*. Cambridge University Press, Cambridge (1988)

[Haj97] D. A. Hajduk, H. Takenouchi, M. A. Hillmyer, F. S. Bates, M. E. Vigild, and K. Almdal. *Macromolecules*, **30**(13), 3788–3795 (1997)

[Has85] H. Hasegawa and T. Hashimoto. *Macromolecules*, **16**(3), 589–590 (1985)

[Hil05] M. A. Hillmyer. *Nanoporous materials from block copolymer precursors - Vol. 189*. Springer Verlag, Berlin - Heidelberg (2005)

[Ish90] K. Ishizu, Y. Yamada, and T. Fukutomi. *Polymer*, **31**(11), 2047–2052 (1990)

[Kno02] A. Knoll, A. Horvat, K. Lyakhova, G. Krausch, G. Sevink, A. Zvelindovsky, and R. Magerle. *Physical Review Letters*, **89**(3), 035501 (2002)

[Lee67] L. H. Lee. *Journal of Polymer Science Part a-2-Polymer Physics*, **5**(6PA2), 1103 (1967)

[Lee88] J.-S. Lee, A. Hirao, and S. Nakahama. *Macromolecules*, **21**(1), 274–276 (1988)

[Lud03] S. Ludwigs, A. Böker, V. Abetz, A. H. E. Müller, and G. Krausch. *Polymer*, **44**(22), 6815–6823 (2003)

[Lud03a] S. Ludwigs, A. Böker, A. Voronov, N. Rehse, R. Magerle, and G. Krausch. *Nature Materials*, **2**, 744 (2003)

[Lud05] S. Ludwigs, K. G., R. Magerle, A. V. Zvelindovsky, and G. J. A. Sevink. *Macromolecues*, **38**(5), 1859–1867 (2005)

[Lud05a] S. Ludwigs, K. Schmidt, and K. G. *Macromolecues*, **38**(6), 2376–2382 (2005)

[Lud05b] S. Ludwigs, K. Schmidt, C. Stafford, E. Amis, M. Fasolka, A. Karim, R. Magerle, and G. Krausch. *Macromolecules*, **38**(5), 1850–1858 (2005)

[Mar96] J. E. Mark. *Physical Properties of Polymers Handbook*. AIP Press, New York (1996)

[Mul96] M. Mulder. *Basic principles of membrane technology, Vol.2*. Kluwer academic publishers, Dordrecht (1996)

[Ndo03] S. Ndoni, M. E. Vigild, and R. H. Berg. *Journal of the American Chemical Society*, **125**(44), 13366–13367 (2003)

[Par06] I. Park, S. Park, H. W. Park, T. Chang, H. C. Yang, and C. Y. Ryu. *Macromolecules*, **39**(1), 315–318 (2006)

[Saw96] L. C. Sawyer and D. T. Grubb. *Polymer microscopy*. Chapman & Hall, London, 2nd edition (1996)

[Sid03] A. Sidorenko, I. Tokarev, S. Minko, and M. Stamm. *Journals of American Society*, **125**(40), 12211–12216 (2003)

[Smi92] D. R. Smith and D. J. Meier. *Polymer*, **33**(18), 3777–3782 (1992)

[Tsa06] L. Tsarkova, A. Knoll, G. Krausch, and R. Magerle. *Macromolecules*, **39**(10), 3608–3615 (2006)

[Tsa06a] L. Tsarkova, A. Knoll, and R. Magerle. *Nano Letters*, **6**(7), 1574–1577 (2006)

[Tsa07] L. Tsarkova. *Nanostructured Soft Matter: Experiment, Theory, Simulation and Perspectives*. Springer Verlag, Heidelberg, ed. a.v. zvelindovsky edition (2007)

[Tur95] A. Turturro, E. Gattglia, P. Vacca, and G. T. Viola. *Polymer*, **36**(21), 3987–3996 (1995)

[Ulb06] M. Ulbricht. *Polymer*, **47**, 2217–2262 (2006)

[vdW96] P. van de Witte, P. J. Dijkstra, J. W. A. van den Berg, and J. Feijen. *Journal of Membrane Science*, **117**(1), 1–31 (1996)

[vR04] C. J. M. van Rijn. *Nano- and Microengineered Membrane Technology*. Elsevier Science, Amsterdam (2004)

[Zal01] A. S. Zalusky, R. Olayo-Valles, C. J. Taylor, and M. A. Hillmyer. *Journals of American Society*, **123**(7), 1519–1520 (2001)

[Zal02] A. S. Zalusky, R. Olayo-Valles, J. H. Wolf, and M. A. Hillmyer. *Journals of American Society*, **124**(43), 12761–12773 (2002)

Chapter 5

Chemical Modification for the Selective Control of Microphase Separation in ABC Triblock Terpolymer Thin Films

ABSTRACT

*We demonstrate an experimental approach to tune the microphase separation of ABC triblock terpolymers by guided variation of both volume compositions and chemical modification of the block copolymer compartments. We overcome a significant instability concerning large area transfers onto support membranes by using polybutadiene-*block*-poly(2-vinylpyridine)-*block*-poly(*tert*-butyl methacrylate) thin films. Moreover, we chemically modified the hydrophobic PB by selective, oxidative hydroboration using 9-borabicyclo[3.3.1] nonane (9-BBN) in order to increase both polarity and surface tension of the PB compartment.*

5.1 Introduction

The increasing technological demand for nanoscale structures has pushed scientists to look at both self- and guided assembly of block copolymers (BC) in thin films. Current applications of block copolymer nanostructures range from nanolithography and electronics [Par03, Seg05] to novel functional synthetic membranes with tailored properties [Ulb06]. The technological potential of BCs is based on their intrinsic rich and intriguing phase behavior in thin films [Kra02]. The resulting microstructures can be chemically modified in order to introduce functionality on the nanoscale dimension.

A rational design of complex BC nanostructures for application in thin film composite (TFC) membranes, which consist of a support membrane (typically poly(ethylene terephthalate; PET) with a deposited thin structured polymer film ('skin'), is intended to overcome current limitations of the state-of-the-art membrane technology, for example limited selectivity, non-uniformity of the pores or non-predictable separation properties. First of all, a thin 'skin' layer from microphase-separated BC structures can be both transformed or even prepared onto a support membrane if thickness and mechanical strength characteristics are combined ideally. Moreover, such a structured synthetic 'skin' has the advantage of an uniform feature-size distribution with the dimensions of potential pores or interconnected channels down to tens-of-nanometer scale.

An essential precondition for such 'skin' layers is the formation of an appropriate microphase-separated morphology such as short standing cylinders, perforated lamella (PL) or a bicontinuous gyroid phase (G) which then may be transformed into porous films by selective removal of one of the components. Several successful examples have been reported about degradation of polydiene compartments by ozonolysis [Lee88, Smi92, Guo06, Oku06] or selective depolymerization of UV-light sensitive compartments [Ban06, Joo06, Lud05, Lud05a, Lud05b].

In contrast to AB diblock copolymer systems, ABC ternary systems show a higher chemical variability and mechanical stability after the selective removal of the third block. Along with diblock copolymer systems or blockcopolymer/homopolymer blends [Yan06] and with block copolymer/surfactant mixtures [Ruo99], ABC triblock terpolymers have been shown to possess high potential as membrane prototypes [Ban06, Lud05a].

In this article, we demonstrate an experimental approach to tune the microphase separation of ABC triblock terpolymers by guided variation of both volume compositions and chemical modification of the block copolymer compartments. Following earlier work on functional polymer membrane templates from ABC triblock terpolymers [Lud03a, Lud03], we overcome their significant instability concerning large area transfers to possible support

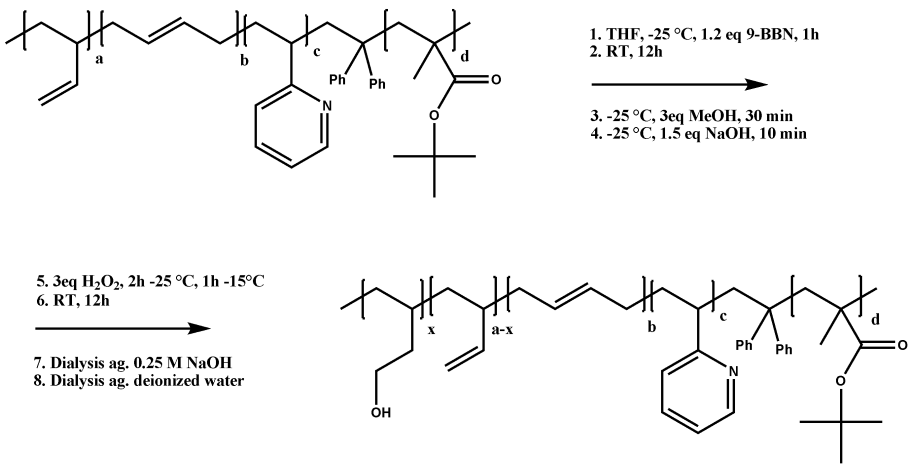

Figure 5.1: *Selective, oxidative hydroboration reaction scheme by use of 9-BBN.*

membranes by substituting a rigid polystyrene (PS) block with a viscous polybutadiene (PB) compartment. Moreover, we chemically modify the hydrophobic PB by selective, oxidative hydroboration using 9-borabicyclo[3.3.1]nonane (9-BBN) [Bro79, Chu88]. This procedure modifies both surface tension and polarity of the PB compartment through the introduction of the hydroxyl functions alongside the backbone.

5.2 Experimental Part

Polymer synthesis. Triblock terpolymers ($B_{14}V_{18}T_{68}{}^{165}$ and $B_{53}V_{24}T_{23}{}^{85}$) were synthesized via sequential living anionic polymerization in THF. All polymers exhibit a narrow molecular weight distribution characterized by polydispersity indices between 1.01 and 1.05. Further synthesis details are presented elsewhere [Spe07]. The molecular parameters of the triblock terpolymers are listed in Table 5.1. All chemicals were purchased from Sigma–Aldrich and used without further purification, unless noted.

Selective hydroboration of polybutadiene compartment. The introduction of additional polar hydroxy groups was realized by the selective oxidative hydroboration as suggested by Chung et *al.* [Chu88] and slightly modified. The reaction scheme is displayed in Figure 5.1.

The whole modification process was performed under nitrogen cover gas. 500 mg of polymer were dissolved in 200 ml dry THF, the solution was degassed via three freeze-thaw cycles and cooled to -25 °C. After 1 hour, 1 eq of 9-borabicyclo[3.3.1]nonane (9-BBN), calculated according to the amount of 1,2-polybutadiene present, was added via syringe and the solution was stirred at this temperature for one more hour. Then the reaction

was allowed to warm up over night. The next day, after cooling to 25 °C, MeOH was added (2.5 eq). After stirring for 30 minutes, NaOH (1.25 eq, 6 N solution in deionized water) was added. After 10 minutes, H_2O_2 (2.25 eq, 30 % solution) was added and the reaction mixture was left for 2 h at -25 °C, 1 h at -15 °C, and finally was warmed to room temperature. Then the solution was concentrated on a rotary evaporator and dialyzed consecutively against 0.25 M NaOH, EtOH, and deionized water. Finally, the precipitate was dissolved in dioxane and freeze dried.

Gel Permeation Chromatography (GPC). All measurements were performed on a set of 30 cm SDV-gel columns of 5 μm particle size having nominal pore sizes of 10^5, 10^4, 10^3 and 10^2 Å with refractive index and UV (λ=254 nm) detection. An elution rate of 1 mL/min with THF as solvent was used.

Small-Angle X-Ray Scattering (SAXS). For studies on the orientation of the microdomains in the bulk samples (dried slowly from chloroform solution at room temperature without stirring), in-situ synchrotron SAXS at the ID2 beamline at the European Synchrotron Radiation Facility (ESRF) was used. The X-ray beam had a diameter of 100 mm. The photon energy was set to 12.5 keV. For the image recording, a two-dimensional CCD camera was installed with a sample distance of 10 m within an evacuated flight tube.

Thin film preparation. For all four polymers presented in this study, we used combinatorial mapping studies as demonstrated by Smith et *al.* [Smi01]. A detailed description of the set-up may is available in the Supporting Information.

For minimizing defects or grain boundaries and equilibrating the microdomain structures, the chain mobility was significantly improved by controlled solvent vapor treatment at a chloroform vapor saturation of 80 % for 72 h for HO-$B_{14}V_{18}T_{68}$[165] gradients. Due to the reduced molecular weight of HO-$B_{53}V_{24}T_{23}$[85] and the corresponding facilitated dewetting, we decreased the solvent annealing time to 24 h. To ensure reproducibility, the developed morphologies were quenched fast with a constant flow of pure dried air.

For the cross-sections, the gradients were initially frozen in liquid nitrogen and subsequently, immediately broken.

Scanning Force Microscopy (SFM). Microdomain structures and film thickness were investigated with SFM (Dimension 3100, Veeco Metrology) operated in Tapping Mode. The spring constant of the silicon cantilevers was in the range between 42-85 nN/m. The corresponding resonance frequency varies between 285 and 385 kHz. Height measurements were performed by scratching the polymer films with a scalpel and measuring the height of the polymer film surface with respect to the underlying silicon substrate. The phase contrast was resolved due to the different physical properties of the components.

Polybutadiene is liquid at room temperature whereas poly(*tert*-butyl methacrylate) and poly(2-vinylpyridine) are in a glassy state at temperatures below 100 °C.

Field–Emission Scanning Electron Microscopy (SEM). We used SEM (LEO 1530, Zeiss) for further characterization of the polymer thin films. Applying the InLens detector with a slow acceleration voltage of 0.5 kV, we received a sufficient material contrast without staining or sputtering.

5.3 Results and Discussion

Both investigated polybutadiene-*block*-poly(2-vinylpyridine)-*block*-poly(*tert*-butyl methacrylate) (BVT) triblock terpolymers with narrow total weight-average molecular weight distribution were synthesized via living sequential anionic polymerization and characterized by GPC and ^{1}H–NMR as described earlier [Spe07]. The main characteristics of $B_xV_yT_z{}^{M_w}$ triblock terpolymers, as well as their hydroborated analogs, are summarized in Table 5.1. The phase behavior of four ABC triblock terpolymers in thin films was analysed with SFM and SEM. Physical characteristics of the homopoymers which are important for the resulting microphase separation and structuring in thin films are summarized in Table 5.2.

Table 5.1: *Thickness dependent Morphologies of investigated BVT Triblock Terpolymers*

Polymer [a]	**PDI** [b]	characteristic film thickness h [nm]			
		h_1	h_2	h_3	h_4
$\mathbf{B_{14}V_{18}T_{68}}^{165}$	1.03	35 ± 2[c]	77 ± 4[c]	97 ± 2[c]	112 ± 2[c]
HO-$\mathbf{B_{14}V_{18}T_{68}}^{165}$	1.10	46 ± 4[d]	71 ± 4[d]	92 ± 1[d]	119 ± 4[d]
$\mathbf{B_{53}V_{24}T_{23}}^{85}$	1.02	46 ± 3[e]	65 ± 4[e]	×[n.m.]	129 ± 6[e]
HO-$\mathbf{B_{53}V_{24}T_{23}}^{85}$	1.05	47 ± 2[f]	72 ± 3[f]	88 ± 3[f]	155 ± 5[f]

[a] Subscripts represent weight fractions of the respective block (in weight %); the superscript denotes the total weight-average molecular weight M_w in kg/mol as determined by SEC in combination with ^{1}H-NMR; [b] Polydispersity determined via SEC. M_w=weight-average molecular weight; M_n=number-average molecular weight; the increase for the modified block terpolymers results from partial interactions with the column material; [c] asymmetric three-component perforated lamella (DPL); [d] hybrid morphology; [e] lamellae; [n.d.] not determined; [f] sponge-like porous morphology

All studied films were prepared by gradient coating from chloroform solutions and annealed for 100 h in chloroform vapor in a temperature controlled cell.

Table 5.2: *Glass Transistion Temperatures of Block Components*

Polymer	T_g [°C] [Gol99]
1,2-polybutadiene	-16
poly(2-vinylpyridine)	104
poly(*tert*-butyl methacrylate)	125 - 130

Thin film phase behavior of $B_{14}V_{18}T_{68}$[165]. The present investigation of this polymer was motivated by the studies on poly<u>s</u>tyrene-*block*-poly(2-<u>v</u>inylpyridine)-*block*-poly(<u>*t*</u>*ert*-butyl methacrylate) (SVT) thin film by Ludwigs et *al.* and all who discovered a thermodynamically stable, three-compartment perforated lamella morphology (PL) representing a promising structure for the preparation of composite membranes. However, all three compartments of SVT are in a glassy state at room temperature which complicates further processing of a thin nanostructured film. Moreover, the observed terrace formation is likely to restrict the separation efficiency of a membrane 'skin' which should possess a homogenous thickness. For this reason, the rigid polystyrene block was replaced by the soft and flexible polybutadiene compartment resulting in BVT block terpolymers [Spe07].

Here we investigated films with thicknesses, Δh, in the range of 35–112 nm. The solvent-annealed samples showed smooth surfaces without any terraces or dewetting artifacts. Figure 5.2 displays a typical 3D-SFM topography image of BVT microstructured films where the bright, mesh-like areas consisted of the two glassy compartments (P2VP, P*t*BMA). The dark round objects represent indentations resulting from the soft PB block (see Table 5.2). A more detailed discussion can be found elsewhere [Spe07].

Removing of the minority compartment via ozonolysis failed due to the harsh conditions necessary for ozonolytic cleavage. Moreover, a detailed investigation of this structure by quasi *in-situ* (QIS) SFM nanotomography demonstrated that the PB block does not penetrate through the whole film (which is a prerequisite for a membrane template), and rather wets the free air surface, whereas P2VP is specifically attracted to the polar silicon substrate (schematic in Figure 5.2 [Spe09]). The resulting morphology has been classified as a distorted three-component perforated lamella (DPL) phase, which is deformed under the strong influence of the surface tensions of the single compartments [Spe09]. The fact that the surface pattern in Figure 5.2 is observed at all studied film thickness indicates that the identified DPL is a surface reconstruction.

Thin film phase behavior of HO-$B_{14}V_{18}T_{68}$[165]. Hydroboration of the PB block was

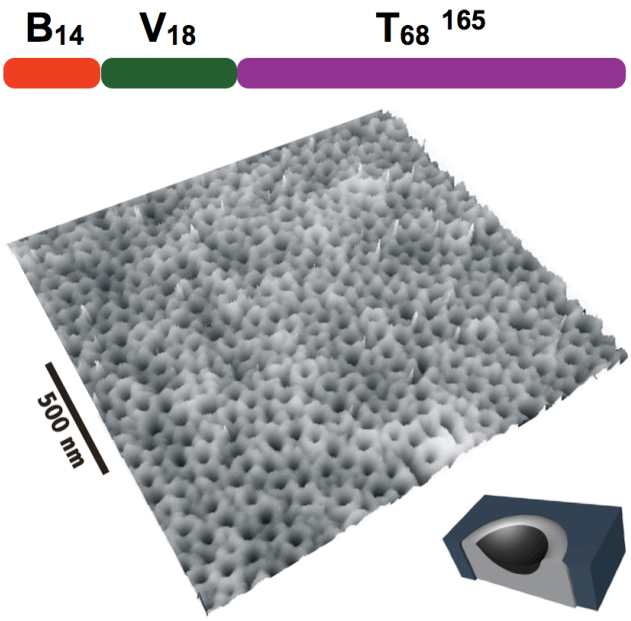

Figure 5.2: *The sketch on top illustrates the polymer composition in dependence of the weight fractions (subscripts) and the total M_n in $\frac{kg}{mol}$. The 3D-SFM height image of a $B_{14}V_{18}T_{68}{}^{165}$ thin film ($\Delta z = 10$ nm) displays a regular mesh-like morphology. The bright areas consist of the two glassy components (P2VP, PtBMA) whereas the dark regions correspond to the soft polybutadiene block which is distorted during SFM tapping. The schematic inset, based on quasi in-situ nanotomography SFM investigations, indicates the asymmetric distorted three-component perforated lamella (DPL) morphology [Spe09].*

performed with the idea to hydrophilize the block and to increase its surface tension in order to reduce the segregation of the PB to the free surface. Upon solvent annealing, gradient films with a thickness in the range of 46-120 nm had a glassy wetting layer prohibiting the imaging of subjacent structures. The film surface was smooth with no topographic features. This observation indicated a film stability towards dewetting [Geo03] which can be explained by high molecular weight of HO-$B_{14}V_{18}T_{68}{}^{165}$ (i.e. high viscosity) and to the strong interaction of the wetting block with the substrate. According to the same arguments, the terrace formation in thin films from BC with a molecular weight more than 100 kg/mol is typically not achieved on a scale of the experimental equilibration times, as the structures are kinetically trapped into metastable states [Tsa07].

Additional SEM measurements revealed a hybrid structure which appeared after the destruction of the top layer by the electron beam: round shaped and elongated objects in Figure 5.3 A can be identified with up-standing and lying cylinders embedded into the PtBMA matrix (destroyed by the electron beam). In contrast to the initial $B_{14}V_{18}T_{68}{}^{165}$, no phase separation between the hydroxylated PB and P2VP compartment could be seen. Merging

both minority blocks results in a volume fraction of 32 : 68 (HO-PB/P2VP : P*t*BMA) which confirmed the microphase separated cylindrical phase. Detailed analysis suggested asymmetric wetting conditions of these films. While the PtBMA majority block wets the free surface, the HO-PB/P2VP combined minority phase is attracted by the silicon substrate. Since due to the volume constrains and the surface energy competition, the minority phase is not able to completely cover the substrate, the wetting layer is randomly perforated with the electron-beam sensitive PtBMA matrix compartment (Figure 5.3 B). The inset in Figure 5.3 presents a schematic of a nanotomographic volume reconstruction of a unit cell structure [Spe09]. A desired outcome is that due to the extended interface within the bulk film combined with the nanoporosity at the substrate interface, these thin films may be used as thin film composite membrane templates for selective adsorption or filtering processes.

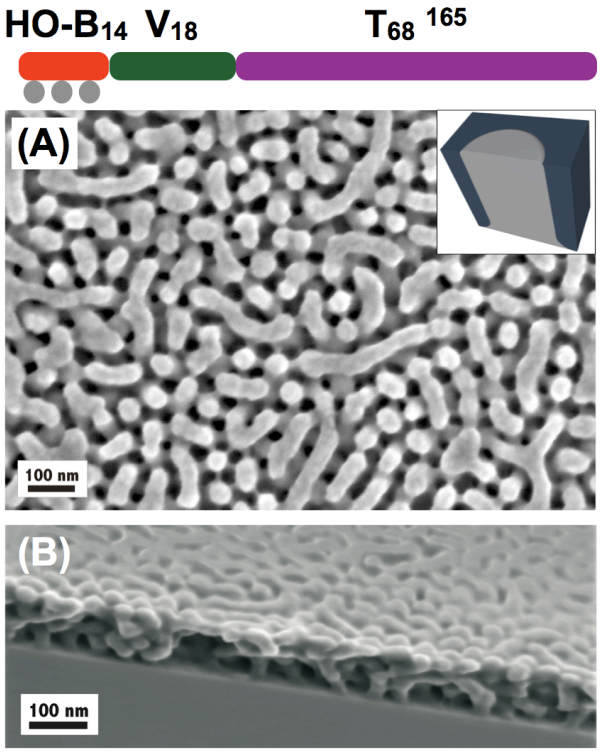

Figure 5.3: *On top, the composition of HO-$B_{14}V_{18}T_{68}{}^{165}$ is schematically illustrated.* ***(A)*** *After the selective degradation of PtBMA during SEM measurements, a hybrid morphology in consequence of asymmetric wetting behavior is revealed. The cross-section* ***(B)*** *points up the network-like microphase separation of the BC system.*

Thin film phase behavior of $\mathbf{B_{53}V_{24}T_{23}}^{85}$. Further design of the microphase separation in ABC block terpolymers was achieved by supplemental improvement of the film processing and its resulting mechanical and resistance stability. Decreasing the total molec-

ular weight of a block copolymer (to 85 kg/mol in our case) shortens the equilibration and processing time, and further miniaturizes the characteristic dimensions of a microphase-separated structure. To facilitate the large area transfer to support membranes, the volume composition of this novel triblock terpolymer was inverted in a way that now the PB compartments forms the majority phase.

Thickness gradients were prepared in the range of 46-129 nm. The annealing time could be reduced to 24 hours. Under longer annealing intervals, the equilibrated morphologies did not show significant changes. A typical height SFM image of $B_{53}V_{24}T_{23}^{85}$ microphase separated structures (shown in Figure 5.4 A) displays the microscopically smoothly featureless surface with typical surface relief structures (round shaped holes with a step height of 67 nm). Terrace formation indicates that the annealing time was sufficient to bring the structures into thermal equilibrium. In bulk, $B_{53}V_{24}T_{23}^{85}$ forms lamella with a dimension of 74 nm (see Figure 5.4 B), and obviously, similar microphase separation is preserved under confinement to a thin film (see Figure 5.4 C).

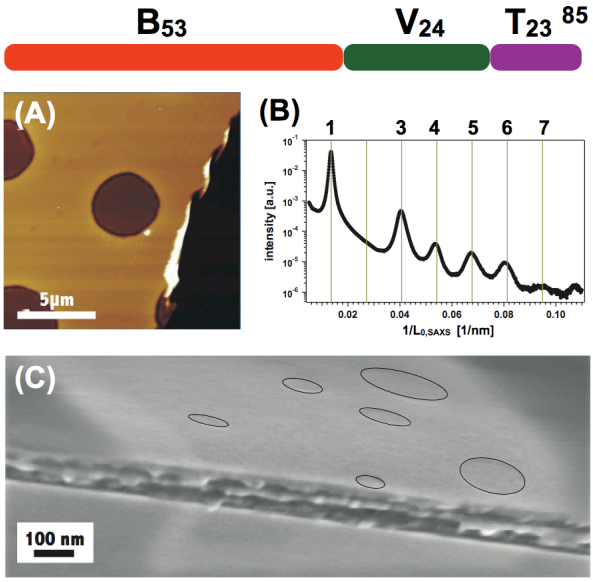

Figure 5.4: *On top, the polymer composition is displayed schematically.* ***(A)****SFM height image ($\Delta z = 150$ nm) illustrates thermal equilibrated structures in terms of terraces. The lamellar separation is confirmed by SAXS measurements* ***(B)*** *in bulk (slowly dried from chloroform solution). Supplementary, the single layers are cleary distinguishable in the cross-section shown in* ***(C)****. As a guide to the eye, the marked borders indicate the terrace formation.*

The in-plane orientation of lamella is dominated by the preferential attraction of the PB block both to the free surface and to the substrate. Although the annealing time is significantly reduced, the in-plane lamella orientation presents little interest in membrane

technology.

Thin film phase behavior of HO-$B_{53}V_{24}T_{23}$[85]. The surface tension and the polarity of the majority PB compartment was selectively adjusted by introducing hydroxyl groups, and films with a thickness in the range of 47-155 nm were investigated. The whole thickness gradient displayed a continuous featureless film with a glassy top layer (similar to HO-B), however without terraces (inset in Figure 5.5 A).

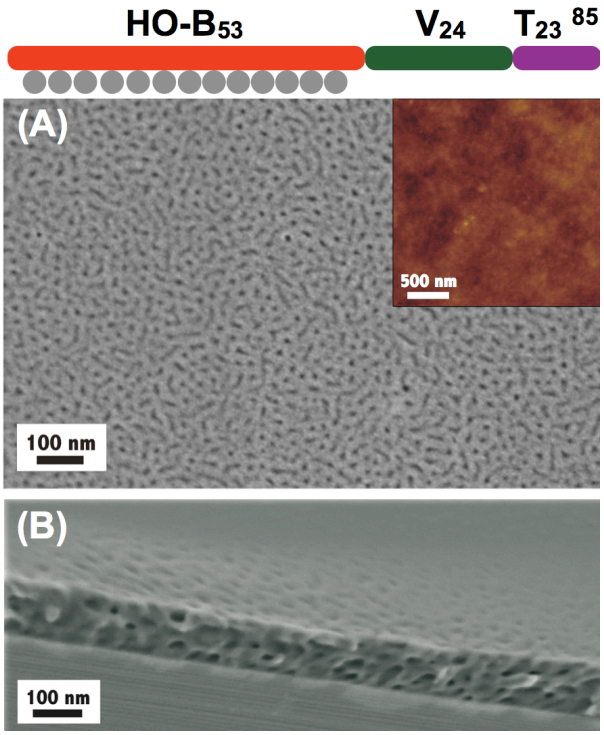

Figure 5.5: *On top, a schematic displays the polymer composition. After the annealing procedure for HO-$B_{53}V_{24}T_{23}$[85], a stiff top layer was found which could not be tapped through by SFM (inset). After the degradation of P*t*BMA during SEM measurements, a porous network was detected* ***(A)****. The cross-section* ***(B)*** *supplements the impression of a sponge-like morphology.*

After SEM measurements, the upper top smooth layer from P*t*BMA appeared to be removed revealing a mesh-like matrix consisting of the HO-PB and P2VP compartments (Figure 5.5 A). The nanoporous structures displayed in cross-sectional SEM (Figure 5.5 B) represent a stable pattern which was detected over the whole studied film thickness. We note that the resulting microphase separation represents the inverse morphology of the $B_{14}V_{18}T_{68}$[165] which was presented above. Successful removal of the minority compartment from both free surface and cavities of the mesh-like pattern results in a sponge-like porous structure. Such nanostructured films satisfy conditions for a large area transfer to e.g. track-etched PET membranes. Moreover, these 'skin' layers possess percolating pores

with a potential for chemical functionalization. Further work will focus on the profound investigation of channel geometry in HO$-B_{53}V_{24}T_{23}$[85] by QIS SFM nanotomography. After the transfer to various support materials, permeability and flux measurements will be performed.

5.4 Conclusion

We have successfully demonstrated the directed influence of selective, oxidative hydroboration on the microphase separation behavior in BVT thin films. Due to their high molecular weight, the studied BVT triblock terpolymers proved to be stable towards dewetting under controlled solvent annealing treatment. The presence of a third compartment facilitates the formation of nanoscale pores. Finally, we fabricated two types of nanoporous films. Due to thickness independence and high homogenity of the pattern over macroscopical areas, both morphologies are highly promising for applications in composite membrane technology.

5.5 Acknowledgement

This research was supported by the VolkswagenStiftung project 'Complex Materials'. A. Sperschneider thanks Heinz Kreijtschi for the technical support concerning the CAD constructions.

5.6 Supporting Information

^{1}H-Nuclear Magnetic Resonance Spectroscopy (^{1}H–NMR). The spectra for all BVT triblock terpolymers were recorded on a Bruker 250 AC spectrometer using either $CDCl_3$ or THF-d_8 as solvent and tetramethylsilane (TMS) as internal standard.

Fast-Fourier Infrared Spectroscopy (FT–IR). For the investigation of the performed hydroboration of the polybutadiene compartment, we used FT–IR for both $B_{53}V_{24}T_{23}{}^{85}$ triblock terpolymer and the hydroxylated one. The spectra were acquired with a Perkin-Elmer, Spectrum One FT-IR spectrophotometer equipped with an ATR sampling unit.

Results for ^{1}H–NMR and FT–IR ^{1}H–NMR of $B_{14}V_{18}T_{68}{}^{165}$ ($CDCl_3$) : δ (ppm) = 8.3–6.3 ((2-vinylpyridine units), 5.5–5.2 (1H: 1,2-PB and 2H: 1,4-PB), 4.9–4.7 (2H: 1,2-PB), 2.3–0.75 (backbone).

^{1}H–NMR of $B_{53}V_{24}T_{23}{}^{85}$ ($CDCl_3$) : δ (ppm) = 8.3–6.3 (2-vinylpyridine units), 5.5–5.2 (1H: 1,2-PB and 2H: 1,4-PB), 4.9–4.7 (2H: 1,2-PB), 2.2–0.75 (backbone). FT–IR (freeze-dried polymer), ν (cm^{-1}) : 3356 (OH), 1723 (C=O vibration of ester), 1639 (C=C), 1392/1366 (tBMA), 1254/1135 (C-O vibration of ester), 1050 (vibration of C-O-H), 993/907 (C=C), 848 (tert-butyl group), 746 (vinyl configuration PB).

^{1}H–NMR of HO$-B_{14}V_{18}T_{68}{}^{165}$ ($CDCl_3$) : δ (ppm) = 8.2–6.3 (2-vinylpyridine units), 3.7–3.6 (R-CH_2-O), 2.2–0.75 (backbone).
^{1}H–NMR of HO$-B_{53}V_{24}T_{23}{}^{85}$ ($CDCl_3$) : δ (ppm) = 8.2–6.3 (2-vinylpyridine units), 3.5–3.4 (R-CH_2-O), 2.2–0.75 (backbone). FT–IR (freeze-dried polymer), ν (cm^{-1}) : 3343 (OH), 1723 (C=O vibration of ester), 1639 (C=C), 1392/1366 (tBMA), 1254/1135 (C-O vibration of ester), 1050 (vibration of C-O-H), 848 (tert-butyl group), 746 (vinyl configuration PB).

For steric reasons, the 1,2 vinyl groups of the polybutadiene will be preferred for selective, oxidative hydroboration reaction whereas the 1,4 PB remains [Tou08]. Thus, initially, the ratios of 1,2 PB and 1,4 PB were determined by ^{1}H–NMR. $B_{14}V_{18}T_{68}{}^{165}$ showed a distribution of 87 % : 13 % (1,2 PB : 1,4 PB). For the second triblock terpolymer, $B_{53}V_{24}T_{23}{}^{85}$, we yielded comparable results, namely 88 % for 1,2 PB and 12 % 1,4 PB what is expected for the anionic polymerization in polar solvents.
After the final oxidation step, an increase in PDI occured. This is most probable due to adsorption on the column caused by the introduction of polar -OH functionalities. Moreover, a slight increase in the elution volume of both hydroxylated BVT triblock terpolymers was detected. This observation is well known and caused by the additional intramolecular H–bondings leading to a reduced gyration radius and subsequently, to a decreased hydrodynamic volume [Mao97, Tuz93]. For a more precise determination of the modification degree, ^{1}H–NMR were recorded. As an example, Figure 5.6 shows the ^{1}H–NMR for

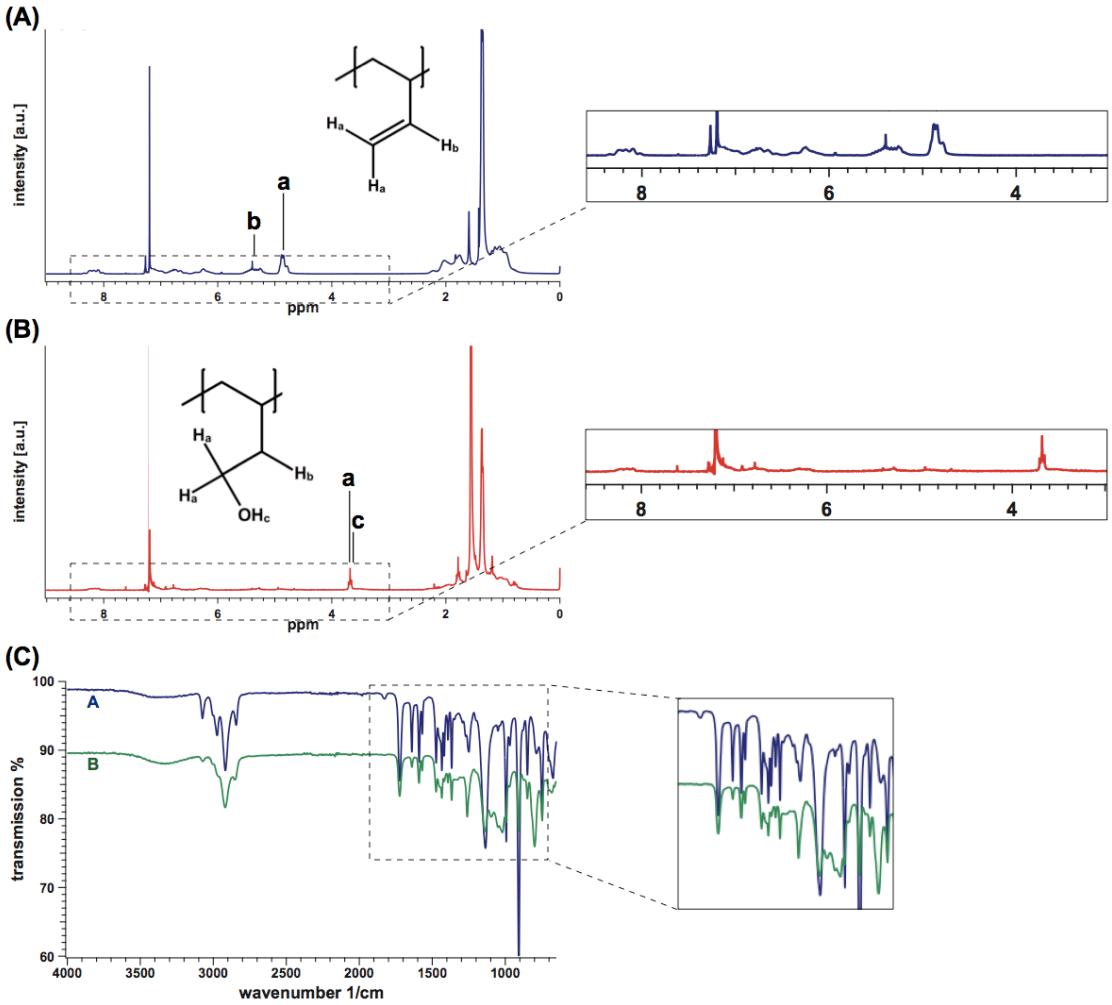

Figure 5.6: *^{1}H–NMR spectra of $B_{14}V_{18}T_{68}$[165] prior to **(A)** and after **(B)** the selective oxidative hydroboration reaction. In **(C)** the corresponding IR spectra is shown (A prior to and B after hydroboration reaction).*

$B_{14}V_{18}T_{68}$[165] before (A) and after hydroboration (B). Both signals of the PB vinyl group, 5.5 – 5.2 ppm and 4.9 – 4.7 ppm, decreased significantly. An additional signal in the range of 3.7 – 3.6 ppm arised revealing the hydroxylated 1,2 PB compartment. By calculating the peak ratio, we determined a successful degree of modification of 69 %. Furthermore, the degree of modification of $B_{53}V_{24}T_{23}$[85], determined by ^{1}H–NMR (not shown here), is 71 %.

The FT–IR spectra shown in Figure 5.6 C before (A) and after hydroxylation (B) supplements the results of the hydroboration reaction. Three main changes in the spectra were observed. In Figure 5.6 C (A) a slight peak at 3356 cm^{-1} representing the OH band is visible. This fact is not surprising because of the thin water layer on both instrument and polymer film. Presumably, the polymer tends to absorb air moisture resulting also in the displayed signal. However, after hydroboration, this OH band increased. In addition, both signals at 993 cm^{-1} and 907 cm^{-1} indicating the vinyl moiety vibration decreased noteworthy whereas in contrast the intensity at 1050 cm^{-1} representing the new vibration (C–O–H) of the hydroborated PB compartment expanded.

Combinatorial Mapping For achieving a continuous thickness gradient, we used combinatorical mapping with the aid of gravity. In contrast to earlier works of Ludwigs et *al.* [Lud05b], we did not use a motor-based set-up.

The desired film thickness gradient can be adjusted by variation of the polymer concentration. In Figure 5.7, a CAD scheme displays the thickness gradient preparation. The sample (2, red) is placed onto a ball-bearing table (1). After the adjustment (horizontally, vertically) of the glass blade (3) by several adjustment screws (4, 6), the polymer solution is applicated and the stopper (5) is released resulting in a constant acceleration in $\overrightarrow{F}$-direction.

For each sample, a polished silicon wafer (1 cm × 7 cm) was stabilized on a fixed ball bearing table equipped with a small winch and a specific weight of 130 g. Subsequently, a glass blade was adjusted to a tilt of approximately 8° and a substrate distance of 0.5 mm. Afterwards, 30 μL of 7 g/L and 10 g/L, respectively, concentrated chloroform polymer solutions were injected between the interspace wafer-glass. With releasing of the fixation, the ball bearing table experienced a constant acceleration and spreading the solution resulting in a defined thickness gradient. We obained film thickness differences between 35 and 155 nm.

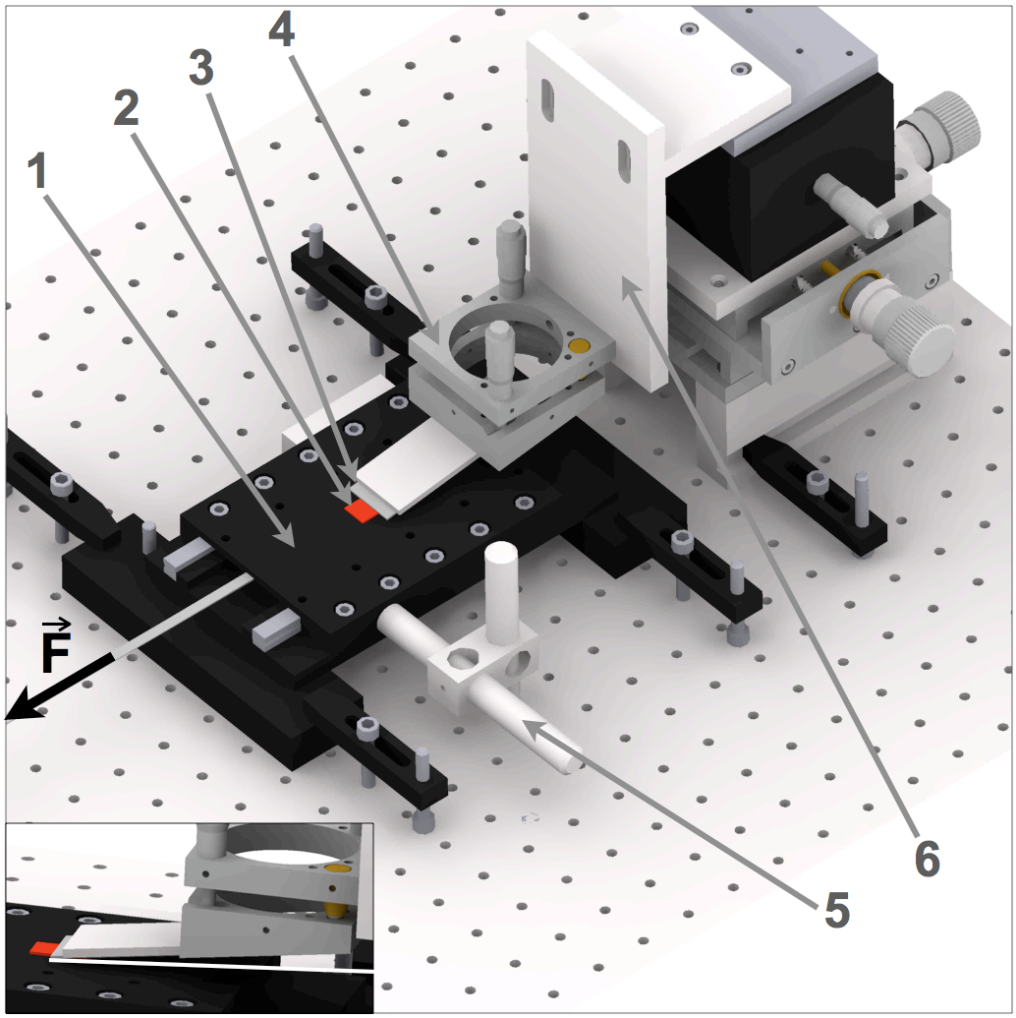

Figure 5.7: *CAD scheme displays the thickness gradient preparation. With the sample (2, red) placement onto the ball-bearing table (1), the glass blade (3) can be adjusted in both horizontally and vertically direction (4, 6). Afterwards, the polymer solution is applicated and, subsequently, the stopper (5) may be released resulting in a constant acceleration of the ball-bearing table where a chosen weight is placed. The thickness gradient is influenced by the acceleration, the concentration of the polymer solution and the tilt angle of the glass blade (inset).*

References

[Ban06] J. Bang, S. H. Kim, E. Drockenmuller, M. J. Misner, T. P. Russell, and C. J. Hawker. *Journal of American Chemical Society*, **128**(23), 7622–7629 (2006)

[Bro79] H. C. Brown and R. A. Coleman. *Journal of Organic Chemistry*, **44**(13), 2328–2329 (1979)

[Chu88] T. C. Chung, M. Raate, E. Berluche, and D. N. Schulz. *Macromolecules*, **21**(7), 1903–1907 (1988)

[Geo03] M. Geoghegan and G. Krausch. *Progress in Polymer Science*, **28**(2), 261–302 (2003)

[Gol99] T. Goldacker. *Dissertation - Überstrukturen in Mischungen aus Blockcopolymeren*. Bayreuth (1999)

[Guo06] S. W. Guo, J. Rzayev, T. S. Bailey, A. S. Zalusky, R. Olayo-Valles, and M. A. Hillmyer. *Chemistry of Materials*, **18**(7), 1719–1721 (2006)

[Joo06] W. Joo, M. S. Park, and J. K. Kim. *Langmuir*, **22**(19), 7960–7963 (2006)

[Kra02] G. Krausch and R. Magerle. *Advanced Materials*, **14**(21), 1579–1583 (2002)

[Lee88] J.-S. Lee, A. Hirao, and S. Nakahama. *Macromolecules*, **21**(1), 274–276 (1988)

[Lud03] S. Ludwigs, A. Böker, V. Abetz, A. H. E. Müller, and G. Krausch. *Polymer*, **44**(22), 6815–6823 (2003)

[Lud03a] S. Ludwigs, A. Böker, A. Voronov, N. Rehse, R. Magerle, and G. Krausch. *Nature Materials*, **2**, 744 (2003)

[Lud05] S. Ludwigs, K. G., R. Magerle, A. V. Zvelindovsky, and G. J. A. Sevink. *Macromolecues*, **38**(5), 1859–1867 (2005)

[Lud05a] S. Ludwigs, K. Schmidt, and G. Krausch. *Macromolecules*, **38**(6), 2376–2382 (2005)

[Lud05b] S. Ludwigs, K. Schmidt, C. M. Stafford, E. J. Amis, M. J. Fasolka, A. Karim, R. Magerle, and G. Krausch. *Macromolecules*, **38**(5), 1850–1858 (2005)

[Mao97] G. Mao, J. Wang, S. Clingman, C. Ober, J. Chen, and T. E.L. *Macromolecules*, **30**(9), 2556–2567 (1997)

[Oku06] A. Okumura, Y. Nishikawa, and T. Hashimoto. *Polymer*, **47**(22), 7805–7812 (2006)

[Par03] C. Park, J. Yoon, and E. L. Thomas. *Polymer*, **44**, 6725–6760 (2003)

[Ruo99] J. Ruokolainen, G. ten Brinke, and O. Ikkala. *Advanced Materials*, **11**(9), 777–780 (1999)

[Saw96] L. C. Sawyer and D. T. Grubb. *Polymer microscopy*. Chapman & Hall, London, 2nd edition (1996)

[Seg05] R. A. Segalman. *Materials Science and Engineering R-Reports*, **48**(6), 191–226 (2005)

[Smi92] D. R. Smith and D. J. Meier. *Polymer*, **33**(18), 3777–3782 (1992)

[Smi01] A. P. Smith, J. F. Douglas, J. C. Meredith, E. J. Amis, and A. Karim. *Physical Review Letters*, **8701**(1), 015503 (2001)

[Spe07] A. Sperschneider, F. Schacher, M. Gawenda, L. Tsarkova, A. H. E. Müller, M. Ulbricht, and J. Köhler. *Small*, **3**(6), 1056–1063 (2007)

[Spe09] A. Sperschneider, M. Hund, A. H. E. Müller, and A. Böker. *Nano Letters*, **submitted** (2009)

[Tou08] A. Touris, K. Kostakis, S. Mourmouris, V. Kotzabasakis, M. Pitsilaklis, and N. Hadjichristidis. *Macromolecules*, **41**(7), 2426–2438 (2008)

[Tsa07] L. Tsarkova. *Nanostructured Soft Matter: Experiment, Theory, Simulation and Perspectives*. Springer Verlag, Heidelberg, ed. a.v. zvelindovsky edition (2007)

[Tuz93] Z. Tuzar and R. Kratochvil. *Surface and Colloid Science*. Springer Verlag, vol. 15 edition (1993)

[Ulb06] M. Ulbricht. *Polymer*, **47**, 2217–2262 (2006)

[Yan06] S. Y. Yang, I. Ryu, H. Y. Kim, J. K. Kim, S. K. Jang, and T. P. Russell. *Advanced Materials*, **18**(6), 709–712 (2006)

Chapter 6

Going beyond the Surface: Revealing Complex Block Copolymer Morphologies with 3D SFM

ABSTRACT

We report on the quasi in–situ *SFM nanotomography which proved to be a key method to effectively obtain a three-dimensional (3D) microdomain structure of a complex ABC triblock morphology. As an example, we studied polybutadiene*-block-*poly(2-vinylpyridine)*-block-*poly(*tert-*butyl methacrylate) (BVT) thin triblock terpolymer films. We realized a controlled erosion of the material by using low-pressure plasma etching inside the SFM with constant high depth resolution down to 1.0 nm. The 3D reconstruction provides insights into the structural behaviour in very thin volume elements reavealing a perforated lamella morphology distorted by surface fields. In addition, we studied in a first step the strong effect of hydroboration on thin film morphologies.*

6.1 Introduction

In recent years, nanotomography turned out to be a promising method to image three-dimensional complex and fragile nanostructures. With the technical advances in the field of microscopy and image processing, nowadays reliable three-dimensional reconstructions of nanoscale objects are feasible representing new challenges for data analysis.

A distinction is drawn between tomography methods based on tilt-series (nondestructive) or on ultrathin sections of the sample (destructive). Nondamaging approaches are achieved using X-ray microscopy [Had94, Che08, Pet08, Par08, Hit08], transmission electron microscopy (TEM) [Fra00, Mid03, Jin00, Rad97] and atom probe field ion microscopy (APFIM) [Mil96]. Moreover, for inorganic bulk samples, such as metals, biominerals or ceramics, focused-ion-beam (FIB) tomography [Dun99, Yeo07, Tom98, Hol06] is commonly used. Harrison et *al.* developed a procedure for layer-by-layer imaging of block copolymers by using scanning electron microscopy (SEM) [Har98, Har98a]. A combination of ultramicrotoming with scanning force microscopy (SFM) suggested by Efimov et *al.* is limited to a step-size of at least 20 nm due to the ultramicrotome setup [Efi07].

Thin film investigations of polybutadiene-*block*-poly(2-vinylpyridine)-*block*-poly(*tert*-butyl methacrylate) (BVT) triblock terpolymers revealed the significant influence of interface interactions between both polymer-substrate and polymer-air leading to a variety of thin film morphologies [Spe07]. Further detailed investigations of these morphologies will be presented in this paper employing a three-dimensional reconstruction method based on scanning force microscopy (SFM).

We basically use nanotomography, a method for volume imaging based on scanning force microscopy (SFM), established by Magerle [Mag00]. This technique combines the erosion of thin specimen layers with the subsequent SFM imaging of each newly exposed surface, thus providing topography information supplemented by the corresponding materials property information which can be detected for instance by SFM tapping mode imaging. With the combination of both, a real-space volume image of the sample can be reconstructed [Mag00, Mag02]. A suitable ablation method for various materials, especially for sensitive polymer materials, is the low-pressure (LP) plasma treatment technique which represents a well established and flexible method since process parameters like gas composition, process pressure and rf power can be adjusted with high accuracy. Thin sample layers can be successively removed in a precise and reproducible way creating neither noteworthy thermal load nor mechanical stress to the specimen [Cha96, Har98]. Moreover, problems encountered in wet chemical etching such as residual solvent on the surface or swelling effects are avoided.

Consequently, the LP plasma technique is a method extensively used for the modification of polymer surfaces, in particular in combination with nanotomography shown by Magerle [Mag00] and Konrad et *al.* [Kon00]. Considering the procedures described in ref. 17 and 21, one has to note that sample investigation by SFM and the plasma apparatus have been used as separated systems. Those so-called *ex-situ* LP plasma treatments lead to time consuming processes for relocating the same sample spot resulting generally in a low performance and in a reduced quantitiy and quality of the SFM data.

The development of the quasi *in-situ* (QIS) SFM [Hun07, Hun], a novel SPM design, solves these problems by separating the sample treatment and the scanning force microscopic examinations temporally and spatially. Thus, experimental limitations of state-of-the-art *in-situ* scanning techniques are removed and furthermore, LP plasma or other aggressive treatments, which are impossible to perform while scanning inside the SFM, are enabled. The quasi *in-situ* working principle was also successfully used to follow the structural evolution of lamellar block copolymers under solvent vapor treatment in presence of high electric fields [Ols06].

6.2 Methods

Quasi *in–situ* (QIS) SFM Nanotomography. Our first results of the quasi *in-situ* SFM nanotomography of two different BVT triblock terpolymer thin films are reported here. The quasi *in-situ* setup utilizes a modified commercial SFM (Dimension^{TM} 3100 equipped with a NanoScope IV SPM controller, NanoScope software including the lithography software option and a hybrid XY closed-loop scanner, all from Vecco Instruments Inc.). A detailed description of the basic setup is given elsewhere [Hun07, Hun]. In this work, the used system additionally features an automatic tip/sample separation (movements of the z-stage of 4.8 mm) with the help of a NanoScript^{TM}. Moreover an automatic and triggered grounding of the sample during scanning was implemented. The plasma etching was performed with a rf power of about 3 W at a process pressure of 5 mbar (atmospheric air). Each of the SFM data sets was acquired with a specific SFM tip (OMCL-AC160TS, Olympus, Japan) operating in TappingMode^{TM}.

Afterwards, the obtained data sets were post-processed using a bunch of self-developed stand alone command-line programs and suitable bash scripts in order to perform image registration and 3D image reconstruction according an voxelization algorithm. The produced 3D image data was further processed and visualised with commercial AMIRA software (Visage Imaging Inc., Carlsbad, USA). The details of the image processing workflow are

described in the supporting information.

BVT Triblock Terpolymers. In this study, we investigated a $B_{14}V_{18}T_{68}{}^{165}$ triblock terpolymer which was synthesized via sequential living anionic polymerization [Spe07] (the subscripts represent the weight fractions of the respective block in weight % whereas the superscript denotes the total average molecular weight in kg/mol). An additional polymer variation was achieved by selective oxidative hydroboration of the polybutadiene compartment resulting in an introduction of a hydroxyl group to the C=C double bonds (according to Refs. [Chu88, Bro74, Mao97, Bök00]). The average modification degree amounts to 69 %.

Thin film preparation. For sample preparation, $B_{14}V_{18}T_{68}{}^{165}$ and HO-$B_{14}V_{18}T_{68}{}^{165}$ polymer thin films were spin-cast from 5 mg/mL and 10 mg/mL chloroform solutions, respectively, onto polished silicon wafers (5 mm × 5 mm). For equilibration of the microdomain structures, the chain mobility was significantly improved by controlled solvent vapor treatment at a chloroform vapor saturation of 80 % for 72 h. To ensure reproducibility, the developed morphologies were quenched with a constant flow of pure dried air.

6.3 Results and Discussion

Determination of the etching rate. Detailed knowledge of the etching behavior of the complex polymers studied here, is a pre-requisite for a reliable 3D reconstruction. The thickness of the removed layers is a critical parameter in the reconstruction algorithm (denoted as product n<d> [Mag00] where n is the number of layers and d is the constant thickness of the removed layer). The calculated thickness of the removed layer determines the surfaces S_n on which the property P_n is measured (z_n(x,y) - n<d>) [Mag00]. In particular, if the etched material consists of several polymer compartments, it is necessary to study the film thickness dependence in detail to avoid errors in the calculation of the 3D reconstruction. We note that only in the simplest case the parameter <d> is constant. Consequently, we use the QIS-SFM to study the film thickness dependence versus the cumulative etching time (Figure 6.1) with the aim to calculate the etch rate functions and to determine suitable exposure times for the following nanotomographic experiments.

For the $B_{14}V_{18}T_{68}{}^{165}$ polymer we found a linear decrease of the film thickness as a function of the cumulative etching time. The rate amounts to (-40.7 ± 0.8) nm/min (Figure 6.1 A). In contrast, the hydroxylated polymer (Figure 6.1 B) possesses, as a result of the hydroboration of the polybutadiene compartment, a reduced number of C=C double bonds providing almost no reactive sites for the plasma-induced bonding cleavage. Therefore the determined etch rate (-28.7 ± 1.0) nm/min is smaller than for the pure polymer.

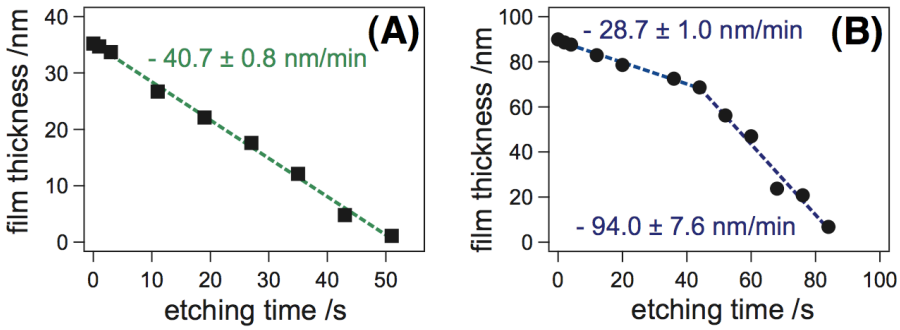

Figure 6.1: *Film thickness plotted as a function of the cumulative etching time including linear fits. The polymer film was fully removed at a defined area of the sample and the height difference between the polymer film and the bare substrate was studied with the quasi in-situ SFM (images not shown).* ***(A)*** *$B_{14}V_{18}T_{68}{}^{165}$. The none-modified polymer shows a linear decrease of the film thickness with a rate of -40.7 ± 0.8 nm/min.* ***(B)*** *HO-$B_{14}V_{18}T_{68}{}^{165}$. A none-linear decrease of the film thickness was approximated by linear fits (-28.7 ± 1 nm/min and -94.0 ± 7.6 nm/min). The cumulative etching time is proportional to the introduced energy into the reaction chamber.*

After 44 s, however, the rate increases significantly up to (-94.0 ± 7.6) nm/min. We assume that the main reason for this behavior is the increase in surface roughness. Due to the subsequent plasma treatments, the surface area increases and therefore the plasma processing is more effective. In addition to the etch rates of the pure and hydroxylated polymers, the rates of the homopolymers were determined and amount to -25 nm/min for polybutadiene (PB), -11nm/min for poly(2-vinylpyridine) (P2VP) and -77 nm/min for poly(*tert*-butyl methacrylate) (P*t*BMA). The high etch rate of P*t*BMA can be explained by its general instability with respect to UV-light or electron beam [Spe07, Saw96].

Quasi *in–situ* SFM nanotomography of $B_{14}V_{18}T_{68}{}^{165}$. Based on these calibration measurements, we decided to use exactly the same etching protocol for our block copolymer samples.

Figure 6.2 a-i displays the results of the successive LP plasma treatment of a $B_{14}V_{18}T_{68}{}^{165}$ polymer thin film. In order to resolve the surface changes, especially while removing the very first material layers, we started with short etching times resulting in a controlled material ablation down to 1 nm. In order to increase time efficiency, we etched the polymer film within nine processing steps by removing 5.4nm thin layers successively with a constant etch rate of (-40.7 ± 0.8) nm/min (Figure 6.1 A). In Figure 6.2 a, the sample surface prior to LP plasma treatment is displayed. The topography image reveals coexisting morphologies of dark stripes and dots embedded in a bright matrix. Comprising the corresponding phase image, the information of two phases with divergent mechanical properties is pro-

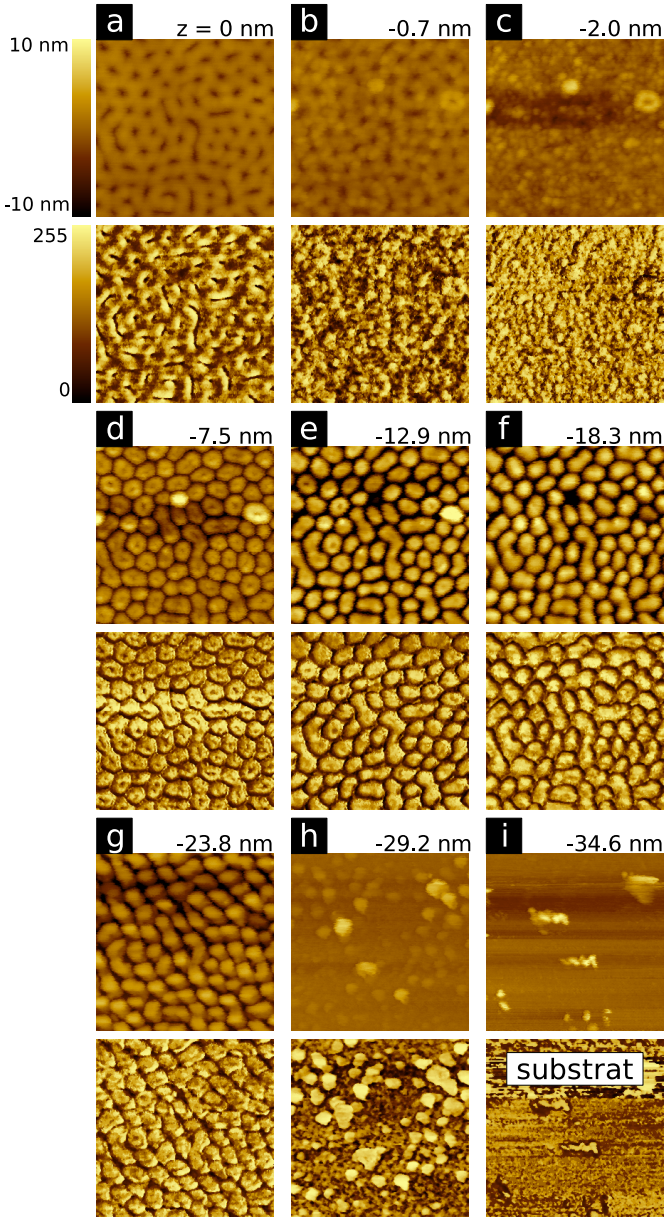

Figure 6.2: *Successive LP plasma etching of a* $B_{14}V_{18}T_{68}{}^{165}$ *triblock terpolymer thin film with the quasi* in-situ *SFM. Cut outs of the post-processed SFM images* (0.73×0.64 μm^2). *Upper rows: topography; lower rows: phase information. The average thickness of the removed material is shown in the top right of the topography images based on the etch rate displayed in Figure 6.1 A. The raw data was acquired by scanning areas of* 3×3 μm^2 *with a resolution of* 1024×1024 *pixels with TappingMode*^{TM} *SFM imaging. The scan area was not changed during data acquisition.*

vided. The polybutadiene compartment which is liquid at room temperature represents the dark color and therefore the soft material. Moreover, the bright and consequently the rigid matrix corresponds to the other glassy polymer blocks (P2VP, P*t*BMA). In addition, due to the similar surface tension γ of PB (24.5 – 32.0 mN/m) [Lee67, Tur95] and P*t*BMA (30.5 mN/m) [Mar07], both compartments are facilitated to segregate to the free surface unlike P2VP which is attracted to the polar silicon substrate. Previous investigations on BVT microphase separation display a comparable thin film behavior [Spe07].

With continuous LP plasma treatment, the hard P*t*BMA block is affected first. Already after 7.5 nm material ablation, the matrix has been almost decomposed (Figure 6.2 d) revealing round shaped objects consisting of a soft PB core surrounded by a stiff P2VP shell. Though, after the next etching step, the phase contrast is partly reduced due to the fast etching rate of PB. With a material erosion of 18.3 nm (Figure 6.2 f) the polybutadiene compartment is completely removed. Thus, we draw the conclusion that this block is located near the free polymer-air interface, not penetrating the whole core-shell objects. Incessant LP plasma treatment leads finally to the stepwise destruction of the P2VP compartment as well.The polymer-substrate interface, however, consists of a wetting layer of poly(2-vinylpyridine) displayed in Figure 6.2 h which has already been shown by Ludwigs

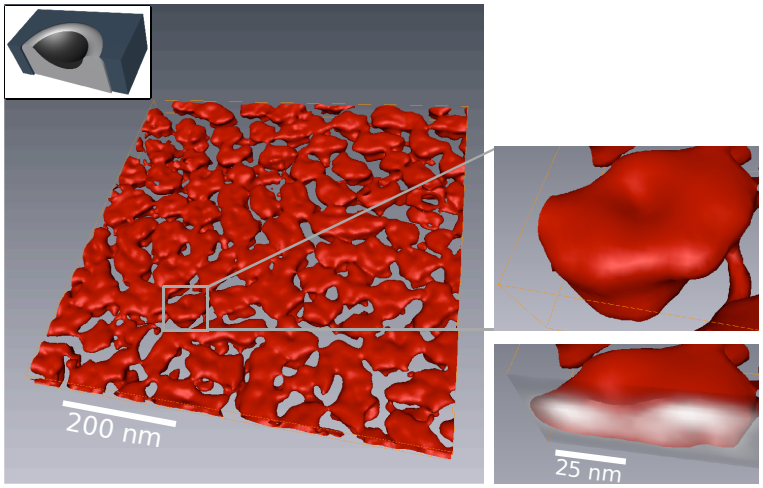

Figure 6.3: *3D reconstruction of the $B_{14}V_{18}T_{68}{}^{165}$ triblock terpolymer thin film based on series of topography and phase images from Figure 6.2 ($250 \times 218 \times 16$ voxels): The P2VP compartment (red) represents the stiff polymer block supplemented by the soft polybutadiene (dark). Here, the matrix material PtBMA is transparent; Inset: schematic drawing representing the microphase separated structure of a single core-shell object embedded in a matrix; the cross-sections clarify the distorted perforated lamella morphology (right images).*

et *al.* for a different PS-*b*-P2VP-*b*-P*t*BMA triblock terpolymer system [Lud03]. The

bare silicon substrate was reached after a material ablation of 34.6 nm.

The phase images and the corresponding height information were used for the three-dimensional reconstruction. Figure 6.3 displays a real-volume reconstruction of the polymer film. Moreover, the inset illustrates schematically the nature of the morphology. The structures result from the strong influence of the polymer surface tensions, as already mentioned. The P2VP middle block tends to preferentially wet the polar silicon substrate while the short PB compartment segregates to the free surface. Thus, a deformed but equilibrated novel morphology was found, which was termed distorted perforated lamella (DPL). Although the investigated thin polymer film is highly sensitive, we succeeded in the reconstruction of a 3D structure from the obtained QIS data yielding insights into the phase separation behavior of the single compartments.

Quasi *in situ* nanotomography of hydroborated $\mathbf{B_{14}V_{18}T_{68}}^{165}$. Figure 6.4 displays results of the successive LP plasma treatment of the HO-$B_{14}V_{18}T_{68}{}^{165}$ polymer. It is clearly seen that the morphology has changed significantly upon hydroxylation.

The surface shown in Figure 6.4 a is rather flat with no recognizable features. In contrast to the pure sample, the hydroxylated polybutadiene compartment does not preferentially segregate to the free surface anymore. Due to the implemented polarity, the surface tension of this block is presumably increased resulting in an almost homogeneous stiff P*t*BMA layer, which cannot be tapped through by the SFM tip. After the first etching step, in both topography and phase images, round objects appear which develop to a microphase separated morphology within additional 2s of treatment and the parallel subsiding of the plasma sensitive P*t*BMA matrix. During this time period, an extremely thin polymer layer of 2.3 nm was removed. As shown in Figure 6.4 c-e, with continuous plasma treatment the structures developped more clearly into round-shaped and elongated objects. For the first seven etching steps, we have found a constant etch rate of -28.7 ± 1.0 nm/min (Figure 6.1 B). After a material ablation of 21.3 nm, a second etchrate of -94.0 ± 7.6 nm/min was approximated. This observation is accompanied by an increasing destruction of the microdomain morphology as shown in the topographic SFM images in Figure 6.4 f-i.

In consequence, the surface roughness increases resulting in an enhanced contact surface for the plasma. Continuous structures were destroyed leading to additional fragments or holes as illustrated in Figure 6.4 h. After a material ablation of 95.3 nm, flat objects remain on the silicon substrate. However, the typical distorted perforated lamella morphology as discussed for $B_{14}V_{18}T_{68}{}^{165}$ thin film, could not be found at any etching step. Due to the hydroxylation of the PB compartment, we detected just one rigid phase consisting of HO-PB and P2VP (bright color) after the decomposition of the matrix. By implementing the

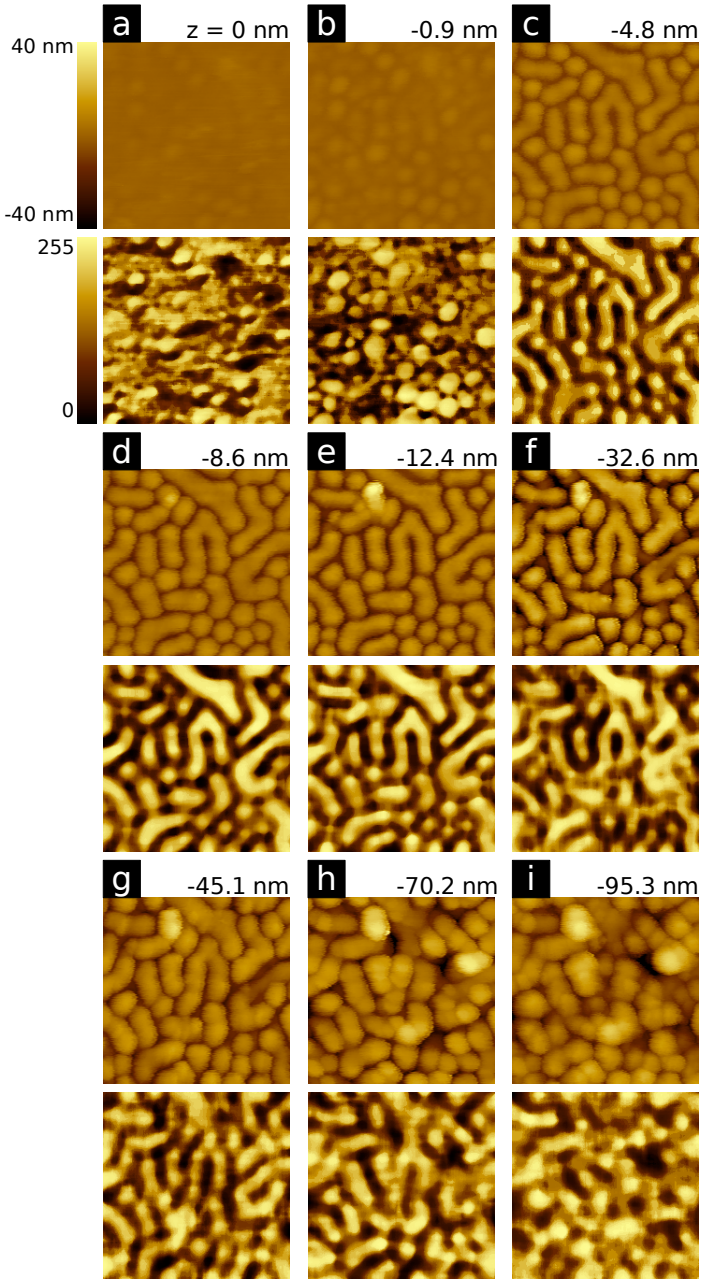

Figure 6.4: *Successive LP plasma etching of a HO-*$B_{14}V_{18}T_{68}{}^{165}$ *triblock terpolymer thin film with the quasi* in-situ *SFM. Cut outs of the post-processed SFM images (*$0.58 \times 0.58\ \mu m^2$*). Upper rows: topography; lower rows: phase information. The average thickness of the removed material is shown in the top right of the topography images based on the etch rate displayed in Figure 6.1 B. The raw data was acquired by scanning areas of* $3 \times 3\ \mu m^2$ *with a resolution of* 1024×1024 *pixels with TappingMode*^{TM} *SFM imaging. The scan area was not changed during data acquisition.*

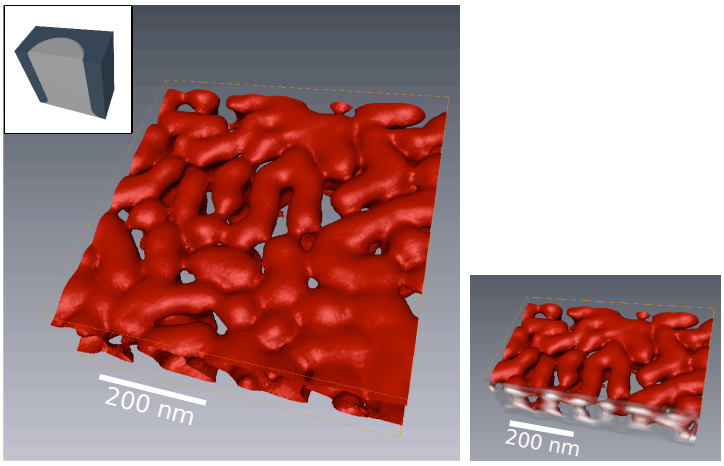

Figure 6.5: *3D reconstruction of the HO-$B_{14}V_{18}T_{68}{}^{165}$ triblock terpolymer thin film based on series of topography and phase images from Figure 6.4 (200×200×36 voxels): The microphase coloured in red is composed of HO-PB and P2VP. Here, the matrix material PtBMA is transparent. The non-linear etching behaviour of the materials was taken into account in the 3D reconstruction; Inset: schematic drawing representing the microphase separated structure of a single round-shaped object embedded in a matrix; the cross-section clarifies the microphase separation behavior (right image).*

hydroxyl group, supplementary intra- and intermolecular hydrogen interactions lead to a reduced microphase separation or even a fully mixed state. Moreover, we expect a shift in the glass transition temperature T_g to higher values resulting in a more glassy state at room temperature. This alteration is accompanied by difficulties in the determination of the material properties by SFM data acquisition. Taking both considerations into account, the decrease of phase information in the SFM measurements can be explained.

For the calculation of the 3D reconstruction, the non-linear etching behavior (seen in Figure 6.1 B) was taken into account. Figure 6.5 displays the reconstructed QIS-SFM data. The round shaped and striped objects penetrate the whole film. The red objects consisting of HO-PB and P2VP seem to wet the polymer-substrate interface partially. The schematic inset in Figure 6.5 represents the microphase separated structure of a single round-shaped object surrounded by a matrix for an improved understanding of the 3D reconstruction.

6.4 Conclusion

In summary, we have shown in a first step that the hydroxylation of the polybutadiene compartment in a BVT triblock terpolymer thin film strongly affects the microphase separation. For $B_{14}V_{18}T_{68}{}^{165}$ we found a distorted perforated lamellae (DPL), round-shaped

objects with a soft indentation embedded in a glassy matrix. With the hydroxylation, we introduced additional polarity via supplementary hydroxyl groups forming presumably intra- and intermolecular hydrogen bonds leading to a reduced microphase separation. Furthermore, with a decrease of the C=C double bonds in the PB block, the glass transition temperature is expected to be shifted to higher values resulting in a glassy state at room temperature for the compartment. Consequently, we observed less distinct differences in materials properties information in SFM phase images. Both effects cause a structural change which could be successfully demonstrated via 3D reconstruction of the SFM data for the two specimen. For the HO-$B_{14}V_{18}T_{68}$[165] polymer film, we solely detected round-shaped and elongated stiff objects after the decomposition of the P*t*BMA matrix.

We present here a high depth resolution QIS-SFM nanotomography procedure circumventing the well known problems of the state-of-the-art *ex-situ* LP plasma treatments (reliability, practicability, manageability). In general, the plasma technique is extremely flexible with respect to the sample treatment. Thus, in the future, this technique will be expanded by using various plasma gases attuned to the specimens' properties. Moreover, the fast growing SPM capabilities realize an improved sensing of material features. Besides, instead of ablating material during the etching treatment, the reverse progression (e.g. plasma deposition process) can be easily achieved with the QIS-SFM setup leading to new insights into the growth of 3D structures. Finally, we note that the quasi *in-situ* SFM used in our experiments has a large potential, which goes significantly beyond the problem studied here.

6.5 Acknowledgement

We thank F. Schacher for the polymer synthesis and H. Schoberth for the fruitful discussions. M. Hund thanks H. Krejtschi (Mechanics, University of Bayreuth), P. Müller and assistants (Mechanical Workshop, University of Bayreuth) and Dr. W. Häfner for the help with the analysis of the cross-correlation algorithm and the integration of his fit algorithm into the software. This project was supported by VolkswagenStiftung in the framework of the project *Complex Materials*. A. Böker acknowledges support by the Lichtenberg-Program of the VW-Stiftung and the SFB481(TP Z2).

6.6 Supporting Information

Our first results of the quasi *in-situ* SFM nanotomography of two different BVT triblock terpolymer thin films are reported here. The quasi *in-situ* setup utilizes a modified commercial SFM (Dimension^{TM} 3100 equipped with a NanoScope IV SPM controller, NanoScope software including the lithography software option and a hybrid XY closed-loop scanner, all from Vecco Instruments Inc.). A detailed description of the basic setup is given elsewhere [Hun07, Hun]. In this work, the used system additionally features an automatic tip/sample separation (movements of the z-stage of 4.8 mm) with the help of a NanoScript^{TM}. Moreover an automatic and triggered grounding of the sample during scanning was implemented. The plasma etching was performed with a rf power of about 3 W at a process pressure of 5 mbar (atmospheric air). Each of the SFM data sets was acquired with a specific SFM tip (OMCL-AC160TS, Olympus, Japan) operating in TappingMode^{TM}.

Post-processing. For a successful reconstruction procedure, the SFM data set passed through standard 2D-image processing tasks like file format conversion, flattening and normalization. Thereby, the developed applications are called from suitable bash scripts. The post-processing of the image data was performed using a self-developed C++ software package, a standard image manipulation toolkit (http://www.imagemagick.org) and a commercial 3D image software (Amira, Visage Imaging Inc., Carlsbad, USA).

The self-developed software consists of small, specialized command-line applications which can be combined to rather complex functionalities by launching them from suitable bash scripts. Another motivation to generate an own software are its tuned functionalities for an effective implementation of controlling a fully automated QIS-SFM which will be described elsewhere. The SFM image series shown in Figure 6.2 and Figure 6.4 were prepared using a SPM software tool (Gwyddion, http://gwyddion.net).

Image registration. For reliable nanotomography, it is indispensable to consider exactly the same area on the sample. The alignment process was performed using rigid image registration based on cross-correlation in spatial domain [Rus02, Man02]. In order to facilitate this process, we implemented the histogram matching technique, whereby a processed image series is produced with each image having approximately the same specified reference histogram [Gon02]. The histogram matched image series was then used in a special script. A first crop command generated a small target image from the very first image of the series. Afterwards, the following command performed cross-correlation by moving the target image to every possible position in the second image of the series. At each location, the cross-correlation value was computed. From this data, the best matching position could be easily extracted and a new current target image was generated. In the

subsequent processing steps, this chain-like computation was repeated resulting in a file holding the best matching coordinates of the target images. An additional application read out this file and produced a bash script containing pairs of commands for every image of the series. To cancel displacements, the first command adds a black margin of suitable size around the image. The displacements were then canceled by performing crop commands with appropriate computed offsets whereas the target position of the first image serves as a reference coordinate.This process is repeated for all images of the series. We note that the used SFM is equipped with a state-of-the-art closed-loop scanner, which drastically reduces image distortions. Non-linear registration methods as described by Scherdel et *al.* [Sch06] are capable to correct also local deformations. The computing time of the cross-correlation could be reduced by taking only cuts of the images or by performing the cross-correlation in frequency domain [Man02].

Tomography computation. A further developed C++ program implemented the 3D reconstruction. In contrast to the algorithm suggested by Magerle [Mag00], the voxelization algorithm used here is capable to take also a nonlinear etching behavior into account (see Figure 6.1 B). For the enhancement of the phase contrast, we used an adaptive mapping algorithm based on the inverse cummulative histogram (Gwyddion software) followed by a suitable 2D median filtering. Special care was taken to realize the computation with correctly scaled topographic data. For this reason, the topographic data was converted into a normalized portable gray map images (PGM) without loss of image information (16 bit per pixel). These images could be easily registered as described above. The original scaling factors were stored for every image file in the PGM-header and were used by the application for re-transformation into scaled height values. It is beyond the scope of this study to describe the use material specific nonlinear ablation functions.

3D visualization and further processing. The produced 3D image data was further processed (Gaussian filters) and visualised with the commercial Amira® 3D software (Visage Imaging Inc., Carlsbad, USA).

References

[Bök00] A. Böker, K. Reihs, J. Wang, R. Stadler, and C. Ober. *Macromolecules*, **33**, 1310–1320 (2000)

[Bro74] H. Brown, E. Knights, and C. Scouten. *Journal of American Chemical Society*, **96**(25), 7765–7770 (1974)

[Cha96] C. Chan, T. Ko, and H. Hiraoka. *Surface Science Reports*, **24**(1–2), 3–54 (1996)

[Che08] J. Chen, C. Y. Wu, J. P. Tian, W. J. Li, S. H. Yu, and Y. C. Tian. *Applied Physics Letters*, **92**(23), 233104 (2008)

[Chu88] T. C. Chung, M. Raate, E. Berluche, and D. N. Schulz. *Macromolecules*, **21**(7), 1903–1907 (1988)

[Dun99] D. N. Dunn and R. Hull. *Applied Physics Letters*, **75**(21), 3414–3416 (1999)

[Efi07] A. Efimov, A. Tonevitsky, M. Dittrich, and N. Matsko. *Journal of Microscopy-Oxford*, **226**(3), 207–217 (2007)

[Fra00] J. Frank. *Atom Probe Tomography: Analysis at the Atomic level*. Kluwer Acedemic/Plenum Press, New York (2000)

[Gon02] R. Gonzalez and R. Woods. *Digital Image Processing*. Prentice Hall International, 2nd edition (2002)

[Had94] W. S. Haddad, I. Mcnulty, J. E. Trebes, E. H. Anderson, R. A. Levesque, and L. Yan. *Science*, **266**(5188), 1213–1215 (1994)

[Har98] C. Harrison, M. Park, P. Chaikin, R. A. Register, D. H. Adamson, and N. Yao. *Macromolecules*, **31**, 2185–2189 (1998)

[Har98a] C. Harrison, M. Park, P. Chaikin, R. A. Register, D. H. Adamson, and N. Yao. *Polymer*, **30**(13), 2733–2744 (1998)

[Hit08] A. P. Hitchcock, G. A. Johansson, G. E. Mitchell, M. H. Keefe, and T. Tyliszcak. *Applied Physics A: Materials Science & Processing*, **92**(3), 447–452 (2008)

[Hol06] L. Holzer, B. Muench, M. Wegmann, P. Gasser, and R. Flatt. *Journal of American Ceramic Society*, **89**(8), 2577–2585 (2006)

[Hun] M. Hund and H. Herold. German Patent No. DE 102004043191 B4 (2006), International Publication No. WO 2005083717 A1 (9 September 2005) and US Patent Application No. US 20080229812 A1 (2008)

[Hun07] M. Hund and H. Herold. *Review of Scientific Instruments*, **78**(6), 063703 (2007)

[Jin00] H. Jinnai, Y. Nishikawa, R. Spontak, S. Smith, D. Agard, and T. Hashimoto. *Physical Review Letters*, **84**(3), 518–521 (2000)

[Kon00] M. Konrad, A. Knoll, G. Krausch, and R. Magerle. *Macromolecules*, **33**(15), 5518–5523 (2000)

[Lee67] L. Lee. *Journal of Polymer Science A-2*, **5**(6), 1103–1118 (1967)

[Lud03] S. Ludwigs, A. Böker, A. Voronov, N. Rehse, R. Magerle, and G. Krausch. *Nature Materials*, **2**, 744 (2003)

[Mag00] R. Magerle. *Physical Review Letters*, **85**(13), 2749–2752 (2000)

[Mag02] R. Magerle. *Lecture Notes in Physics*. Springer-Verlag, Heidelberg (2002)

[Man02] B. Mantooth, Z. Donhause, K. Kelly, and P. Weiss. *Review of Scientific Instruments*, **73**(2), 313–317 (2002)

[Mao97] G. Mao, J. Wang, S. Clingman, C. Ober, J. Chen, and T. E.L. *Macromolecules*, **30**(9), 2556–2567 (1997)

[Mar07] J. Mark. *Physical Properties of Polymers Handbook*. Springer, Berlin, 2nd edition (2007)

[Mid03] P. A. Midgley and M. Weyland. *Ultramicroscopy*, **96**(3–4), 413–431 (2003)

[Mil96] M. K. Miller. *Polymer microscopy*. Chapman & Hall, London, 2nd edition (1996)

[Ols06] V. Olszowka, M. Hund, V. Kuntermann, S. Scherdel, L. Tsarkova, A. Böker, and G. Krausch. *Soft Matter*, **2**(12), 1089–1094 (2006)

[Par08] C. R. Parkinson and A. Sasov. *Dental Materials*, **24**(6), 773–777 (2008)

[Pet08] J. Petrasch, P. Wyss, R. Stampfli, and A. Steinfeld. *Journal of American Ceramic Society*, **91**(8), 2659–2665 (2008)

[Rad97] L. H. Radzilowski, B. O. Carragher, and S. I. Stupp. *Macromolecules*, **30**(7), 2110–2119 (1997)

[Rus02] J. Russ. *The Image Processing Handbook*. CRC press, 4th edition (2002)

[Saw96] L. C. Sawyer and D. T. Grubb. *Polymer microscopy*. Chapman & Hall, London, 2nd edition (1996)

[Sch06] S. Scherdel, S. Wirtz, N. Rehse, and R. Magerle. *Nanotechnology*, **17**(3), 881–887 (2006)

[Spe07] A. Sperschneider, F. Schacher, M. Gawenda, L. Tsarkova, A. H. E. Müller, M. Ulbricht, and J. Köhler. *Small*, **3**(6), 1056–1063 (2007)

[Tom98] B. Tomiyasu, I. Fukuju, H. Komatsubara, M. Owari, and Y. Nihei. *Nuclear Intruments & Methods in Physics Research Section B-Beam Interactions with Materials and Atoms*, **137**, 1028–1033 (1998)

[Tur95] A. Turturro, E. Gattiglia, P. Vacca, and G. T. Viola. *Polymer*, **36**(21), 3987–3996 (1995)

[Yeo07] T. S. Yeoh, J. A. Chaney, M. S. Leung, N. A. Ives, Z. D. Feinberg, J. G. Ho, and J. U. Wen. *Journal of Applied Physics*, **102**(12), 123104 (2007)

Danksagung

Das Gelingen dieser Arbeit wäre ohne das passende Umfeld mit den vielen hilfsbereiten Personen nicht möglich gewesen. Dafür möchte ich mich bedanken bei:

Prof. Georg Krausch, der es mir ermöglichte, ein interessantes und interdisziplinäres Thema in seinem Arbeitskreis zu bearbeiten. Seine zahlreichen Ratschläge und sein Optimismus waren eine große Unterstützung. Prof. Axel Müller für die tolle Aufnahme in den Arbeitskreis der Makromolekularen Chemie II, seine stetige Diskussionsbereitschaft und die grosse Unterstützung. Meinen beiden Chefs für die ermöglichten Freiräume, um eigene Ideen zu verwirklichen.

Prof. Alexander Böker und PD Dr. Larisa Tsarkova für die anregenden Diskussionen, Ratschläge und Aufmunterungen.

Felix Schacher für die Einführung in die hohe Kunst der Anionischen Polymerisation, seine Diskussionsfreude und seine enormen Geduld auf Flugreisen.

Ganz besonderer Dank gilt allen ehemaligen und jetzigen Mitgliedern der Arbeitsgruppen der PC II und der MC II für das anregende und unterhaltsame Arbeitsklima. Mein besonderer Dank gilt:

Dr. Wolfgang Häfner für seine grosse Unterstützung bei mathematischen, physikalischen und TEXnischen Problemen.

Heiko Zettl für die geduldige Einführung in die Welt des Programmierens, seine unglaubliche Hilfsbereitschaft und seinen andauernden Diskussionsdrang. Darüber hinaus bedanke ich mich bei ihm und seiner Frau Ute für die grandiosen kulinarischen Abende und für die gute Freundschaft.

Markus Hund für den Optimismus und der unglaublichen Ausdauer bei den Nanotomographie-Experimenten.

Anne Horn, Stephanie Hiltl, Adriana Mihut und Nathalie Mougin für die wissenschaftlichen Diskussionen, aber auch für die lustige Abendunterhaltung und das allgegenwärtige Verständnis.

Heiko Schoberth für sein allwissendes Auge für graphische Lösungen und seine Einführung in die Welt der Computersimulationen.

Natürlich möchte ich mich hiermit auch beim Grenoble-Team für die stetige Ausdauer bei den Dünnfilmexperimenten bedanken.

Und natürlich allen anderen, auch ehemaligen, Mitgliedern der PC II und MC II Arbeitsgruppen: Anne Horn, Michaela Hoffmann, Andriana Horvat, Sven Hüttner, Günther Jutz, Dr. Armin Knoll, Dr. Sergej Koutouzov, Carmen Kunert, Ute Zettl, Dr. Violetta Olszowka, Gustav Sauer, Dr. John Bosco Stanislaus, Dr. Denys Zimin, Clemens Liedel, Christa Weber, Daniel Kluge, Thomas Czubak, Nicole Popp, Kerstin Schindler, Alexandra Schweikart, Dr. Stephan Schmidt, Johann Erath, Julia Gensel, Öznur Kaftan, Eva Max, Melanie Pretzl, Katja Trenkenschuh, Christian Kuttner, Anja Goldmann, Joachim Schmelz, Andreas Hanisch, Susanne Edinger, Andre Gröschel, Annette Krökel, Annika Ochs, Stefan Reinicke, Thomas Ruhland, Dr. Holger Schmalz, Sandrine Tea, Dr. Markus Burkhardt, Dr. Manuela Schumacher und Andrea Wolf für die gute Zusammenarbeit.

Ein ganz besonderer Dank gilt Sybille Zimmermann und Gaby Rösner-Oliver für die Hilfsbereitschaft in bürokratischen und organisatorischen Belangen sowie für die gute Versorgung mit Nervennahrung.

Meiner Familie danke ich für die große Unterstützung während des Studiums und der Promotion. Besonders danke ich meinen Ehemann Dirk für sein riesigesVerständnis während der Endphase.

Erklärung

Die vorliegende Arbeit wurde von mir selbstständig verfasst und ich habe dabei keine anderen als die angegebenen Hilfsmittel und Quellen benutzt.

Ferner habe ich nicht versucht, anderweitig mit oder ohne Erfolg eine Dissertation einzureichen oder mich der Doktorprüfung zu unterziehen.

Bayreuth, 27. Juli 2009

Alexandra Sperschneider